



Ion selectivity in multi-channel CDI

Permselectivity of porous carbon
capacitive membrane electrodes used in
multi-channel capacitive deionisation

Ruben Vos

Ion selectivity in multi-channel CDI

Permselectivity of porous carbon
capacitive membrane electrodes used in
multi-channel capacitive deionisation

by

Ruben Vos

to obtain the degree of Master of Science
at the Delft University of Technology,
to be defended publicly on Monday April 22, 2024 at 10:00 AM.

Student Number:	1378988
Supervisor:	R.M. Hartkamp
Daily-supervisor:	N.J.H. Boon
Thesis Duration:	April, 2023 - April, 2024
Faculty:	Faculty of Mechanical Engineering, Delft

Preface

Climate change is a hot topic in the modern industrial age. Media are regularly writing about alternatives to fossil fuels and rising global temperatures. Energy technologies that deal with climate change have always been my main areas of interest. Climate change is not only causing a rise in global temperatures, but also causing droughts. This is what happened in Cape Town in 2018, where the water reserves in the various lakes around the city almost dried up. Capacitive deionisation (CDI) is a desalination technology that could help resolve these water shortages. This is what motivated me to do my research on the permselectivity of membranes used in CDI. I enjoyed the experimental work which was the cornerstone of my thesis. Sometimes it was challenging to get the setup working as intended, but the bigger the challenge the bigger the reward when the setup is finally working.

I would like to thank my two supervisors Remco Hartkamp and Niels Boon, who helped me doing my selectivity measurements. Their experience and feedback during our weekly meetings helped me to improve the measuring setup and provided valuable insights on the topic of permselectivity. Secondly, I would like to thank Irem Gurbuz for instructing me on how to use the Porolux Revo porometer. Irem helped me with operating the porometer during my first experiment. I would also like to thank Eszter Má dai, Prasad Gonugunta and Prasaanth Ravi Anusuyadevi from Materials Science, for their time and effort in performing the SEM imaging. The SEM images gave invaluable insights into the pore size data.

With this report, my master's thesis and my studies at the TU Delft have come to an end. Looking back on my time as a student, I can see how much I have grown. I can only say that I am very grateful for the support and presence of my family and friends. Thanks, Mum and Dad, for our talks whenever I felt the need to exchange ideas with someone. Antoine, thanks for your ideas and suggestions when I got stuck on the electrical interference problem. I am closing with you, Mariska. Your love and support in the smallest things allowed me to perform at my best.

*Ruben Vos
Delft, April 2024*

Summary

Due to climate change, more places around the world are dealing with freshwater shortages. There is plenty of salt water on earth, but this is not suitable for human consumption, agriculture, or for use in many industrial processes. Among desalination technologies a new technology started to emerge called "capacitive deionisation" (CDI). A conventional CDI cell consists out of two electrodes with a potential applied to them. The electrostatic charge on the electrodes attracts the ions from the feed water that flows in between these electrodes. Recent years have seen the introduction of a new cell architecture with multiple electrodes and multiple water channels parallel to each other. A cell consists out of four electrodes. The potential on the outer electrodes is the driving force, and the inner electrodes function as selective membranes between the channels. The inner electrodes therefore serve two functions and are called capacitive membrane electrodes (CME). The water is deionised due to the migration of ions through the CME, from the inner channel (low salinity) to the outer channels (high salinity). Since multi-channel CDI is relatively new, a thorough investigation of the effect of electrostatic charge and the microstructure of the CME on its deionisation performance is still lacking. This led to the following main research question: *How large is the effect of the pore size distribution on the ion transport and selectivity of porous carbon capacitive membrane electrodes?* This thesis sought an answer to this question by testing five different CME materials via an experimental approach.

An experimental measuring setup was built, with a source measuring unit (SMU), a power supply, and a cell holding the CME. The charging of the cell and measuring procedure were all controlled by a relay board and Arduino. The measuring procedure was as follows: each experiment consists out of a positive and negative charge cycle. Each cycle has a charging phase, a floating phase (the cell is disconnected from the power supply), and a short-circuit phase. During each phase, the membrane potential (V_m) and the electrical potential of the CME (V_{CME}) w.r.t. one of the reference electrodes was recorded. Knowing the salt concentrations and V_m , the permselectivity (P) can be calculated.

The materials that were studied, were all research samples with varying compositions and thicknesses. Each material showed a different permselectivity (P), ionic resistance (R_m) and fluid flow through the membrane (Q). The membrane materials should not be compared based on permselectivity alone. A highly selective membrane with high ionic resistance is not considered to be desirable. Therefore, two performance parameters were used to compare the materials: P/V_{CME} and P/R_m . When looking at the ratio of P/V_{CME} , no membrane material really stood out from the rest. However, when looking at P/R_m clearly material 09/04 had the advantage. Material 09/04 was decently selective with a permselectivity of 0.56 [-], but it showed a much lower ionic resistance of 19.91 [Ω] for its membrane area. These are desirable qualities in a CME, and therefore material 09/04 should be considered in a CDI cell.

The pore size measurements were conducted with a porometer that utilises the capillary flow technique, where the fluid flow is recorded as the pressure on the membrane is increased. First, a wet measurement with wetting liquid is carried out, followed by a dry measurement. From the difference in pressure between these measurements, the pore size distribution can be calculated. The pore size measurements showed that the most occurring pore sizes were between 20 [nm] and 80 [nm], which is in the mesopore range to the smaller macropore range. Scanning electron microscopy (SEM) imaging was used to verify the porometer results, as the porometer has a lower measuring limit of 20 [nm]. From the SEM images, it was verified that there were almost no pores below the 20 [nm] limit.

When comparing the results between the permselectivity measurements and the pore size measurements the following correlation was found: membrane materials that showed higher fluid permeability also showed lower ionic resistances. This can be explained the following way: if the liquid can easily permeate through the CME, then the ions will also easily diffuse through. Finding a correlation between the fluid permeability and the ionic resistance, does give the confidence that there must be a connection between the physical properties and the electrical/permselectivity properties of a CME. To achieve good deionisation performance in multi-channel CDI, CMEs must offer low ionic resistance when ions are forced to migrate from low to high salinity, while still being permselective when ions want to migrate back from high to low salinity.

Contents

Preface	i
Summary	ii
List of Figures	vi
List of Tables	vii
Nomenclature	viii
1 Introduction	1
1.1 Research questions	2
1.2 Objectives	2
1.3 Thesis outline	3
2 Theoretical framework	4
2.1 CDI working principle	4
2.2 CDI cell architectures	5
2.3 Multi-channel CDI systems	6
2.4 CDI performance metrics	7
2.4.1 Maximum salt adsorption capacity	7
2.4.2 Average salt adsorption capacity	7
2.4.3 Charge and current efficiency	8
2.5 Electrical double layer	8
2.6 Porosity of carbon electrodes	9
2.7 Selective ion separation by CDI	10
2.8 Measuring membrane selectivity	11
2.9 Literature discussion	11
2.10 Diffusivity of ionic species in electrolytes	12
2.11 Derivation of permselectivity equation	13
3 Methodology	18
3.1 Thesis approach	18
3.1.1 Experimental setup	18
3.1.2 Data processing	18
3.1.3 Discussion of the results and recommendations for further research	18
3.2 Selectivity measurements	19
3.2.1 Measuring setup overview	19
3.2.2 Measuring equipment	21
3.2.3 Measuring procedure	21
3.2.4 Membrane materials	23
3.2.5 Problem solving	25
3.3 Pore size measurements	26
3.4 SEM imaging	27
4 Cell Design	28
4.1 Design and fabrication of different cell components	28
4.2 Cell design overview	31
5 Results	34
5.1 Results of a typical experiment	34
5.2 Testing for various conditions	35
5.2.1 Varying amount of salt concentrations	36

5.2.2	Tuning the amount of discharge during floating phase	37
5.2.3	Using a different salt	39
5.2.4	Applying different charge potentials	39
5.2.5	Influence of stirring mixture on selectivity	41
5.2.6	Exchanging concentrations	41
5.2.7	Reduction of CME selectivity after charge cycling	42
5.3	Permselectivity and resistivity results	43
5.4	Porosity measurements	47
5.5	SEM Imaging	48
6	Discussion	51
7	Conclusion & Recommendations	55
7.1	Conclusion	55
7.2	Recommendations for future research	56
	References	58
A	Code files	61
A.1	Python Code	61
A.2	Arduino code	65
B	Combined short-circuit measurements	68
C	Pore size measurements	69
D	SEM figures	73

List of Figures

2.1	The adsorption phase in a CDI cell	4
2.2	The desorption phase in a CDI cell	5
2.3	Various CDI cell architectures	6
2.4	The working principle of multi-channel CDI	7
2.5	Experimental data on the charge and current efficiency for MCDI and FCDI [9]	8
2.6	Figure A: Gouy-Chapman-Stern model and figure B: modified Donnan model to describe the ion concentration [9]	9
2.7	The ASAC times vs interparticle porosity [7]. The transport is either limited because of the absence of transport ways (due to tight packing of the material), or due to the pathways being too long (as a result of the packing being too loose).	10
2.8	Schematic of the experimental setup to measure the electrochemical potential [24]	11
2.9	This figure shows a snapshot of the multi-channel cell described in section 2.3. If the CME would be perfectly selective there would be no J_- flux and optimal J_+ flux. Here, the selectivity describes the effectiveness of the deionisation process.	16
3.1	Raw sketch of the side-view of the cell. The cell has two compartments with the CME in between. With probes close to the membrane. The CME is charged w.r.t. one counter electrode.	19
3.2	Schematic overview of the selectivity measurements setup	20
3.3	The measuring setup in the lab	20
3.4	Progression of measurement phases over time during an experiment	22
3.5	Wiring schematic of the relay board	24
3.6	The soldered together filter. A 3.3 [nF] capacitor in parallel, and a 100 M Ω resistor in series	25
3.7	Various degrees of membrane wetting with wetting liquid. Picture source: Training slides Porolux Revo [37]. Used with written permission from Aptco Technologies NV	26
3.8	Graph of a pore size distribution, for illustrative purposes Information source: Training slides Porolux Revo [37]. Used with written permission from Aptco Technologies NV	26
3.9	The process of the wet measurement. Picture source: Training slides Porolux Revo [37]. Used with written permission from Aptco Technologies NV.	27
3.10	The process of the dry measurement. Picture source: Training slides Porolux Revo [37]. Used with written permission from Aptco Technologies NV.	27
4.1	CAD model of the cell compartments	29
4.2	Final cell compartments	29
4.3	CAD drawing in Solidworks of the cell	31
4.4	The fully completed cell	32
5.1	Membrane potentials during a typical experiment. The figures on the left show V_{CME} and V_m during full charge cycles. At around 1250 [s] (and 4750 [s]), there is a clear jump in the curves. This denotes the change from the charge phase to the floating phase. The figures on the right show V_{CME} and V_m during the floating phase.	35
5.2	Increasing the salt concentrations reduces the permselectivity of the CME. It is hypothesised, that at higher concentrations more ions will be located in the EDL. This reduces the apparent membrane potential, which reduces the permselectivity.	37
5.3	These two experiments were performed back to back. This clearly indicates that short-circuiting the cell during the floating phase is beneficial to get the complete discharge curve in a timely manner.	38
5.4	By increasing the number of short-circuit times during the floating phase, the more the CME gets discharged, and the smaller the membrane potential gets at the end of the floating phase. From these figures it is clear that 15 times makes sure that the CME is completely discharged.	38

5.5	Permselectivity for a monovalent (KCl) salt on the left, and the permselectivity for a divalent salt (CaCl_2) on the right. Ca^{2+} has a much smaller diffusion coefficient, and it needs two electrons to be attracted by the CME. This leads to a different membrane potential and therefore a different permselectivity.	39
5.6	The permselectivity for increasing charge potentials on the CME. Increasing the charge potential has a lasting effect on the permselectivity, even when the CME is discharged. Which can be observed by comparing the permselectivities at the end of the floating phase, when the CME is discharged. Figure d shows the permselectivity of an oxidised membrane. The charge potential is 1 [V], but after two experiments with higher potentials.	40
5.7	Permselectivity during positive floating, with and without stirring the solutions. From this figure, it is clear that stirring increases the permselectivity both in the positive and negative range. . .	41
5.8	In the figure on the left permselectivity experiment was carried out with salt concentrations in the normal configuration. In the figure on the right, the concentrations were reversed. Meaning that the ions will now migrate in the opposite direction through the CME, resulting in a permselectivity that is inverted.	42
5.9	Selectivity after 10 cycles, where positive and negative cycles alternate. Each point in the graph is all the way at the end of a positive or negative cycle. Meaning that the CME is completely discharged.	43
5.10	Comparing CME material based on two performance metrics	45
5.11	Permselectivity for different materials. For each figure the green curve correlates with the positive cycle (first occurring), and the red curve with the negative cycle (second occurring). As time progresses the curves move inward. The x-axis shows the electrical potential of the CME in Volts w.r.t. one reference electrode. The permselectivity is on the y-axis and has no units. . .	46
5.12	Pore size measurement results for material 09/04. This figure on the left shows the data points of the measurement, where the pressure data points were recorded with their respective fluid flows. The wet and dry curves did not converge, unfortunately. The porometer software has the capability to recalculate the dry curve with an exponential approximation. This is what happened in the figure on the left. The curve in the figure on the right is the calculated PSD from the data from the curve on the left. It is clear from this figure that most pores are between 20 and 80 [nm]. That is in the mesopore and lower macropore range. As was discussed in section 2.6, the mesopores play a key role in the permselectivity of CMEs.	48
5.13	The surface of material 04/21 at a magnification 100,000x. From the scale at the bottom, it can be deduced that most pores are larger or in the order of 20 [nm]. Few pores are smaller than 20 [nm]. This validates the pore size measurements from the porometer which has a lower measuring limit of 19.4 [nm], see section 5.4.	49
5.14	SEM figure of the cross-section of material 04/21 at a magnification 7,000x. A network of carbon black and binder is surrounded by graphite particles. As the carbon black and binder fill the space between the graphite particles, it is therefore plausible that the pore structure is running continuously through the thickness of the material.	50
6.1	The curves through the data point guide the eye, to show that generally speaking, a higher membrane resistance indicates a higher permselectivity.	52
6.2	The data points of the fluid flow at MFPS are plotted against the 4 different membrane resistances of each material. The curves through the data points are drawn to indicate the trend that membranes with high fluid flow, also demonstrate low ionic resistance.	52
6.3	The fluid flow data is plotted w.r.t. the permselectivity data of each membrane. Only the positive curve suggests a trend that higher fluid flows lead to lower permselectivities. The negative curve does not show any correlation or trend. Also in this figure, the curves through the data points are merely a visual aid to help see a trend.	54
B.1	Overlaying permselectivity curves for 3 experiments with varying amount short-circuit intervals. The curves from short-circuiting 3 times and 6 times do not meet at the middle point. Indicating that the CME has not been completely discharged yet.	68
D.1	SEM figures with increasing magnification of the surface of material 04/21	77
D.2	SEM figures with increasing magnification of the cross-section of material 04/21	80

List of Tables

3.1	The standard high and low concentrations of KCl in water. Used in all experiments, except for the experiments in subsection 5.2.1.	23
3.2	Composition of membrane materials	24
4.1	Fabricated components with a short description	30
4.2	Bill of materials of the cell	33
5.1	Permselectivity and resistance data for different CME materials	43
5.2	Pore size measurements for different membrane materials	47

Nomenclature

Abbreviations

Abbreviation	Definition
ASAC	Average salt adsorption capacity
BET	Brunauer-Emmett-Teller
CA	Carbon aerogels
CAD	Computer aided design
CDI	Capacitive deionisation
CME	Capacitive membrane electrode
FCDI	Flow CDI
EDL	Electrical double layer
GCS	Gouy-Chapman-Stern
i-CDI	inverse-CDI
IEM	Ion exchange membrane
MCDI	Membrane capacitive deionisation
mD	modified Donnan
MFPS	Mean flow pore size
MP	Maximum pore size
MPS	Mean pore size
mSAC	Maximum salt adsorption capacity
PDE	Partial differential equation
PMMA	Poly(methyl methacrylate)
PNP	Poisson-Nernst-Planck
PSD	Pore size distribution
PVDF	Polyvinylidene fluoride
RO	Reverse osmosis
SEM	Scanning Electron Microscopy
SHE	Standard hydrogen electrode
SMU	Source measuring unit
SP	Smallest pore size

Symbols

Symbol	Definition	Unit
A_{wire}	Cross-sectional area of an electrical wire	[m ²]
C_H	Higher salt concentration	[g l ⁻¹]
C_i	Molar concentration of species i in the bulk of the fluid	[mol L ⁻¹]
c_i	Molar concentration of species i inside the membrane	[mol L ⁻¹]
C_L	Lower salt concentration	[g l ⁻¹]
\mathbf{D}	Electric displacement field vector	[C s ⁻²]
D	Pore diameter	[m]
D_i	Diffusivity of species i	[m ² s ⁻¹]
E	Electric field	[N C ⁻¹]
e	Elementary charge	[C]
F	Faraday constant	[C mol ⁻¹]
I	Current	[A]
J_i	Ionic flux of species i	[mol m ⁻² s ⁻¹]
k_b	Boltzmann constant	[J K ⁻¹]
l_{wire}	Length of an electrical wire	[m]
M_i	Mobility of species i	[m ² s ⁻¹ V ⁻¹]
P	Permselectivity	[-]
P_{pore}	Pore pressure	[Pa]
Q	Volumetric flow rate	[m ³ s ⁻¹]
R_m	Ionic resistance of a membrane	[Ω]
R_{wire}	Resistance of an electrical wire	[Ω]
S	Selectivity	[-]
t	Time	[s]
T	Temperature	[K]
u	Bulk velocity	[m s ⁻¹]
V_{CME}	Potential between CME and 1 reference electrode	[V]
V_m	Membrane potential	[mV]
V_t	Thermal voltage	[V]
z_i	Valence of species i	[-]
γ	Surface tension of a fluid	[N m ⁻¹]
ϵ	Electric permittivity	[F m ⁻¹]
Λ	Charge efficiency	[%]
λ	Current efficiency	[%]
μ	Chemical potential	[J mol ⁻¹]
ρ	Free charge density	[C m ⁻³]
ρ_{wire}	Specific resistance of an electrical wire	[Ω m]
ϕ	Potential	[V]

1

Introduction

An increasing number of places are dealing with freshwater shortages due to climate change. Most of the earth's surface is covered in water, but this is salt water that cannot be used for human consumption, agriculture, or for use in many industrial processes. Salt water is not a simple mixture of water and salt grains, because it is different on a molecular level: when salt gets dissolved in water the ionic bonds are broken down and ionic particles start to interact with the individual water molecules. From an energetic perspective, salt dissolves in water because it prefers to be in a lower free-energy state. For NaCl this is an endothermic process: dissolution increases enthalpy but the gain in entropy of the (now) mobile ions makes the process favourable nonetheless. Consequently, salt does not spontaneously go out of solution. This explains why removing salt from water is not a straightforward filtration process.

The oldest method to desalinate water is by evaporating the water and then condensing the water vapour again. This is an energy intense distillation method that also occurs in nature as the well-known water cycle. Salt water distillation, though energy intense, is capable of producing highly pure water that contains virtually no ionic species. This method is still used today to produce distilled water for laboratory purposes [1]. Water distillation has been the dominant method to produce potable water until the late sixties. Recently, water distillation got a renewed interest in the form of solar distillation [2]. Here, the heat of the sun is used to produce distilled water.

Water distillation eventually got replaced by a process called reverse osmosis (RO). In the US, the first large scale RO desalination plant started producing 11.4 million litres of potable water in 1977, Cape Coral (Florida, USA) [3]. Currently, RO is the most widely used desalination technology [4]. Reverse osmosis works on the principle of pushing the salt water through a membrane that is only permeable to water molecules and not to the ionic species. Osmosis is the natural process where the solvent (in this case water) can move through a semipermeable membrane from a fluid low in salinity to a fluid high in salinity. An osmotic pressure can be observed when the solvent migrates through the membrane. Reverse osmosis works in the opposite direction, and it has to overcome the osmotic pressure. This explains why RO has to work at high pressures and consumes considerable amounts of energy. From a mass perspective, it can be said that RO removes the water from salt water.

A completely different technology that got a lot of attention in recent years, is called "capacitive deionisation" (CDI). Brackish water desalination with CDI can be considerably less energy intense compared to RO and distillation [5, 6]. CDI removes the ionic species directly from salt water instead of removing water from salt water. In CDI, the deionisation process is initiated by applying a potential over a set of electrodes (called a cell) as water is passing through or by the electrode. The charged particles adhere themselves to the electrodes in the so-called electrical double layer (EDL) via electrostatic attraction. When the electrodes are completely saturated with salt, the process is reversed and all the salt is released into a waste stream. This setup is the conventional CDI cell architecture that operates in cycles. Cycling between a product stream and a waste stream of water. Many CDI cell architectures have been developed in the past years (see section 2.2), such as: flow-by cells, flow-through cells, membrane CDI, and inverted CDI.

Recently, a new CDI cell architecture has been developed, with multiple channels parallel to each other that run under continuous operation. In this cell architecture, the ionic species migrate from channel to channel driven by an electrostatic potential. The advantage of this method is that the product and the reject flows are separated at all times, permitting a more continuous operation. This research will focus on the ion transport through the electrodes. The electrodes that separate the channels also function as membranes, therefore called capacitive membrane electrodes (CME). Depending on the electrostatic charge of the CME, the CME will either become a cation exchange membrane or an anion exchange membrane. As the method is relatively new, a thorough investigation of how electric charge and the microstructure of the CME affect its performance is still missing. For example, the permselectivity, which is a membrane property that describes the ratio of the migration of positive ionic species, over the total number of ions migrating through the membrane.

1.1. Research questions

Before the research questions can be formulated, first a problem statement must be given:

Problem statement "In conventional CDI cell architectures, the porosity of the carbon material has been linked to the salt adsorption rate of CDI electrodes [7], and the micropores had the largest contribution to the maximum salt adsorption capacity (mSAC). The porosity of the CMEs can be quantified with a pore size distribution. As of yet it is not fully known how the pore structure affects the ion transport and ion selectivity of CMEs."

The research questions are given below. The main research question is supported by the sub-questions. These sub-questions have to be answered first before the main research question can be answered.

Main research question: *How large is the effect of the pore size distribution on the ion transport and selectivity of porous carbon capacitive membrane electrodes?*

Sub questions:

- What will the experimental setup look like such that it can measure the ion transport and ion selectivity of a CME?
- How can a mathematical model be built such that it can describe the permselectivity of the CME in terms of measurable electrostatic potential and ion concentrations?
- How can the pore size distribution of a CME be measured and which units quantify the pore size distribution?
- How can the measured pore size distributions be linked to the experimental values for ion selectivity and transport capability?
- How can the experimental results be correlated to each other?

1.2. Objectives

The main objective of this research is to determine whether there is a clear correlation between the pore size distribution and the ion transport and ion selectivity of CMEs made of porous carbon materials. A list of sub-objectives is given below:

- Build a mathematical model that describes the permselectivity of the CMEs as a function of the electrostatic potential and the ion concentrations
- Experimentally measure the ion transport and selectivity of a CME
- Experimentally measure/quantify the pore size distribution of a CME
- Compare experimental results to determine if there is a correlation between the pore size distribution and ion transport and ion selectivity of the CMEs

1.3. Thesis outline

Chapter 2 explains how CDI exactly works and discusses the theoretical framework. Chapter 3 discusses the methodology, what the measuring procedure is, and how the data is processed. The cell design of the measuring setup is discussed in chapter 4. Chapter 5 shows all results and reflects on them with intermediate discussions. Chapter 6 discusses the final results and seeks to find correlations between the data. Finally, chapter 7 concludes this research by answering the research questions and giving recommendations for future research.

2

Theoretical framework

Capacitive deionisation as a concept was proven to work in 1960, but it only started to get attention from researchers in the last 20 years [8]. During those years much research has been performed on CDI cell architectures, materials, and advancements in the theoretical understanding of CDI. This chapter gives an overview of the working principle behind CDI, the many cell architectures that are out there, and the mathematical relation between the permselectivity and the membrane potential.

2.1. CDI working principle

A basic CDI cell consists out of a pair of porous carbon electrodes. Salt containing feed water is fed between the electrodes. By applying a potential over the electrodes, they start to charge up. The charge on the electrodes starts to attract the oppositely charged ionic species in the water. The more internal surface area the electrodes have, the higher the capacitance, the more ions it can absorb from the water. These ions accumulate in a very thin layer close to the carbon-water interface, which is called the electrical double layer (EDL). This process of attracting the ions from the water produces a product stream of deionised water. This process of removing salt from the water is depicted in Figure 2.1.

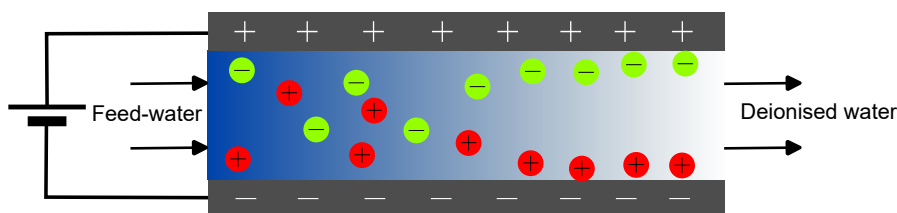


Figure 2.1: The adsorption phase in a CDI cell

At some point, the cell is completely saturated with salt. When the maximum salt adsorption limit has been reached, the cell must be short-circuited or reversed to release all the ions back into the water. The reversal of the process produces a waste stream as can be seen in Figure 2.2. When all the ions are released, then the cell can be charged again to produce fresh water. This means that a conventional CDI cell has to cycle between charge and discharge phases. The cell itself is a straightforward component, but the cycling between phases makes fluid handling downstream of the cell complex.

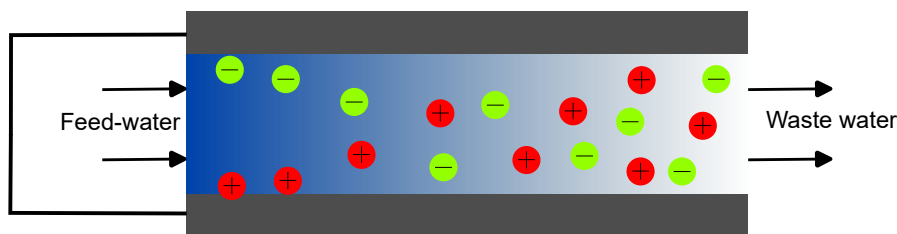


Figure 2.2: The desorption phase in a CDI cell

2.2. CDI cell architectures

As mentioned in the introduction, there are many CDI cell architectures. Many of these are extensively described and discussed in literature [9]. The most common cell architectures are briefly discussed and an overview is given in Figure 2.3.

The conventional cell design is a cell consisting of two porous electrodes where the salt water flows in between. Here the flow of water and the direction of the electric field are perpendicular to each other, therefore it is called a "flow-by" cell as can be seen in Figure 2.3a. In a flow-by cell, there is a spacer between the electrodes to provide structural support, to prevent the electrodes from short-circuiting, and to guide the fluid flow between the electrodes. A different approach is a setup where the flow of water and electric field are in the same direction, this is called a "flow through" cell (see Figure 2.3b). Here, the feed water goes straight through the electrodes themselves. The advantage of such a cell is that the spacer that sits between the electrodes can be much thinner. That is because the spacer does not have to guide the fluid flow between the electrodes anymore, as the fluid flow is now perpendicular to the electrodes. A thinner spacer means that the cell can be more compact and that the cell ionic resistance will be reduced [9].

An important variant of the flow-by cell design is by applying a selective membrane or coating on the electrodes. These membranes are permeable to either cations or anions and are called ion exchange membranes (IEM). This type of cell architecture is called "membrane CDI" (MCDI), see Figure 2.3c. The main advantage of MCDI is the improvement of charge efficiency (see subsection 2.4.3 on charge efficiency) compared to conventional CDI [9]. That is because the IEMs repel the co-ions and let the counter-ions through to be adsorbed by the electrode. The downside of utilising IEMs is the increased material cost of the cells. Depending on the operational costs, utilising MCDI may be less economical compared to conventional CDI [10]. In recent years, much research has been performed on membrane materials, manufacturing processes and the operation of MCDI cells [11–15]. MCDI has been proven to be a viable technology to deionise water with moderate salinities, as MCDI is now commercially used by desalination companies like Voltea (Texas, USA) [16].

Recently, another variant of the flow by cell has been developed by Gao *et al* [17], where the electrodes were chemically surface treated. This resulted in an inverse behaviour of the charging and discharging process, therefore calling it inverse-CDI (i-CDI) Figure 2.3d. The chemical treatment of the surface of the electrode caused the electrode to possess fixed charges. This resulted in the spontaneous formation of the electrical double layer (EDL) (see section 2.5). The ions from the solution are stored in the EDL. When the cell is charged the fixed charges in the electrodes are neutralised and ions are released back into the solution.

Cell architecture depicted in Figure 2.3e is derived from the flow-by cell, but configuration E (called a desalination battery) utilises one or more faradaic electrodes instead of capacitive electrodes. Faradaic electrodes are non-capacitive and are beyond the scope of this research. The reader is referred to Biesheuvel *et al* [18] if the reader is interested in knowing more about Faradaic processes in CDI.

The final cell configuration is the flow cell depicted in Figure 2.3f and it is called flow-CDI (FCDI). FCDI utilises carbon flow electrodes. These carbon flow electrodes form a slurry of carbon particles mixed with the feed water. These carbon flow electrodes are also beyond the scope of this research. The reader is referred to Zhang *et al* [19] and Shin *et al* [20] if the reader is interested in the recent developments of FCDI.

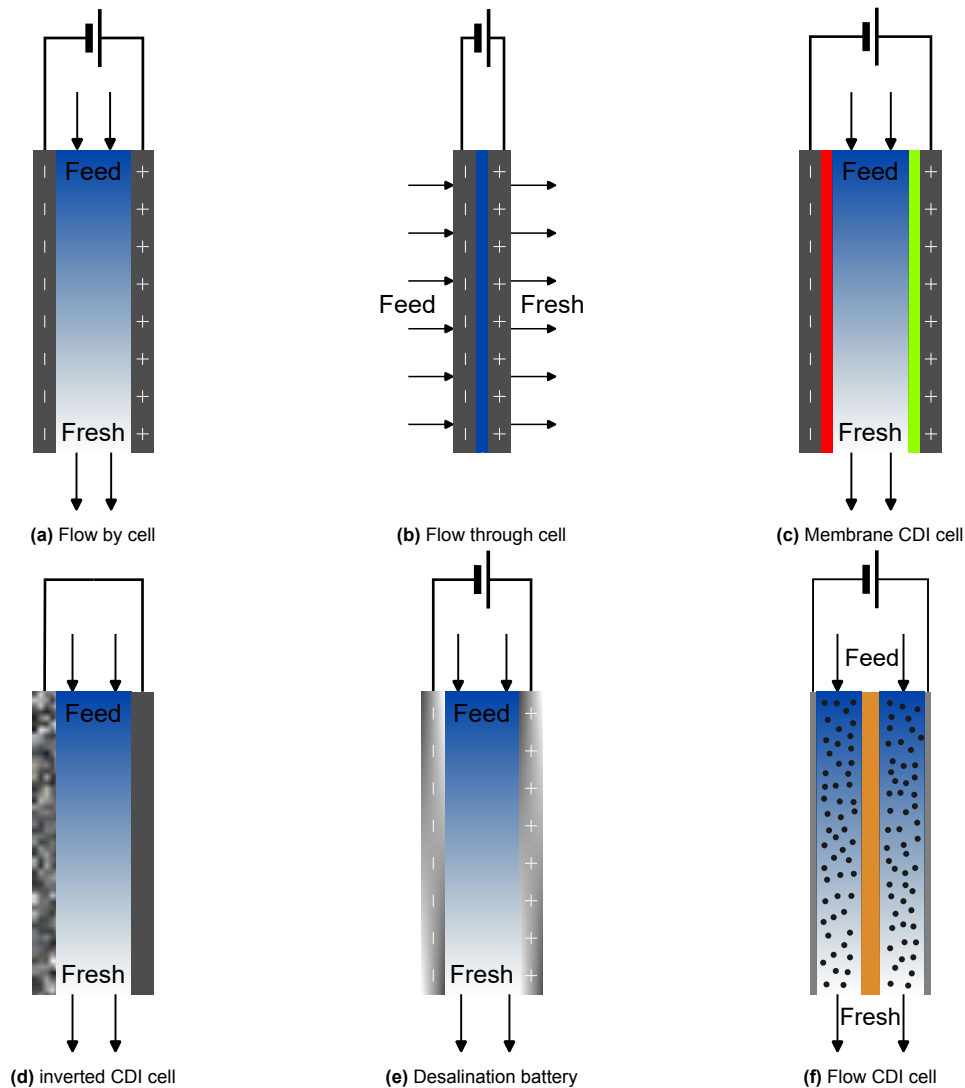


Figure 2.3: Various CDI cell architectures

2.3. Multi-channel CDI systems

Recent years have seen the introduction of a new architecture (depicted in Figure 2.4) with multiple channels. This new architecture has a continuous flow of water instead of cycling between product streams and waste streams. This can be achieved by having multiple channels parallel to each other. There is an inner and outer set of electrodes with an alternating potential applied to them. It should be noted that Figure 2.4 shows a snapshot at which the inner electrodes have a maximum charge, and the outer electrodes have no charge. The potential on both pairs of electrodes is 90 degrees out of phase. For example, when the inner right electrode is positive, the outer right electrode has no charge yet but it starts to become positive. In this situation, an anion could enter the inner right electrode and as the outer right electrode gets charged positively it will pull the anion through to the next channel. The outer electrodes are the driving force behind the system and the inner electrodes function as selective membranes between the channels. From here on in this document the inner electrodes are referred to as capacitive membrane electrodes (CMEs).

The potential on the electrode pairs is alternating in four phases. In the first phase, the CMEs charge up. In the second phase, the outer electrodes charge up to pull the ions through the CMEs. In the third phase, the polarity of the CMEs is reversed and in the final phase, the polarity of the outer electrodes is reversed. And the cycle starts over again. This cell architecture is fairly new and as of today it is not fully known which variables (and in what magnitude) optimise the transport of ions through the CMEs.

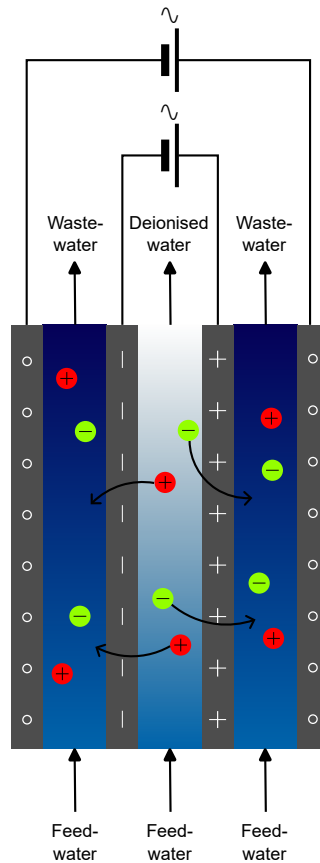


Figure 2.4: The working principle of multi-channel CDI

The information about the multi-channel CDI cell was obtained through personal communication with N.J.H. Boon, see its patent [21].

2.4. CDI performance metrics

There are several ways the performance of a CDI cell can be measured to compare different CDI technologies with each other. These are standard practices in CDI research to be able to make fair comparisons [9]. The most important metrics are the maximum salt adsorption capacity (mSAC), average salt adsorption capacity (ASAC) and charge efficiency. These metrics are discussed in the following subsections.

2.4.1. Maximum salt adsorption capacity

The mSAC is reached by applying a constant voltage on the cell for an extended period of time. When the cell is completely charged, no more extra salt gets adsorbed. This equilibrium is reached when the gradient of the conductivity of the cell is equal to zero. The amount of salt removed can be calculated by measuring the difference in salinity between the feed water and the desalinated water multiplied by the fluid flow. The mSAC is then defined by dividing the mass of the removed salt (in [mg]) by the mass of the electrode (in [g]). The mass of the electrode must be carefully reported though, as it affects the mSAC. The mass of the electrode should be clearly defined as either the entire mass of the electrode or just the mass of the effective carbon component that adsorbs the salt. Porada *et al* [7] found that the porosity of the carbon material of the electrodes had a considerable influence on mSAC. What they found was that the micropores of a size smaller than 1.1 [nm] contributed the most to the mSAC.

2.4.2. Average salt adsorption capacity

The ASAC differs from mSAC in the sense that a time component is involved. The ASAC is defined as the mass of the removed salt divided by the mass of the electrode and time [$\text{mg g}^{-1} \text{min}^{-1}$]. Choosing shorter charging times could lead to a higher ASAC. A capacitor charges up fast at first, because the charge on a

capacitor increases inverse exponentially to a final value. The last bit of charge on a capacitor is only accepted at a slow pace. Therefore, not completely charging the CDI cell and then discharging could lead to a higher ASAC.

2.4.3. Charge and current efficiency

The last important metrics are the charge and current efficiency. The current efficiency as a performance metric has been adopted from the field of electrodialysis [9] [22]. Here the current efficiency λ [%] is related to the change in salinity ($c_{in} - c_{out}$) in $[\text{mol m}^{-3}]$, the volumetric flow rate \dot{Q} in $[\text{m}^3 \text{s}^{-1}]$, the Faraday constant F $[\text{C mol}^{-1}]$ and the current I [A]. The current efficiency describes what the electrical requirements are for deionising a fixed flow rate of water with a certain drop in salinity.

$$\lambda = \frac{(c_{in} - c_{out}) \dot{Q} F}{I} \times 100 \quad (2.1)$$

The charge efficiency Λ is similar to the current efficiency as it describes the required electrical energy to deionise a fixed volume of water with a certain drop in salinity. The electrical energy for a fixed cell voltage is equal to $E = \int_{t_0}^{t_1} I dt$. Then, the charge efficiency can be described as:

$$\Lambda = \frac{(c_{in} - c_{out}) Q F}{\int_{t_0}^{t_1} I dt} \times 100 \quad (2.2)$$

Equation 2.2 is less relevant for cell architectures that are operating at a constant current, such as MCDI [9].

2.5. Electrical double layer

In nature, positively and negatively charged particles balance each other such that a material is electrically neutral. This means that in an aqueous solution, the concentrations of cations and anions must be the same. This becomes different however near the surface of a charged electrode. Because of the charge on the electrode, it will attract the counter-ion and repel the co-ion in the solution. There will be a higher concentration of either cations or anions in a thin layer that covers the electrode. This thin layer is called the "electrical double layer" (EDL) and in this layer is where the ions are "stored" when the electrodes are charged.

The first mathematical models that described the EDL were the Helmholtz and the Gouy-Chapman model [9]. Stern combined both models into one model, naming it the Gouy-Chapman-Stern (GCS) model. However, these models are not very accurate at capturing the physics of the EDL of porous materials. The Helmholtz model assumes that the EDL only contains counter-ions in a flat plane. The GCS model assumes a charge efficiency of one [9], which means that every charged particle in the electrode attracts one counter-ion from the solution. This is clearly not case when looking at Figure 2.5. Figure 2.5 shows that the charge λ is only close to 1 when the salt concentrations are very low.

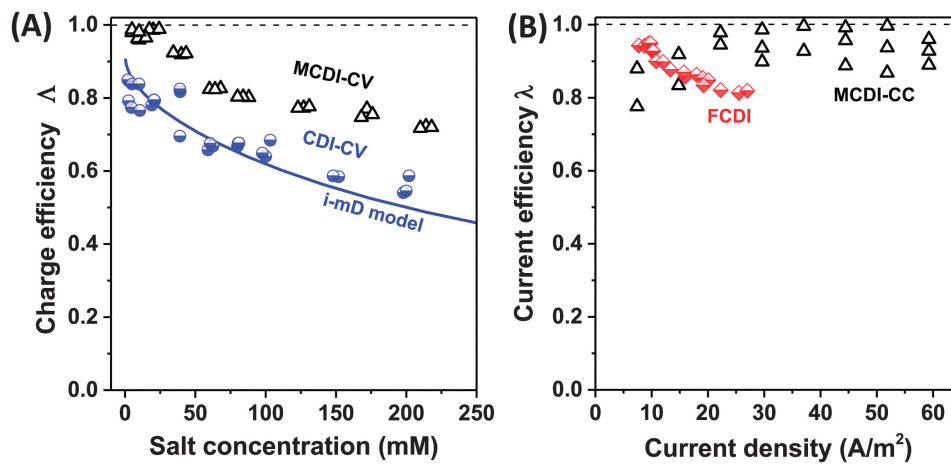


Figure 2.5: Experimental data on the charge and current efficiency for MCDI and FCDI [9]

Porous materials contain micropores, mesopores and macropores. These pore sizes are defined as follows: micropores fall in the sub 2 [nm] range, mesopores between 2 [nm] and 50 [nm], and macropores are larger than 50 [nm]. In the micropores, the EDLs of the pore walls start to overlap. This means that the entire volume of a micropore becomes the EDL, as can be seen in Figure 2.6B. The modified Donnan model (mD) describes the salt adsorption in the micropores more accurately compared to the Helmholtz and GCS models when the pore size are smaller than the thickness of the EDL. The mD model assumes that the ions are stored in the *volume* of the micropore [9].

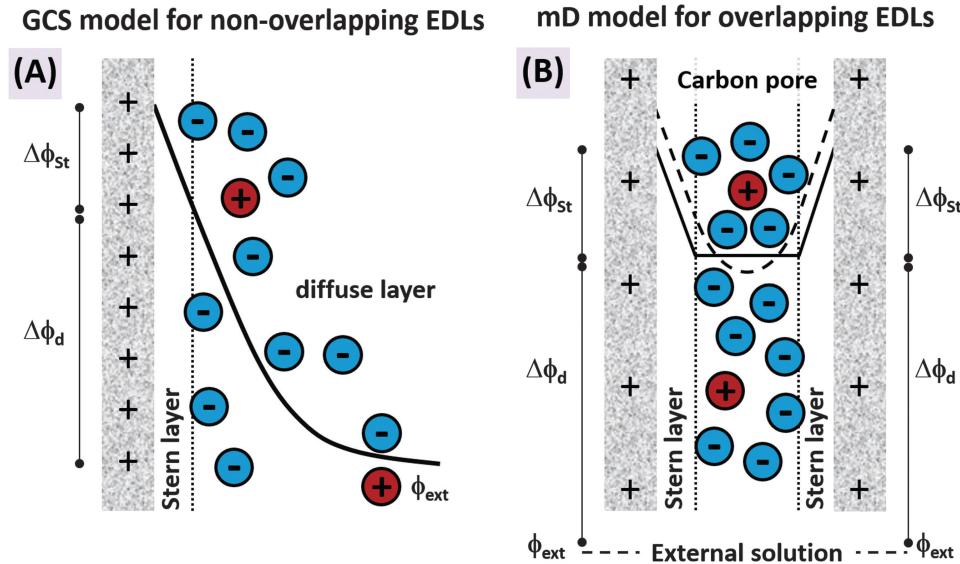


Figure 2.6: Figure A: Gouy-Chapman-Stern model and figure B: modified Donnan model to describe the ion concentration [9]

2.6. Porosity of carbon electrodes

Porada *et al* [7] showed that there is a correlation between the pore size distribution (PSD) of porous carbon electrodes and the deionisation performance of those electrodes. The old belief was that there should be almost no overlap between EDLs inside the pores of carbon material for optimal adsorption of ions in the EDL. The optimal pore size to avoid overlapping EDLs is in the pore size range of mesopores [7]. New research showed that electrodes high in mesopores did not have the highest mSAC. The more porous a carbon material is, the higher the surface area. A high surface area means that more ions can be adsorbed. The downside of highly porous materials though, is the long pathways that the ions have to travel to get adsorbed. Meaning that adsorption times are longer. For a good capacitance and short adsorption time, a combination of micro-, meso- and macropores is most optimal. Porada found that an interparticle porosity of a little over 40 % gave the shortest times for ASAC. Figure 2.7 shows that the adsorption time increases when the interparticle porosity either becomes too small or too high. A small interparticle porosity means that the ion transport pathways are absent, because the electrode packing is too dense. A high interparticle porosity means that the transport pathways are too long, because the electrode packing is too loose.

A more recent study performed by Zhang *et al* [23] found that carbon electrodes with a more compact microstructure had the highest mSAC. In their study carbon aerogels (CA) with different microstructures were prepared by drying them at ambient pressures. Several samples were prepared, and the microstructure was varied by changing the ratio of resorcinol to catalyst (R/C). The CA-200 sample had a R/C ratio of 200, and showed the highest mSAC. A BET analysis on CA-200 showed that the average pore diameter was 2.14 [nm], and it showed that sample CA-200 had the highest micropore specific surface area. Via SEM imaging it was confirmed that the CA-200 sample had the finest microstructure. Their research concluded that the micropores play a vital role in the storage of ions, and that the mesopores provide the transport pathways for the ions to migrate through the microstructure.

The literature discussed in section 2.6 studied the effects of the interparticle porosity of conventional porous carbon electrodes. Here the ions migrate *into* the microstructure of the electrode and are absorbed in the EDL. Porada showed that there is a correlation between the interparticle porosity and the salt adsorption capacity

of electrodes. CMEs are different compared to conventional electrodes however, because the ions have to migrate *through* the microstructure. The interparticle porosity for optimal ion transport through the CMEs is still unknown. It is therefore hypothesised that there should also be a correlation between the PSD and the ion transport through the CMEs of multi-channel CDI. Zhang concluded in their research that the mesopores provided the migration pathways, whereas the micropores were responsible for ion storage. Therefore, it is expected that the mesopores will play an important role in the ion transport through the microstructure of the CMEs.

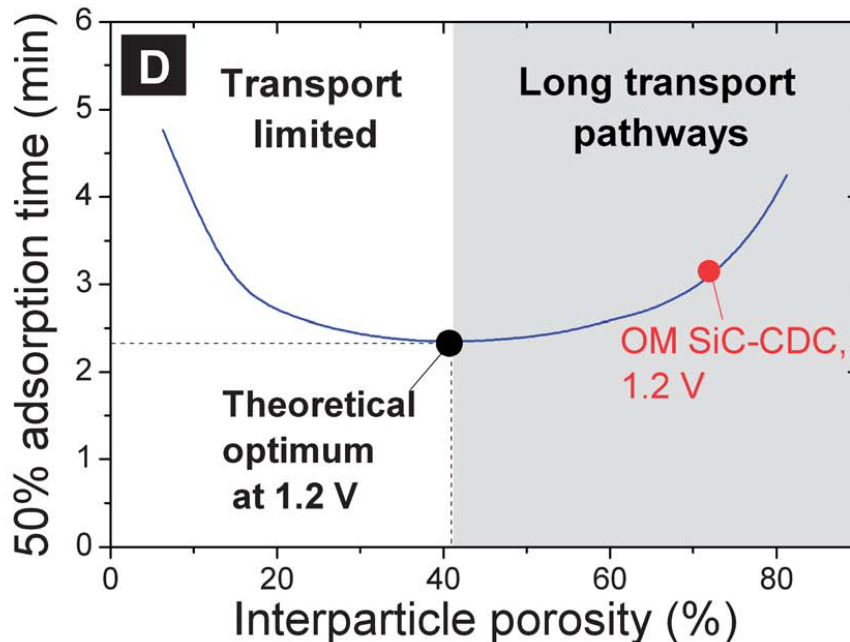


Figure 2.7: The ASAC times vs interparticle porosity [7]. The transport is either limited because of the absence of transport ways (due to tight packing of the material), or due to the pathways being too long (as a result of the packing being too loose).

2.7. Selective ion separation by CDI

Selective ion separation means that a specific ion is removed from the solution. For example, selectively removing Li^+ ions from a solution for lithium recovery. Or, selectively removing Na^+ ions but not Ca^{2+} ions. Selective ion separation is either done to remove or recover a specific chemical element, or to remove ions with a specific valence. Zhang *et al* [8] has performed an extensive state-of-the-art review on selective ion separation by CDI. There are several mechanisms to remove ions from the feed water.

- Ion conductors in the packing between the electrodes. The packing is in the bulk solution. If the packing is made with ion conductors, then this creates pathways and increases the migration rate for the desired ion to be adsorbed.
- The use of ion exchange membranes. IEMs provide pathways through its microstructure for specific ions, but block the competing ions from being adsorbed.
- Pore size sieving by the electrode's microstructure. The microstructure of an electrode can be tuned for specific pore size distributions. The pore size distribution affects the adsorption behaviour of ions, by acting as a pore size sieve. The adsorption rate of larger ions will be lower for smaller pores.
- Chemical bonding at the surface. This is done by functional groups in the electrode material. For example an alcohol group ($-\text{OH}$) forming hydrogen bonds.
- Faradaic electrodes. Selective separation can also be achieved by providing Faradaic reactions, which allow specific chemical reactions to take place with target species that have to be removed.

2.8. Measuring membrane selectivity

The permselectivity of an IEM can be determined experimentally by placing the IEM between two solutions with different salinities (Cha [24]). Suppose an IEM would be perfectly selective for cations. Then the cations would move from the high concentration solution to the low concentration solution, and the anions would be blocked. Due to a mismatch in the number of charged particles in both solutions, a membrane potential will start to build up. This potential is associated with an electric field across the membrane and, thus, an electric force in the opposite direction of the ionic current. This mechanism makes sure that the system reaches a state in which the charge transport across the membrane vanishes. The permselectivity is obtained by measuring the electrochemical potential difference between the two solutions, and compare this potential with the 'ideal' potential that would develop for perfectly selective membranes. Cha's experimental setup makes use of two single-junction electrodes that work as reference electrodes. The single-junction electrodes consisted out of Ag–AgCl electrodes encased in a glass tube filled with a 3M aqueous solution of sodium chloride. In the setup depicted below Figure 2.8, the solutions are constantly thoroughly mixed to achieve a homogeneous solution.

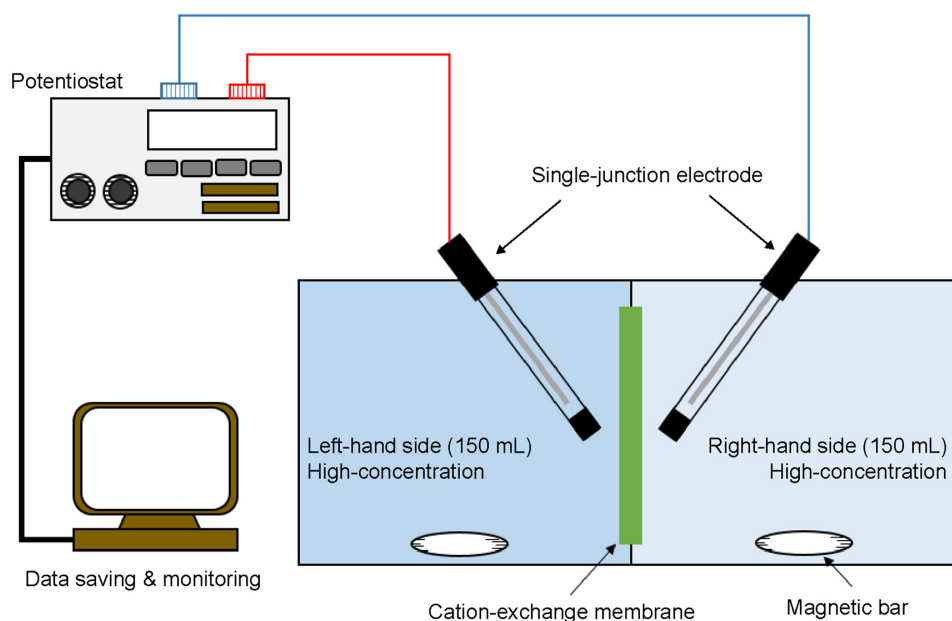


Figure 2.8: Schematic of the experimental setup to measure the electrochemical potential [24]

2.9. Literature discussion

The literature discussed in section 2.6 studied the effects of the interparticle porosity of conventional porous carbon electrodes. Here the ions migrate *into* the microstructure of the electrode and are absorbed in the EDL. Porada showed that there is a correlation between the interparticle porosity and the salt adsorption capacity of electrodes. CMEs are different compared to conventional electrodes however, because the ions have to migrate *through* the microstructure. The interparticle porosity for optimal ion transport through the CMEs is still unknown. It is therefore hypothesised that there should also be a correlation between the PSD and the ion transport through the CMEs of multi-channel CDI. Zhang concluded in their research that the mesopores provided the migration pathways, whereas the micropores were responsible for ion storage. Therefore, it is expected that the mesopores will play an important role in the ion transport through the microstructure of the CMEs.

The selectivity mechanisms discussed in section 2.7 do not explain the selectivity behaviour of CMEs. CMEs are active membranes (their potential changes over time), that only differentiate between positively and negatively charged particles. When the CME is positively charged it provides pathways through the microstructure for anions, and vice versa for cations. Therefore, CMEs function as ion conductors. Up until now no research in CDI literature has been found that investigates the selectivity of electrodes by modelling them as ion conductors. It is expected that CMEs with better transport pathways, become less selective. For example, if a CME allows all cations to pass through, it is likely that some anions will come along as well.

2.10. Diffusivity of ionic species in electrolytes

The diffusivity and migration of ionic species in electrolytes can be described with the so-called Poisson-Nernst-Planck (PNP) equations [25, 26]. These equations help to improve our understanding of the mechanisms that drive the migration of ionic species in electrolytes. In order to derive the PNP equations, one starts with the mass conservation Equation 2.3. The $\frac{\delta c_i}{\delta t}$ term describes the change of ionic concentration with respect to time. The term $u \nabla c_i$ is the convection term, where u denotes the background velocity of the solvent. The $\nabla \cdot J_i$ is the divergence of the ionic flux. Equation 2.3 can be simplified by assuming a steady problem without any convection. Then $\frac{\delta c_i}{\delta t}$ and $u \nabla c_i$ drop from the equation.

$$\frac{\delta c_i}{\delta t} + u \nabla c_i + \nabla \cdot J_i = 0 \quad (2.3)$$

$$J_i = M_i c_i \nabla \mu_i \quad (2.4)$$

$$M_i = \frac{D_i}{k_b T} \quad (2.5)$$

$$\nabla \mu_i = \frac{k_b T}{c_i} \nabla c_i + z_i e \nabla \phi \quad (2.6)$$

J_i is the ionic flux, which is described by Equation 2.4 to 2.6. M_i is known as the mobility of the ionic species i , where D_i is the diffusivity, k_b the Boltzmann constant and T the absolute temperature. The gradient in chemical potential $\nabla \mu_i$ for a dilute solution is described by $k_b T$, the natural logarithm of the concentration of species i , z_i the valence of species i , e the elementary charge and $\nabla \phi$ the gradient in electrostatic potential. Combining Equation 2.4 to 2.6 gives Equation 2.7.

$$J_i = -D_i \left[\nabla c_i + \frac{z_i e c_i}{k_b T} \nabla \phi \right] \quad (2.7)$$

Equation 2.7 relates the flux J_i to the gradient of the concentration of species i and the gradient of the electrostatic potential. Finally, Equation 2.7 can be substituted into Equation 2.3 to arrive at the well-known Nernst-Planck equation.

$$\boxed{\frac{\delta c_i}{\delta t} + u \nabla c_i - \nabla \cdot \left[D_i \left(\nabla c_i + \frac{z_i e c_i}{k_b T} \nabla \phi \right) \right]} = 0 \quad (2.8)$$

The Nernst-Planck equation still has one too many unknowns. This is where the Poisson equation becomes necessary to solve the system. To derive a relationship between the electrostatic potential and the concentration gradient, one starts with the Poisson equation for the free charge density ρ . Here \mathbf{D} is the electric displacement field vector.

$$\rho = \nabla \cdot \mathbf{D} \quad (2.9)$$

The electric displacement field vector is described by the electric permittivity ϵ and the electric field E . The electric field is defined as the negative of the gradient of the applied potential.

$$\mathbf{D} = \epsilon E \quad (2.10)$$

$$E = -\nabla \phi \quad (2.11)$$

Combining Equation 2.9 to 2.11 yields Equation 2.12 for the free charge density.

$$\rho = -\nabla \cdot (\epsilon \nabla \phi) \quad (2.12)$$

Another way of describing the free charge density is by using a mean field approach. Here the electric charges from all the ions per unit volume are summed up.

$$\rho = \sum_i z_i e c_i \quad (2.13)$$

Equation 2.14 is the result when Equation 2.12 and Equation 2.13 are combined. This equation relates the potential ϕ to the ionic concentration c_i .

$$-\nabla \cdot (\epsilon \nabla \phi) = \sum_i z_i e c_i \quad (2.14)$$

Equation 2.8 and Equation 2.14 together form the so-called "Poisson-Nernst-Planck" equations. Together they form a set of n equations and n unknowns.

$$\begin{aligned} \frac{\delta c_i}{\delta t} + u \nabla c_i - \nabla \cdot \left[D_i \left(\nabla c_i + \frac{z_i e c_i}{k_b T} \nabla \phi \right) \right] &= 0 \\ -\nabla \cdot (\epsilon \nabla \phi) &= \sum_i z_i e c_i \end{aligned} \quad (2.15)$$

The electric permittivity is usually constant, in which case the Poisson equation simplifies to:

$$-\epsilon \nabla^2 \phi = \sum_i z_i e c_i \quad (2.16)$$

Simplifying the PNP-equations

The PNP-equation can be simplified by stating that the system:

1. is steady-state: this means that any term w.r.t. time $\frac{\delta}{\delta t} = 0$
2. has no convection: $u \nabla c_i$ is the convection term and drops out of the equation
3. is a 1D problem: any nabla term reduces to $\frac{d}{dx}$

Then the PNP-equations simplify to:

$$\begin{aligned} \frac{d}{dx} \left[D_i \left(\frac{dc_i}{dx} + \frac{z_i e c_i}{k_b T} \frac{d\phi}{dx} \right) \right] &= 0 \\ \frac{d^2 \phi}{dx^2} &= \frac{-1}{\epsilon} \sum_i z_i e c_i \end{aligned} \quad (2.17)$$

Equations 2.17 are a set of two nonlinear PDEs, where the Nernst-Planck equation is 1st order, and the Poisson equation 2nd order. Solving these equations analytically is challenging, and only possible by further simplifying the problem. This is beyond the scope of this thesis, as the thesis will focus on experimental work. If the reader is interested in solutions to the PNP-equations, plenty of articles have been written about solving the PNP-equations, such as [27–30]. The resulting set of Equations 2.17 do answer the question, "What is the physical mechanism that drives the migration of ionic species in electrolytes?". It shows that the migration of ionic species is driven by the concentration gradient $\frac{dc_i}{dx}$ and the gradient in electrostatic potential $\frac{d\phi}{dx}$.

2.11. Derivation of permselectivity equation

As was mentioned in section 2.3, it is not fully known which variables (and in what magnitude) affect the ion selectivity of the inner electrodes, the CMEs. First, a definition for the selectivity is needed. In literature, the selectivity of ion exchange membranes (IEMs) is described by the ion transport number. According to Micari *et al* (2022) [31]: "The permselectivity can be defined as a function of the transport number of ions through

the membrane" (p132). The transport number of species i is the fraction of the total number of ionic species carried by species i through the membrane [31]. The selectivity can also be written in flux terms [32]: the selectivity can be defined as the ratio of the flux of species i over the total flux of species i and j combined, that are migrating through the membrane. In equation form, it looks as follows:

$$S_i = \frac{J_i}{J_i + J_j}$$

$$S_j = \frac{J_j}{J_i + J_j}$$

Combining both equations by subtraction yields the selectivity equation for IEMs:

$$S = \frac{J_i - J_j}{J_i + J_j} \quad (2.18)$$

Permselectivity of CMEs In Equation 2.18, the selectivity $S = 0$ (not selective at all) when $J_i = J_j$, and $S = 1$ (perfectly selective) when $J_j = 0$. During an experiment J_+ and J_- are not easily measurable quantities. Therefore, the permselectivity will be rewritten in more familiar terms. Below, the general equation for the chemical potential is given:

$$\mu_i = \mu_i^0 + k_b T \ln C_i + z_i e \phi \quad (2.19)$$

Where:

- μ_i^0 is the chemical potential in standard conditions
- k_b is the Boltzmann constant
- T is the temperature in Kelvin
- C_i is the concentration of species i in the bulk
- z_i is the valence of species i
- e is the elementary charge
- ϕ is the electrostatic potential

For a system in equilibrium, with a higher chemical potential region (H), and a lower chemical potential region (L):

$$k_b T \ln C_i^L + z_i e \phi^L = k_b T \ln C_i^H + z_i e \phi^H \quad (2.20)$$

The difference in chemical potential for both mono-valent cations and anions, between regions H and L:

$$\Delta\mu_+ = k_b T \ln \frac{C_+^H}{C_+^L} + e(\phi^H - \phi^L)$$

$$\Delta\mu_- = k_b T \ln \frac{C_-^H}{C_-^L} - e(\phi^H - \phi^L) \quad (2.21)$$

In Equation 2.21, $(\phi^H - \phi^L)$ denotes the membrane potential V_m . Combining Equation 2.4 and 2.5 to get an equation for ion fluxes for both positive and negative species. Here, the membrane thickness d is added to the equation. Because the selectivity is taking place in the membrane space, not in the bulk.

$$J_+ = \frac{D_+}{k_b T d} c_+ \Delta\mu_+$$

$$J_- = \frac{D_-}{k_b T d} c_- \Delta\mu_- \quad (2.22)$$

The process in the cell described in chapter 4 is of the *non-driven* kind, meaning that ions naturally migrate from high salinity to low salinity through the CME. Therefore, no desalination is taking place in this cell. Here, the selectivity describes a membrane property instead of a cell property, namely the preferential permeation of specific ionic species, i.e. permselectivity. The permselectivity is dependent on the *charge* on the CME in the cell described in chapter 4. For a non-driven system it can be stated that: $J_+ = J_-$. By imposing $J_+ = J_-$, no imbalance can occur between cations and anions in the bulk of the fluid, as ions are migrating from high salinity to low salinity. Substituting Equation 2.21 and 2.22 into $J_+ = J_-$, k_b , T , and d drop out from the flux equations. Also the ratio C_+^H/C_+^L should equal ratio C_-^H/C_-^L , as there cannot be an imbalance of cations and anions in the bulk. Then, the following result is obtained:

$$D_+c_+ \left[k_b T \ln \frac{C_+^H}{C_+^L} + e(\phi^H - \phi^L) \right] = D_-c_- \left[k_b T \ln \frac{C_-^H}{C_-^L} - e(\phi^H - \phi^L) \right] \quad (2.23)$$

Recollecting terms:

$$(D_+c_+ - D_-c_-) \cdot k_b T \ln \frac{C_+^H}{C_+^L} = -(D_+c_+ + D_-c_-) \cdot e(\phi^H - \phi^L) \quad (2.24)$$

Rewriting gives the following result for the permselectivity P :

$$P = \frac{D_+c_+ - D_-c_-}{D_+c_+ + D_-c_-} = -\frac{e(\phi^H - \phi^L)}{k_b T \ln \frac{C_+^H}{C_+^L}} \quad (2.25)$$

Equation 2.25 is the final result that relates the permselectivity P to the membrane potential $(\phi^H - \phi^L)$. It should be clearly stated that Equation 2.25 is valid for non-driven systems, where $J_+ = J_-$. Here, c_+ and c_- are the concentrations inside the membrane, induced by a potential on the CME. The following quantities are treated as 'constants' in a non-driven system:

- e : elementary charge
- k_b : Boltzmann constant
- T : temperature, assumed to be constant throughout a measurement
- C^H/C^L ratio of concentrations, assumed to be constant throughout a measurement

If the concentration ratio $C_H/C_L = 1.00 [\text{g l}^{-1}] / 0.25 [\text{g l}^{-1}] = 4$, and the temperature is 293 [K], then for a perfect permselectivity of $S = 1$, the maximum theoretical membrane potential in an isolated, non-driven system would be 35.6 [mV].

Selectivity in a multi-channel system The selectivity Equation 2.18 for IEMs was derived earlier in this section, this equation however does not apply to the *driven* multi-channel CDI cell depicted in Figure 2.9. The deionisation process aims to migrate ions from low to high salinity. Figure 2.9 shows a snapshot, where the cations will want to move from the inner channel to the outer channel, driven by the electrostatic potential from the outermost electrodes. The anions want to move from the outer channel to the inner channel, due to the concentration gradient and the electrostatic potential. In this snapshot, it is the task of the CME to prevent the migration of anions. If the CME would be perfectly selective there would be no flux of anions (J_-) and optimal flux of cations (J_+). If the CME was not selective at all, then the deionisation process would not be very effective. In this situation selectivity is not the most accurate term, rather it should be seen as a "charge efficiency". The selectivity here describes the effectiveness of the deionisation process. Or, for a given amount of current going through the cell, what is the net flux of ions migrating from the inner channel to the outer channel?

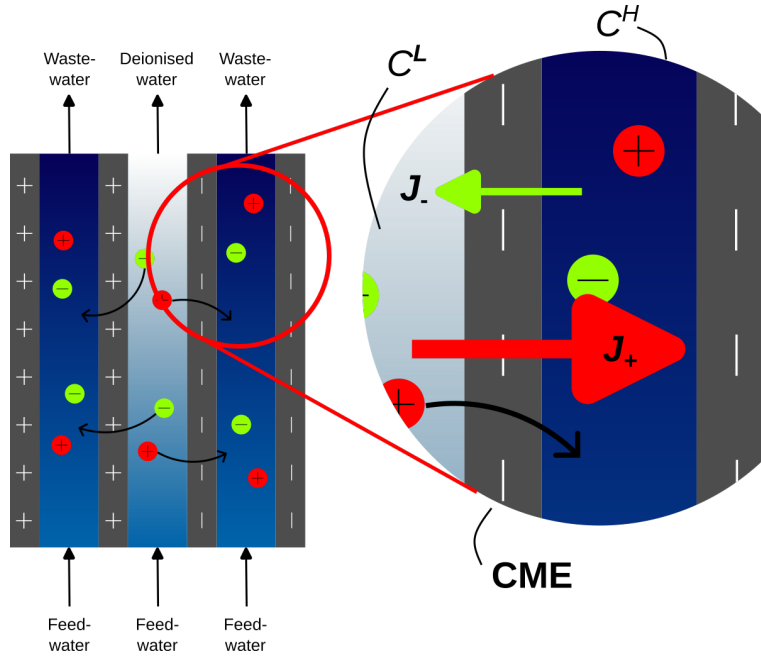


Figure 2.9: This figure shows a snapshot of the multi-channel cell described in section 2.3. If the CME would be perfectly selective there would be no J_- flux and optimal J_+ flux. Here, the selectivity describes the effectiveness of the deionisation process.

An important detail to note is the fact that J_+ and J_- have opposing directions in Figure 2.9. Equation 2.18 describes the selectivity for a system of an IEM, where both cation and anions migrate in the same direction, from high salinity to low salinity. Therefore, Equation 2.18 is rewritten by inverting the sign in front of the J_- term, which gives Equation 2.26:

$$S = \frac{J_+ + J_-}{J_+ - J_-} \quad (2.26)$$

Equation 2.26 seems to have a singularity when $J_+ = J_-$, then the selectivity would go to infinity. As stated earlier, the selectivity can be thought of as a charge efficiency. $J_+ = J_-$ would occur when no current is going through the system. If ions are moving without any current driving the system, then that would imply infinite selectivity. To derive an equation for the cell selectivity: one starts by substituting Equation 2.21 and 2.22 into Equation 2.26, k_b , T , and d drop out from the flux equations. Also the ratio C_+^H/C_+^L should equal ratio C_-^H/C_-^L , as there cannot be an imbalance of cations and anions in the bulk. Therefore, the plus and minus subscripts can be dropped from C^H and C^L .

$$S = \frac{D_+c_+ \left[k_b T \ln \frac{C^H}{C^L} + e(\phi^H - \phi^L) \right] + D_-c_- \left[k_b T \ln \frac{C^H}{C^L} - e(\phi^H - \phi^L) \right]}{D_+c_+ \left[k_b T \ln \frac{C^H}{C^L} + e(\phi^H - \phi^L) \right] - D_-c_- \left[k_b T \ln \frac{C^H}{C^L} - e(\phi^H - \phi^L) \right]} \quad (2.27)$$

Rewriting by collecting D^+ , c^+ , D^- , c^- terms:

$$S = \frac{k_b T \ln \frac{C^H}{C^L} [D_+c_+ + D_-c_-] + e(\phi^H - \phi^L) [D_+c_+ - D_-c_-]}{k_b T \ln \frac{C^H}{C^L} [D_+c_+ - D_-c_-] + e(\phi^H - \phi^L) [D_+c_+ + D_-c_-]} \quad (2.28)$$

Equation 2.28 has quite a few unknowns, such as c_+ and c_- . It is difficult to say what the concentrations are inside the membrane. Therefore, the permselectivity Equation 2.25 is used and rewritten:

$$P = \frac{D_+c_+ - D_-c_-}{D_+c_+ + D_-c_-}$$

$$D_-c_- = D_+c_+ \left(\frac{1-P}{1+P} \right) \quad (2.29)$$

Substituting Equation 2.29 into Equation 2.28 gives:

$$S = \frac{k_b T \ln \frac{C^H}{C^L} \left[D_+c_+ + D_+c_+ \left(\frac{1-P}{1+P} \right) \right] + e(\phi^H - \phi^L) \left[D_+c_+ - D_+c_+ \left(\frac{1-P}{1+P} \right) \right]}{k_b T \ln \frac{C^H}{C^L} \left[D_+c_+ - D_+c_+ \left(\frac{1-P}{1+P} \right) \right] + e(\phi^H - \phi^L) \left[D_+c_+ + D_+c_+ \left(\frac{1-P}{1+P} \right) \right]}$$

D_+c_+ can now be dropped from the equation:

$$S = \frac{k_b T \ln \frac{C^H}{C^L} \left[1 + \left(\frac{1-P}{1+P} \right) \right] + e(\phi^H - \phi^L) \left[1 - \left(\frac{1-P}{1+P} \right) \right]}{k_b T \ln \frac{C^H}{C^L} \left[1 - \left(\frac{1-P}{1+P} \right) \right] + e(\phi^H - \phi^L) \left[1 + \left(\frac{1-P}{1+P} \right) \right]}$$

Which can be simplified to:

$$S = \frac{k_b T \ln \frac{C^H}{C^L} \left[\frac{2}{P+1} \right] + e(\phi^H - \phi^L) \left[\frac{2P}{P+1} \right]}{k_b T \ln \frac{C^H}{C^L} \left[\frac{2P}{P+1} \right] + e(\phi^H - \phi^L) \left[\frac{2}{P+1} \right]}$$

Which can be simplified to:

$$S = \frac{k_b T \ln \frac{C^H}{C^L} + e(\phi^H - \phi^L)(P)}{k_b T \ln \frac{C^H}{C^L}(P) + e(\phi^H - \phi^L)} \quad (2.30)$$

Equation 2.30 is an interesting result as it relates the selectivity of a CDI cell to the permselectivity of its CME. This is the final result that relates the selectivity S to the membrane potential $(\phi^H - \phi^L)$ and the following 'constants':

- e : elementary charge
- k_b : Boltzmann constant
- T : temperature, assumed to be constant throughout a measurement
- C^H/C^L ratio of concentrations, assumed to be constant throughout a measurement

It should be clearly stated that Equation 2.30 is valid for driven multi-channel systems, where the selectivity is defined as: $S = (J_+ + J_-)/(J_+ - J_-)$. It can be said for the following limit case: that when a system is strongly driven by a potential $(\phi^H - \phi^L)$, and the concentration ratio (C^H/C^L) can be neglected w.r.t. to that potential, that $S \approx P$.

3

Methodology

After the theoretical framework has been finished the methodology can be worked out. The methodology explains the experimental approach of the thesis. Section 3.1 gives an overview of the project approach. Section 3.2 explains how the selectivity measurements are performed. Followed by section 3.3 that sheds light on the pore size measurements. Finally, section 3.4 discusses how SEM imaging is performed.

3.1. Thesis approach

This thesis has an experimental approach with 3 parts. The first part is the experimental setup. This part covers the selectivity measurements, pore size measurements, and SEM imaging. The second part is where the data processing takes place. Here, the data is documented, analysed, and correlations are found. The third part covers the discussion and reflection of the results and the recommendations for further research. All three parts are broken down into different objectives below.

3.1.1. Experimental setup

- Perform lab experiments to measure the ion selectivity of the CME. The ion selectivity of the CME causes either cations or anions to move more easily through the membrane. The selectivity of the CME is determined by measuring the membrane potential. Therefore, a measuring setup with a cell is needed.
- Identify which variables during the selectivity measurements have an effect on the membrane selectivity.
- Perform measurements with these variables and quantify their effect on the selectivity.
- Develop a methodology to quantify the pore size distribution and micro-structure of the CMEs. The Process & Energy Department of Mechanical Engineering has access to a Porolux Revo porometer. This device will directly give a pore size distribution.
- To verify the results from the porometer, scanning electron microscopy (SEM) images will be taken. SEM imaging allows to see the material at a large magnification, such that individual pores become visible.

3.1.2. Data processing

- Separate the different signals in the data, filter the data, and perform calculations with the data.
- Reflect on the data, whether the data is usable or that the data should be discarded.

3.1.3. Discussion of the results and recommendations for further research

- Compare the results from the selectivity measurements, pore size measurements, and SEM imaging. Reflect on the findings and answer the main research question.
- Give recommendations for further research.
- Collect everything in this report and give an oral presentation.

3.2. Selectivity measurements

The permselectivity of a CME can be determined by measuring the membrane potential (V_m) of a CME. The membrane potential is measured by placing the membrane in an aqueous environment with different salinities on either side. The membrane potential is sensed by two probes close to the membrane on either side. These probes are made out of tubing and pipette tips containing salt water from the cell. The probes carry an ionic signal that is later on transduced in an electrical signal by two Ag-AgCl reference electrodes. To be able to measure the reference potential between the two Ag-AgCl electrodes, a bridge was added with two 3-way switches. To meet all these requirements a measuring setup with a cell was built. A first raw sketch of the cell is depicted below in Figure 3.1.

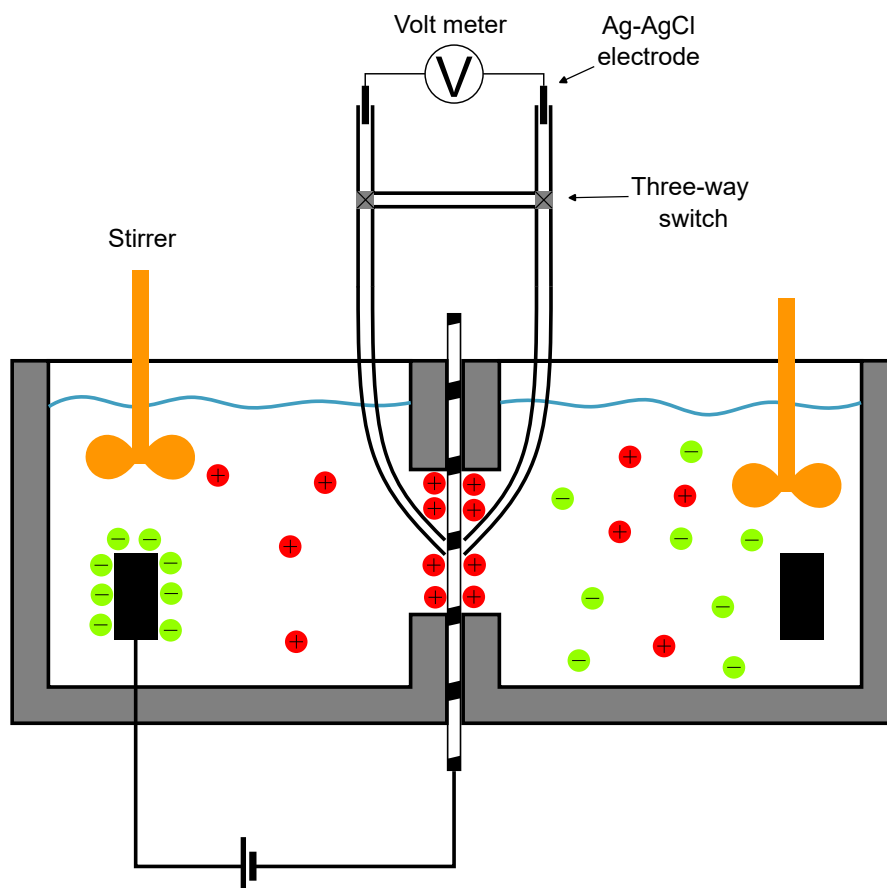


Figure 3.1: Raw sketch of the side-view of the cell. The cell has two compartments with the CME in between. With probes close to the membrane. The CME is charged w.r.t. one counter electrode.

3.2.1. Measuring setup overview

Figure 3.2 gives a visual overview of the entire selectivity measurement setup. The "relay board/Arduino" controls how the power supply and source measuring unit SMU are connected with the cell. Figure 3.2 only gives a simplified logic diagram of the "relay board/Arduino" combo. A much more detailed wiring scheme for the relay board is given in subsection 3.2.3. The relay board has been set up in such a way that the cell can be charged in different phases. These phases will be discussed in subsection 3.2.3. Furthermore, the relay board also controls which signal is being measured by the SMU. The first signal is the membrane potential V_m , which is defined as the potential measured across the membrane between points 1 and 3 in Figure 3.2. The second signal, V_{CME} , is defined as the CME potential measured w.r.t. to one of the reference electrodes. V_{CME} is measured between points 2 and 3. Figure 3.3 shows how the schematic overview from Figure 3.2 translates to an actual setup in a lab environment.

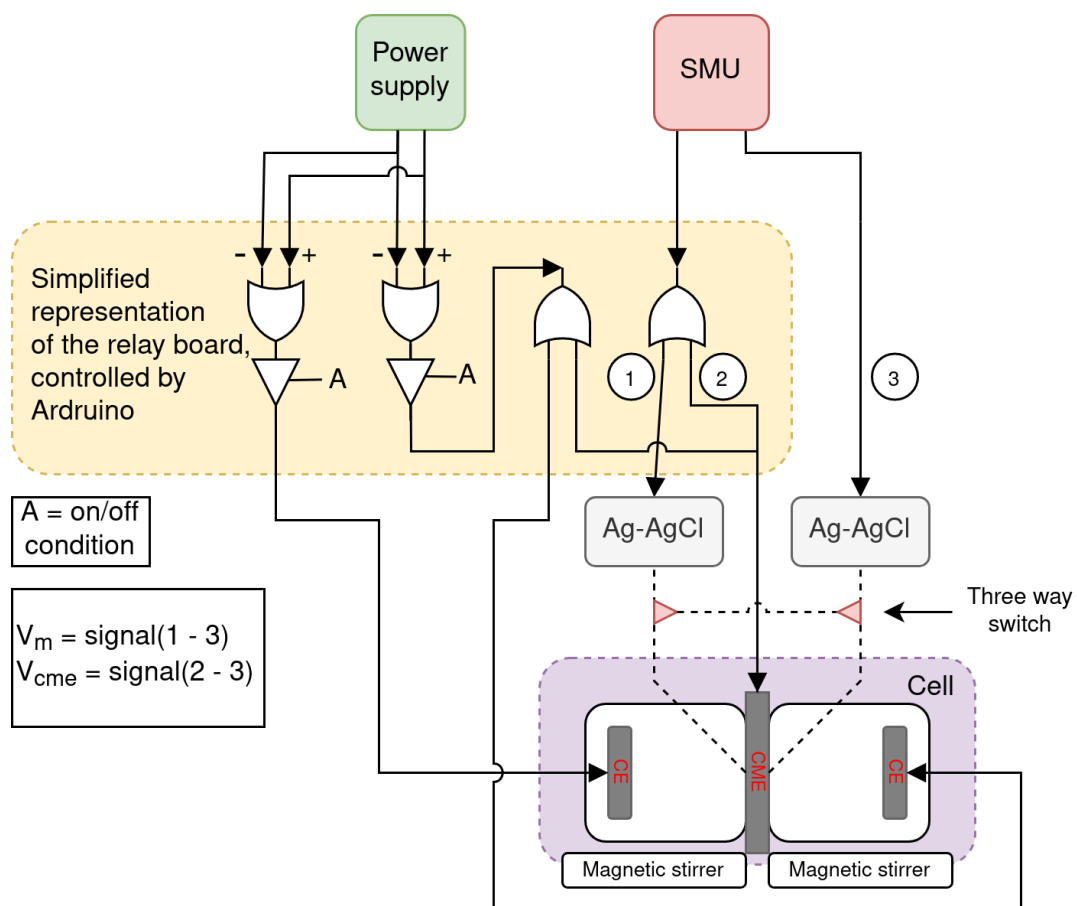


Figure 3.2: Schematic overview of the selectivity measurements setup

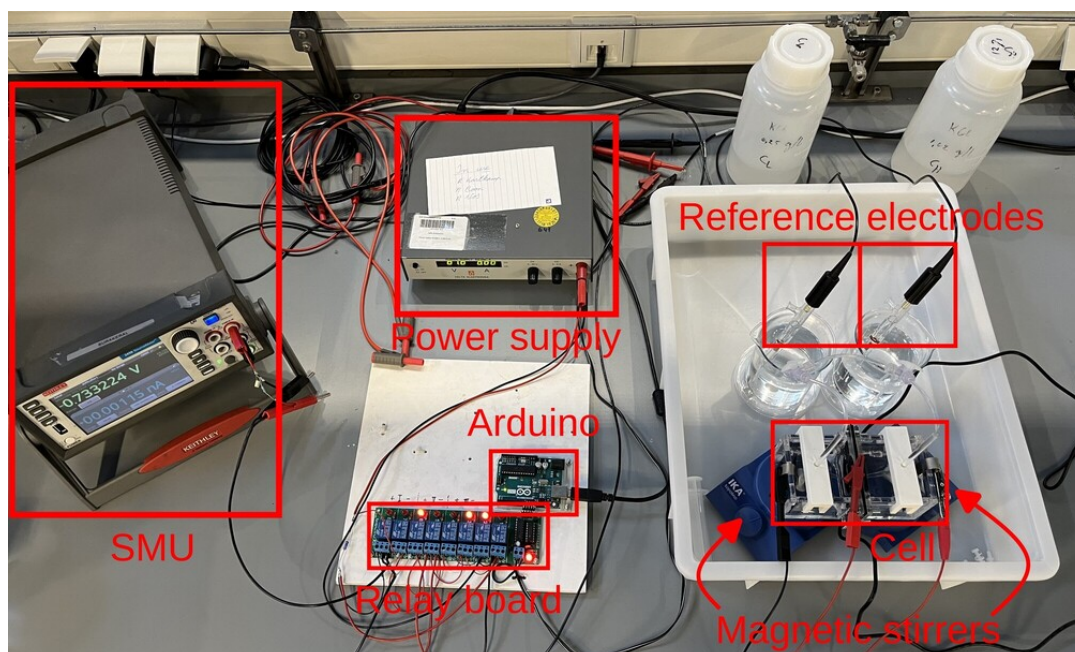


Figure 3.3: The measuring setup in the lab

3.2.2. Measuring equipment

The selectivity measurements require quite a bit of equipment before any measurements can be done. Below a list is given of the most important components.

- **Keithley 2450 SMU:** A source measuring unit (SMU) such as a Keithley 2450, has a remarkably high input resistance. To validate the use of such equipment, first an estimation is made of the resistance in the cell circuitry. The probes in the experimental setup that measure the membrane potential, are made of tubing that contains salt water from the cell. These tubes work similarly to traditional metal wiring, carrying the signal from the membrane to the Ag-AgCl reference electrodes. To get an order of magnitude of the resistance in the cell circuit, consider the resistance of a wire, see Equation 3.1. Here, ρ_{wire} denotes the specific resistance, l_{wire} the length of the wire, and A_{wire} the cross-sectional area of the wire.

$$R_{wire} = \rho_{wire} \cdot \frac{l_{wire}}{A_{wire}} \quad (3.1)$$

In the case of the tubing, ρ_{wire} is determined by the conductivity of salt water at specific concentrations. The cross-sectional area is determined by the inner diameter of the tubing. Tong *et al* [33] describe the relationship between varying KCl-concentrations and the conductivity of the solution. From their data, it was estimated that at a KCl concentration of $0.25 \text{ [g l}^{-1}\text{]}$, the conductivity was equal to $0.434 \text{ [mS cm}^{-1}\text{]}$. The specific resistance is the inverse of the conductivity, which equals $2.303 \text{ [k}\Omega \text{ cm]}$. The inner cross-sectional area of tubing with a diameter of 1.5 [mm] equals $1.767 \times 10^{-2} \text{ [cm}^2\text{]}$. Using Equation 3.1 to calculate the resistance R_{wire} for tubing that is 50 [cm] long, yields a resistance of $6.52 \times 10^6 \Omega$. This is in the order of mega ohms, validating the choice to use a Keithley 2450 SMU with an input resistance of $>10 \text{ [G}\Omega\text{]}$ [34].

- **Ag-AgCl reference electrodes:** General purpose silver-silverchloride (3M KCl) reference electrodes from Sigma-Aldrich were used [35]. Ag-AgCl reference electrodes are extensively used in chemistry and biology research. The advantage of using Ag-AgCl reference electrodes is that they provide a very stable redox reaction between the silver wire and the solution in the reference electrodes. In this measurement setup they function as a transducer, where an ionic signal is converted to an electrical signal.
- **Power Supply:** In order to charge the cell a power supply is necessary, capable of delivering a few volts at near zero amps. Therefore, an "ES 030-5" power supply from Delta Elektronika was used.
- **Arduino.** An "Arduino uno" was used to control the relay board, by turning each relay independently on or off. An Arduino is a microcontroller made from a single circuit board. It has a main chip that can be programmed through the Arduino IDE software. Appendix A shows the Arduino code that was programmed on the board.
- **Relay board:** The relay board consists out of 8 relays, that can be independently turned on or off by the Arduino board. A wiring scheme that shows how the relay board is connected in the measurement setup is given in Figure 3.5. The relay board allows to measure 2 different potentials (described in Figure 3.2) with one SMU. Furthermore, the "relay board/Arduino" combination allows to charge/discharge the cell positively/negatively in any particular length and order. Subsection 3.2.3 describes in detail how the cell is charged and discharged.
- **Mixing tables:** Magnetic stirrers were placed under the cell to continuously mix the solutions. It was assumed at first that stirring the mixture would be beneficial for the selectivity measurements, ensuring that the bulk fluid is properly mixed. The magnetic stirrers were provided by the lab.
- **The cell.** The cell itself had to be designed and built up from scratch. No on-the-shelf components (except for nuts and bolts) were used. Chapter 4 describes in detail how the cell was designed and built.

3.2.3. Measuring procedure

The setup has several signals running from the cell to the SMU. Also, the cell is connected to the power supply to be able to charge the cell (CME), both positively and negatively. How these tasks are performed and in which order is explained in this subsection.

Time scheme of each measurement Each measurement is divided into two cycles, and each cycle is divided into multiple phases. Figure 3.4 gives a clear overview of how these phases are ordered and how

long they take. Below a numerated list is given with a brief description for each phase. The Arduino and relay board together control all the phases. The code on the Arduino board can be found in Appendix A.2.

1. During a charge phase of 1200 [s] the cell is charged by the power supply, at a nominal voltage of 1 [V]. In the cell, the CME is charged w.r.t. to one of the counter electrodes.
2. After the charge phase the membrane resistance across the thickness is measured for 20 [s]. The resistance is measured by recording the membrane potential as an electrical current passes through. A more detailed description is given below in paragraph "Measuring membrane resistance".
3. The next phase is the floating phase of 1800 [s]. In this phase, the CME will slowly lose its charge, which is beneficial, as it allows the membrane potential to be measured as a function of the CME's potential w.r.t. the reference electrode. However, as it turns out, the self-discharging of the CME is rather slow. That is why the cell is short-circuited, in order to get a complete picture of the discharge curve of the CME. During the floating phase, the cell is short-circuited for short intervals of 20 [s], which occur for n-number of times during 1800 [s]. These short-circuit intervals help to discharge the CME. Section 5.2.2 gives a more detailed explanation on why this is beneficial.
4. After the floating phase the membrane resistance is measured again.
5. Before the next cycle starts, first the cell is short-circuited for 600 [s] to make sure that it is completely discharged. Then the next cycle can start from a clean slate.

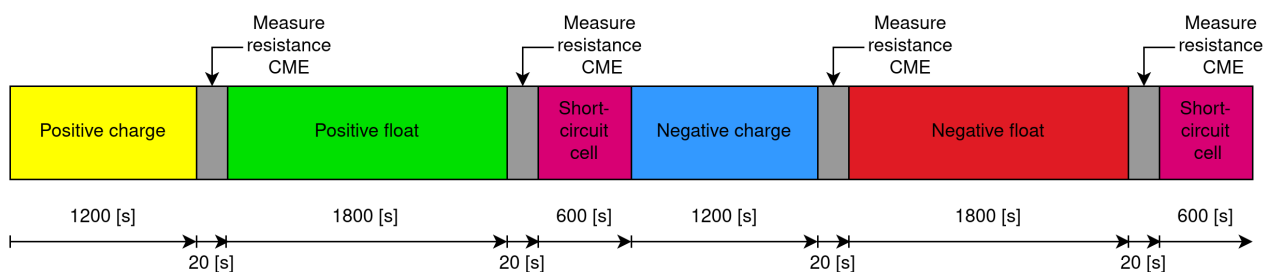


Figure 3.4: Progression of measurement phases over time during an experiment

Measuring potentials During the charging and floating phase, either the membrane potential (V_m) or the electrical potential of the CME (V_{CME}) (w.r.t to one of the reference electrodes) is measured. These measurements take 10 [s] each and are continuously alternating, as the SMU cannot measure two potentials simultaneously. This meant that the data of two potentials was in one data stream, which complicated the data processing, but this was not insurmountable. Measuring either V_m or V_{CME} is also controlled by the Arduino and relay board. Adding a second SMU could also solve the issue of measuring two potentials at the same time, but since these devices are not cheap, that would have been quite a hefty financial investment.

Measuring membrane resistance Besides measuring V_m and V_{CME} , also the electrical resistance across the thickness of the membrane is measured. The reason being that the electrical resistance across the thickness originates from the ionic resistance of the membrane. The idea is that ions are charged particles and show similar behaviour to electrons when transferring energy and carrying signals. The resistance was measured by adding an extra counter electrode to the cell, such that each compartment has one. For a 20 [s] time period a potential was applied on these counter electrodes. This means that a small (in the order of <1 [mA]) current was going through the CME. While a current was going through the CME, the membrane potential was recorded. This potential was compared to the membrane potential without a current going through the CME. The difference between these two potentials is the actual resultant potential from the current going through the CME.

Knowing the membrane potential of and the current through the CME, the resistance can be calculated through Ohm's law. The current through the CME could not be measured directly, which meant that a resistor was added to the positive line from the power supply. This resistor had a small resistance of 10 [Ω]. By measuring the potential drop over the resistor, and knowing its resistance, the current could be calculated. This current is equivalent to the current through the CME. This meant that in this setup, the SMU had to measure 3 potentials in total, although not all three simultaneously for the entire length of the experiment.

Wiring scheme relay board In Figure 3.5 a detailed wiring diagram is given how the relay board is connected in the measuring setup. Below a list of input and output signals and currents is given.

Input signals and currents:

- Positive pole power supply
- Negative pole power supply
- Positive lead SMU
- Negative lead SMU

Output signals and currents:

- Charge current counter electrode 1
- Charge current CME
- Charge current counter electrode 2
- Signal from the CME
- Signal from reference electrode 1
- Signal from reference electrode 2
- Signal from the positive pole of the resistor
- Signal from the negative pole of the resistor

Relay numbers 1,2,3, and 4 control how the cell is charged, floated, or short-circuited. The membrane resistance measurements are controlled by relay number 5. Relay numbers 6,7, and 8 control which signal is measured by the SMU. The table in Figure 3.5 gives a clear overview which relays must be turned on, or off for a specific setting.

Mixing salt with water The salt solutions used to perform measurements were made in the following way: demineralised water was taken and mixed with a predetermined amount of potassium chloride (KCl). This was done by mass measurement. A specific amount of salt was weighed in an empty container. After this step approximately 998.18 [g] of water was added. Water has a density of 998.18 [g L⁻¹] at 20 [°C] [36]. The temperature was not recorded, but it was assumed to be around 20 [°C]. With the water density and the added mass of salt and water, the concentration in [g L⁻¹] can be calculated. For completeness, the molar concentrations were calculated with the molar mass of KCl, $M_{\text{KCl}} = 74.55$ [mol L⁻¹].

Table 3.1: The standard high and low concentrations of KCl in water. Used in all experiments, except for the experiments in subsection 5.2.1.

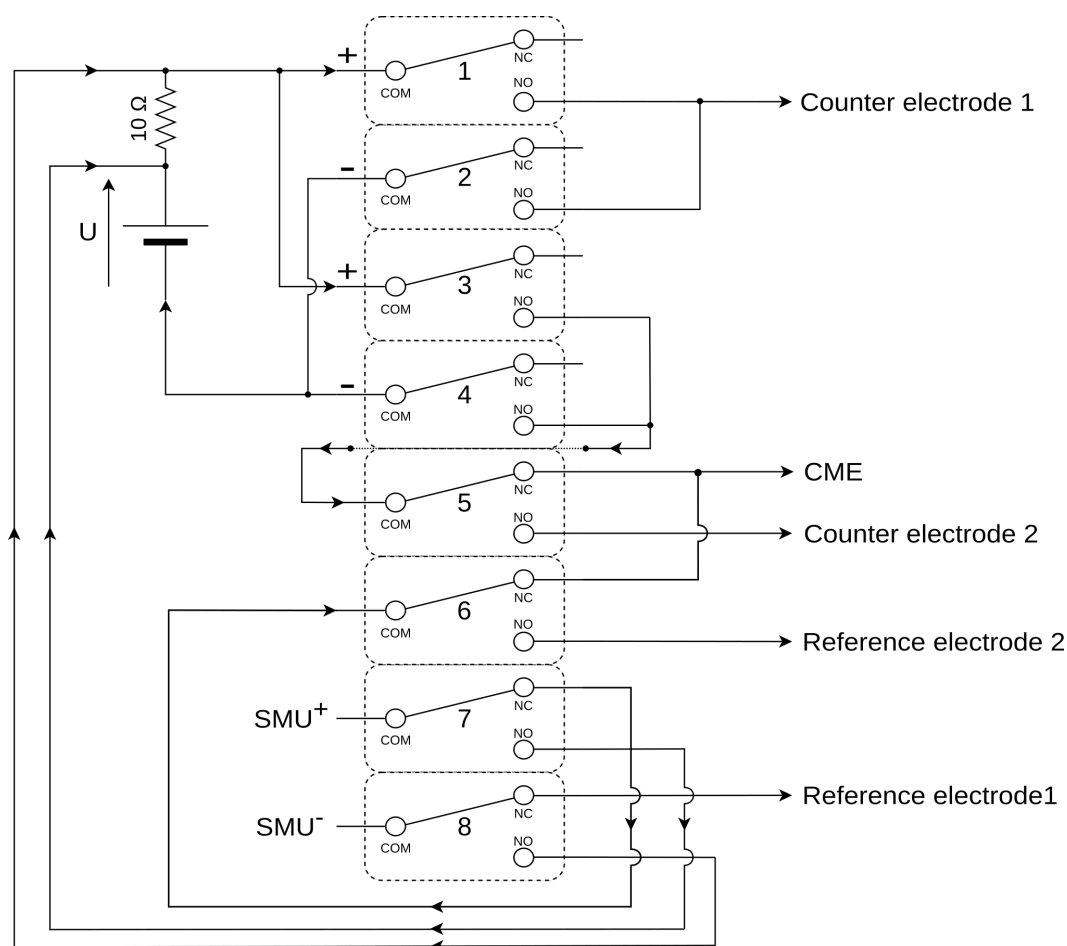
	Mass ratios [g/g]	Concentration in [g L ⁻¹]	Molar concentration [mol L ⁻¹]
C_L	0.25/998.18	0.25	3.353×10^{-3}
C_H	1.00/998.18	1.00	1.341×10^{-2}

3.2.4. Membrane materials

The CMEs that were studied in this thesis are all research samples that were used to study various ratios of graphite, carbon black and binder. These samples were made prior to September 4th, 2023. The solid components are carbon black for the capacitance of the CME, graphite for the electrical conductance of the CME, and PVDF as a binder to hold it all together. Of course, there is also a solvent present when making these CMEs, but it evaporates off. Below in Table 3.2 an overview is given of the composition, as well as the thickness of the materials. It should be noted that although material 04/21 is made with the same ratios, a coarser graphite was used. The gradient material was also made with similar ratios, but as the name suggests, the membrane was made with a gradually changing thickness. The thickest part was 25 microns and the thinnest part was 5 microns. During testing, it was found that at 5 microns the membrane lost its structural integrity, which meant that large holes nullified the permselectivity. Therefore, only the thickest part at 25 microns of the gradient material was used.

Table 3.2: Composition of membrane materials

Material	Carbon black [wt%]	Graphite [wt%]	PVDF [wt%]	Thickness [μm]
04/21	4.61	50.40	44.99	65
06/01#1	4.61	50.40	44.99	75
06/01#2	6.17	33.66	60.17	45
Gradient	6.17	33.66	60.17	25
09/04	12.22	16.29	71.49	20



	Relay 1	Relay 2	Relay 3	Relay 4	Relay 5	Relay 6	Relay 7	Relay 8
Positive charge CME	O	I	I	O	O	-	-	-
Positive float CME	O	I	O	O	O	-	-	-
Negative charge CME	I	O	O	I	O	-	-	-
Negative float CME	O	O	O	I	O	-	-	-
Positive charge CE s	O	I	I	O	I	-	-	-
Negative charge CE s	I	O	O	I	I	-	-	-
Short circuit cell	O	I	O	I	O	-	-	-
Measure CME vs RE1	-	-	-	-	-	O	O	O
Measure RE2 vs RE1	-	-	-	-	-	I	O	O
Measure V_{res}	-	-	-	-	-	O	I	I

Legend:	
Must be turned on	I
Must be turned off	O
May be turned on/off	-

Figure 3.5: Wiring schematic of the relay board

3.2.5. Problem solving

As explained in section 2.11, the membrane potential is theoretically limited to 35.6 [mV] for perfectly selective membranes, when standard concentrations are considered. However, during some of the earlier measurements, improbably high membrane potentials were observed, in the order of 30 [mV]. Then the measurements would indicate near perfect selectivity. Also, sometimes the values for the membrane potential showed many fluctuations, causing the data to be hard to interpret. The following possible causes were investigated:

- Interference from the ether being picked up by non-shielded cables. This was solved by using shielded cables wherever possible. The noise in the signal did go down after making the change. When trying to measure a signal in the order of [mV], shielded cables should be used to prevent noise in the signal. The noise itself was causing voltage fluctuations in order multiple [mV].
- It has also been observed that the magnetic stirrers were causing interference with the cabling. Unfortunately, not every cable could be shielded. This problem was solved by using a higher voltage scale on the SMU. The Keithley 2450 SMU has a built-in mathematical noise filter. At higher voltage scales the noise filter filters more noise out of the signal due to the lower resolution at those scales.
- Chapter 4 describes how the cell was designed and built. There it is stated that the cell is not perfectly leak free. The nuts and bolts used to hold the cell together are made from galvanised steel. Because faradaic reactions might occur between the salt water and the galvanised steel, they were replaced with nylon bolts and nuts.
- Air bubbles in the tubes were causing weird membrane measurements. When air bubbles form in the tubes the electrical connection between the reference electrode and pipette tip is interrupted. Therefore, the system was flushed before every measurement to make sure that the tubes were free of air bubbles.
- The tubes have also been checked for leaks to make sure that it does not affect the measurements.
- After all previous measures were taken still some noise was left in the signal. This was ultimately solved by adding a physical filter right at the input ports of the SMU. This filter consisted out of a 3.3 [nF] capacitor in parallel to the positive and negative pole and a 100 M Ω resistor in series in the positive line. This filter completely resolved the noise issue. Even to the point that the voltage scale of the SMU could be brought back to its original scale at 2 [V]. This meant that the measurements could be performed at a higher resolution again.
- Ultimately, it was figured out that the high membrane potentials were caused by polarisation of the membrane. The polarisation has been caused by performing resistance measurements that were done repetitively at regular intervals during the floating phase. This old measuring procedure was replaced by only measuring the membrane resistance once before the floating phase and once after the floating phase. This completely reduced the polarisation of the membrane, and the measurements gave normal results again.

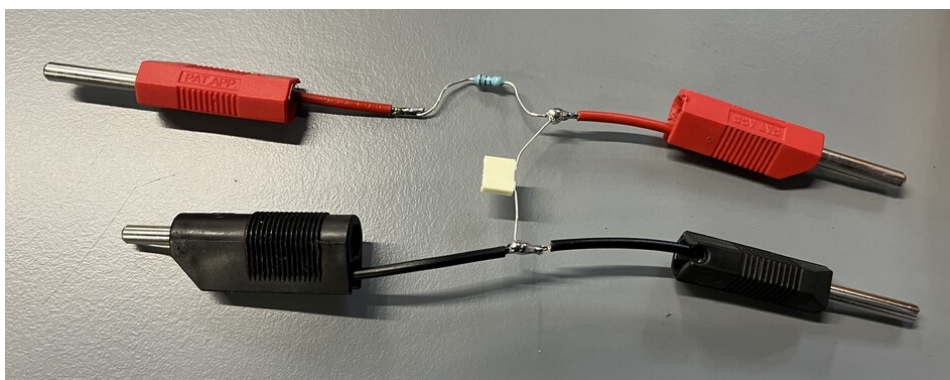


Figure 3.6: The soldered together filter. A 3.3 [nF] capacitor in parallel, and a 100 M Ω resistor in series

3.3. Pore size measurements

The pore size distributions were estimated using a Porolux Revo porometer. This device directly gives the distribution, together with the following data points:

- Maximum pore size
- Mean flow pore size
- Mean pore size
- Minimum pore size

This porometer works on the principle of capillary flow inside the pores. Before inserting the membrane into the porometer, the membrane is first wetted with a wetting liquid. Next, the wet measurement is carried out, where gas is administered to the membrane. The gas will first push out the wetting liquid through the largest pores, and subsequently it will push out the liquid at the smaller pores [37]. This working principle can be seen in Figure 3.9. The pressure needed to displace a liquid from a pore is called the pore pressure. The capillary pore pressure can be related to the surface tension γ and pore diameter D with Equation 3.2, the so-called Young-Laplace equation [37]. The membrane is wetted perfectly when the surface of the fluid film is parallel to the membrane, see Figure 3.7. Meaning that $\cos(\theta) = 1$:

$$P_{pore} = \frac{4\gamma \cdot \cos(\theta)}{D} \quad (3.2)$$

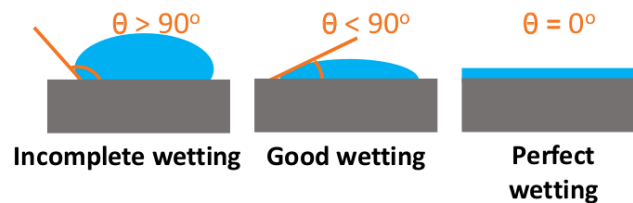


Figure 3.7: Various degrees of membrane wetting with wetting liquid.

Picture source: Training slides Porolux Revo [37]. Used with written permission from Aptco Technologies NV

Followed by the wet measurement, the dry measurement is carried out. Here, the gas will go straight through the membrane, see Figure 3.10. Because there is no wetting liquid inside, there is less resistance for the gas to move through. At the end of the wet measurement, the membrane has become dry. Therefore, when comparing the wet and dry measurements, they should both give the same fluid flow for higher pressures. This principle can be seen in Figure 3.8. At first, the dry curve is above the wet curve for lower pressures, simply because the dry membrane offers less resistance. But for higher pressures, the dry curve and wet curve have to converge and run parallel.

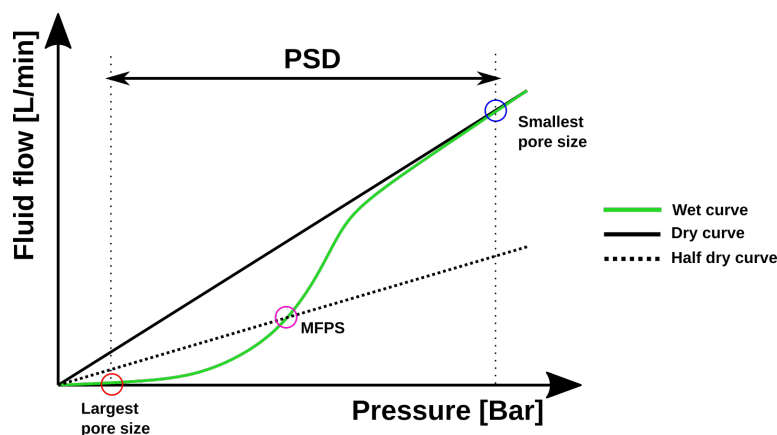


Figure 3.8: Graph of a pore size distribution, for illustrative purposes

Information source: Training slides Porolux Revo [37]. Used with written permission from Aptco Technologies NV

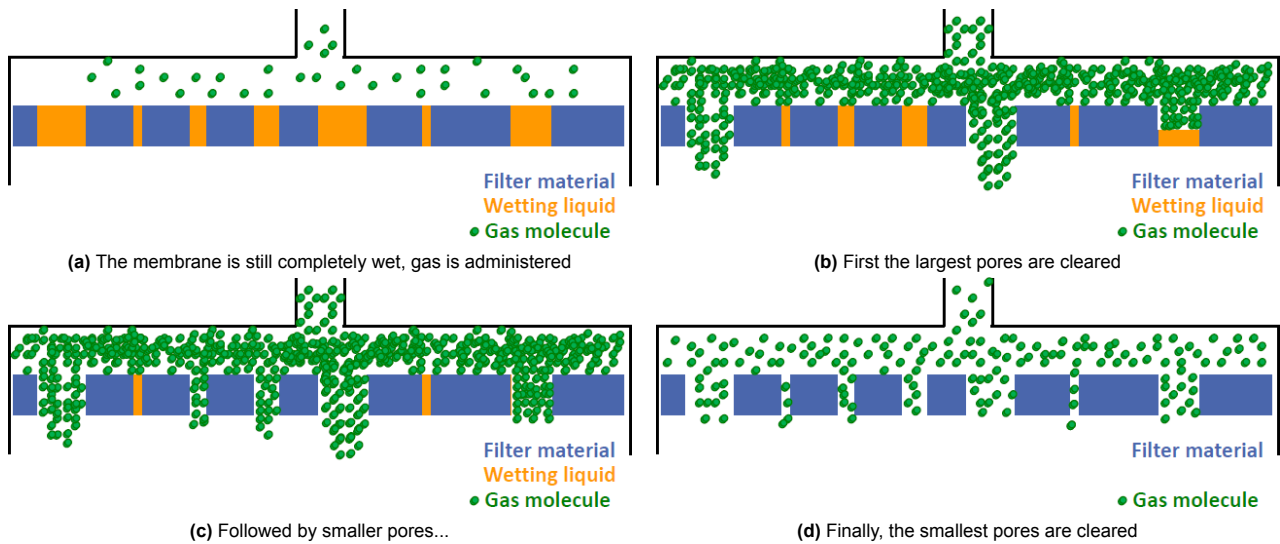


Figure 3.9: The process of the wet measurement.

Picture source: Training slides Porolux Revo [37]. Used with written permission from Aptco Technologies NV.

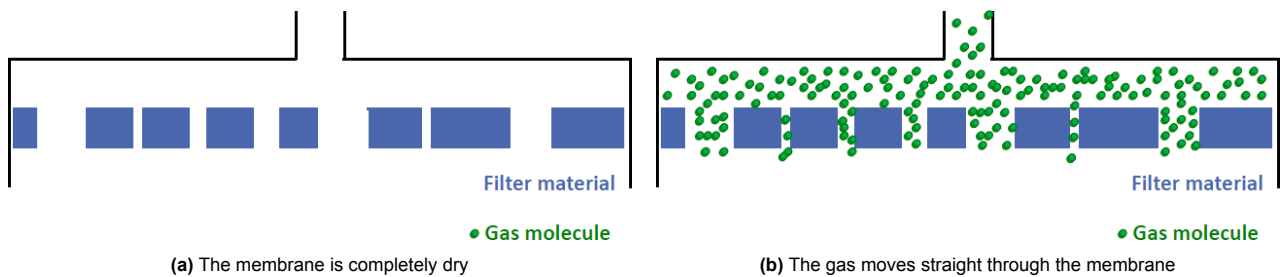


Figure 3.10: The process of the dry measurement.

Picture source: Training slides Porolux Revo [37]. Used with written permission from Aptco Technologies NV.

3.4. SEM imaging

A Jeol scanning electron microscope (model JSM-6500F SEM) is present in the lab of the TU Delft, and it can only be operated by trained staff. SEM imaging is used in this thesis as a validation method for the pore size measurements from section 3.3. The lower measuring limit from the Porolux Revo is 19.4 [nm]. Therefore, SEM imaging will be used to verify whether smaller pores are present in the material. A magnification of at least 100,000x is needed to magnify 20 [nm] to 2 [mm] on a computer screen. Only then can it be visually concluded from an SEM image whether smaller pores are present or not.

The material viewed should be conductive, for an electron microscope to work. Fortunately, this is the case for all CME materials. The viewing procedure is as follows: the magnification of the sample is increased with incremental steps until the highest magnification is reached. At each step, the image is corrected for spherical and cylindrical aberration. When the image is clear at the highest magnification, then (while zooming out) the views are recorded at each step as the magnification is decreased by increments. By working in this order the sharpest possible images will be created of the sample at varying magnifications.

4

Cell Design

The goal of the design is to have a cell that is capable of measuring the membrane potential of the CME. This is achieved by designing a cell with 2 compartments, between these 2 compartments is the CME. The cell was designed and built in a short amount of time, therefore the design will not be ideal. However, in this thesis the main research question does not revolve around a design problem. The main research question revolves around whether the permselectivity depends on the pore size distribution. The only design requirements were:

- The compartments must be large enough for them to be workable.
- The holes in the compartments must be large enough to provide easy access to the exposed CME surface area.
- The entire design must be simple and quick to make.
- The design must retain its structural integrity.

4.1. Design and fabrication of different cell components

A few parts of the cell are on the shelf components. Most other components had to be designed and fabricated. The following paragraph together with Table 4.1 discuss the design and fabrication of the components.

Cell compartments The compartments were designed such that they each hold 150 ml of water. A hole in the base plate with a 40 [mm] diameter has been cut where the CME is positioned. 40 [mm] was an arbitrary choice, but it was chosen to provide plenty of exposed CME surface area. CMEs are fragile membranes, with thicknesses less than 100 [μm]. A 40 [mm] hole in the base plate allowed for careful placement of the probes close to the CME, without causing damage. To compare length scales, the typical thickness of a CME is less than 100 [μm]. That is a ratio of $0.1[\text{mm}]/40[\text{mm}] = 0.0025$. A high ratio means that it is reasonable to assume, that the ion migration through the CME is taking place in 1D only.

The compartments are built up out of a base plate, side walls and a floor. These pieces were shaped such that they fit together like pieces of a puzzle. Another advantage is that the pieces are "2D objects" with a constant thickness, which means that they can easily be laser-cut from a sheet of material. The pieces have a jigsaw like shape, as can be seen in Figure 4.1. This gives the compartment more rigidity when the pieces are glued together. The material of the compartment was chosen to be PMMA, because of its transparency. Figure 4.1 show the CAD design in Solidworks of the compartment consisting out of 2D pieces.

After the design was finished, the PMMA pieces of the compartments were laser-cut by a "Lion 900, L9A-1112-1" automated laser cutting machine. Next, the pieces were glued together with Acrifix 1R 0192. Acrifix is specifically used to glue PMMA, and it hardens under the influence of UV light. Therefore, the compartments were left in sunlight to harden the glue out. As a final step, the connecting interfaces were sanded with 600-grid sandpaper. This last step ensures a smooth surface and that any glue residue is removed. A smooth surface helps to prevent leakage of water once the cell is assembled. Figure 4.2 shows the fabricated result.

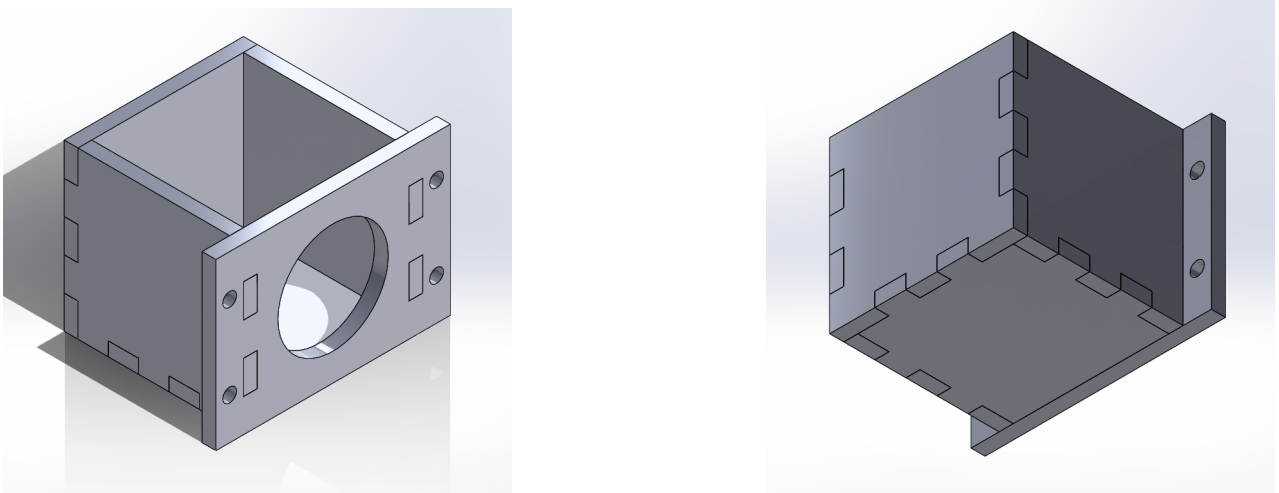


Figure 4.1: CAD model of the cell compartments

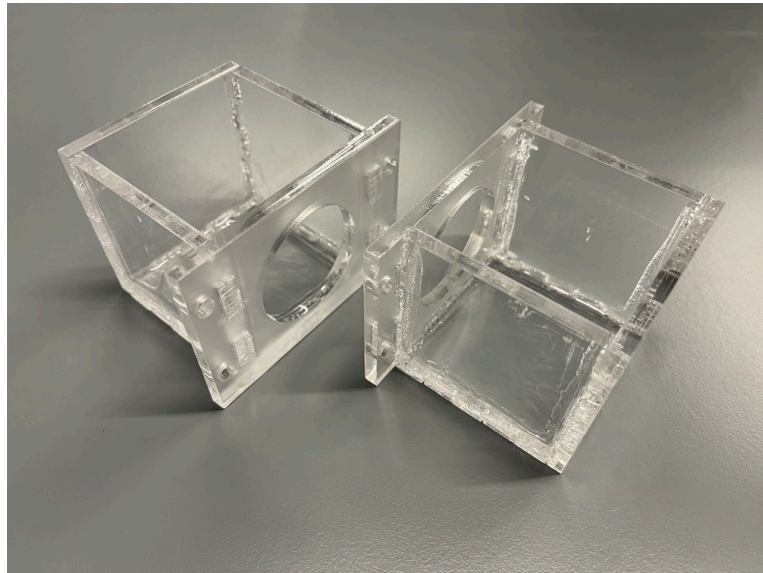
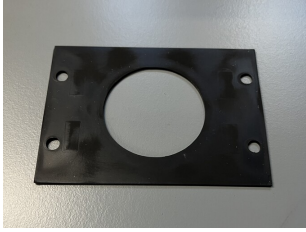

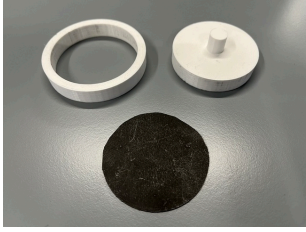
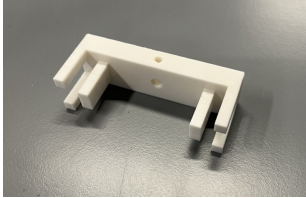

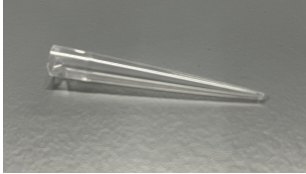



Figure 4.2: Final cell compartments

Table 4.1: Fabricated components with a short description

Description	Component
<p>The gaskets were sized and shaped to match the connecting interface of the compartments. These gaskets were laser-cut from 1.15 mm thick EPDM rubber material at the university's laser cutting facilities.</p>	
<p>The current collector is made from 0.05 mm thick Grade 1 Titanium. The current collector is situated in an environment (consisting of salt water solutions and electric currents) that promotes corrosion. Therefore, titanium was chosen as the material for the current collector, because of its corrosion resistance. The titanium was cut by water jet at the cutting facilities of the TU Delft, due to its small thickness.</p>	
<p>To cut the CME in a nice round shape, a die and punch were designed. The die and punch were 3D printed from their CAD drawings. For clarity: the CME is the black circle in the figure on the right.</p>	
<p>The bracket has the sole purpose of holding the tubing in place. To keep the assembly simple (i.e. no screws necessary), a tight fitment was used to keep it in place. The bracket was also drawn in Solidworks. From these drawings it was 3D printed as well.</p>	
<p>The tubing has a 45-degree elbow. This was fabricated by sawing pieces of PMMA tubing at an angle. The cutting interfaces were sanded down to smooth them out. Next PMMA pieces were glued together with Acrifix 1R 0192 to form an elbow.</p>	
<p>The pipette tips were cut off from regular industry pipettes. They were cut at length such that they would fit in the cell. The pipette tips had a friction fitment on the tubing.</p>	
<p>The brackets were made from grade 2 titanium, and were fabricated using hand tools</p>	

4.2. Cell design overview

As was mentioned earlier in this chapter, a cell with two compartments was designed. One compartment is meant for the high concentration solution, and the other for the low concentration solution. The membrane is sandwiched between the connecting interface of both compartments. A current collector is sitting on top of the membrane to provide current to it. Two rubber gaskets are also positioned between the compartments to prevent leaking of the cell. This assembly is bolted together with 4 screws, 4 nuts, and 8 rings. The counter electrode is hanging from a clip on the side of one of the compartments. The clip is also serving the purpose of being a current collector to the counter electrode. The membrane potential is measured by two measuring probes. These probes consist out of a bracket, tubing and a pipette. The bracket has the simple task of holding the tubing and positioning the pipette tips close to the membrane. By placing the pipette tips close to the membrane ohmic losses will be reduced, allowing for more accurate membrane resistance measurements. A bill of materials of the cell is given in Table 4.2. Figure 4.3a show the CAD design in Solidworks, and an exploded side view of the cell is given in Figure 4.3b.

Reflection on cell design As was mentioned at the start of this chapter, the cell was designed and built in a quick manner, to be able to quickly start measuring and not spend too much time on designing and building. To qualitatively reflect on the design requirements:

- During experiments it turned out that the compartments were sufficiently large enough to be workable.
- The selectivity of the CMEs could be measured effectively, due to sufficient exposed surface area of the CME.
- Cell was designed and built in only a couple of days.
- The cell's structural integrity never failed.

The downside of the design was that it was not completely leak-free. The estimated leakage rate was two teaspoons of fluid per 24 hours. This was deemed to be at such a low level, that it would not affect experimental results. Therefore, the state of the design was left as is. A second design iteration could be performed to perfect the cell, making sure that it is leak-free. This could be achieved by enlarging the flange of the compartments. Furthermore, the flange could also be extended such that it runs along the top and bottom as well as the sides of the compartments. With more flange area more screws can be added to the cell. These added screws will increase pressure on the gaskets, making sure that the cell becomes leak free.

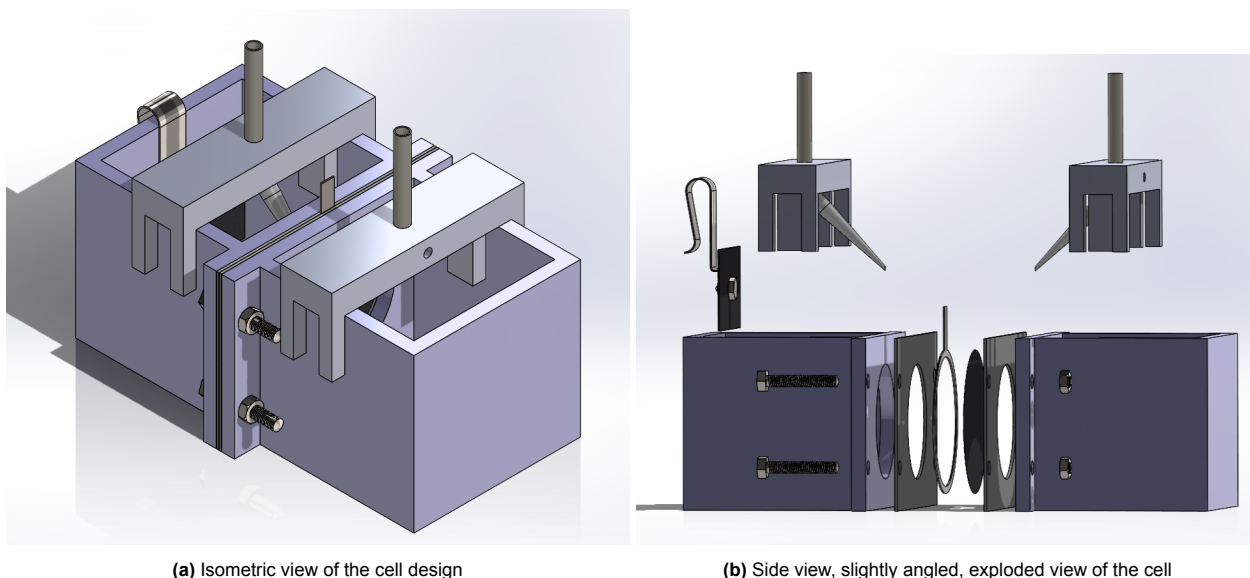


Figure 4.3: CAD drawing in Solidworks of the cell

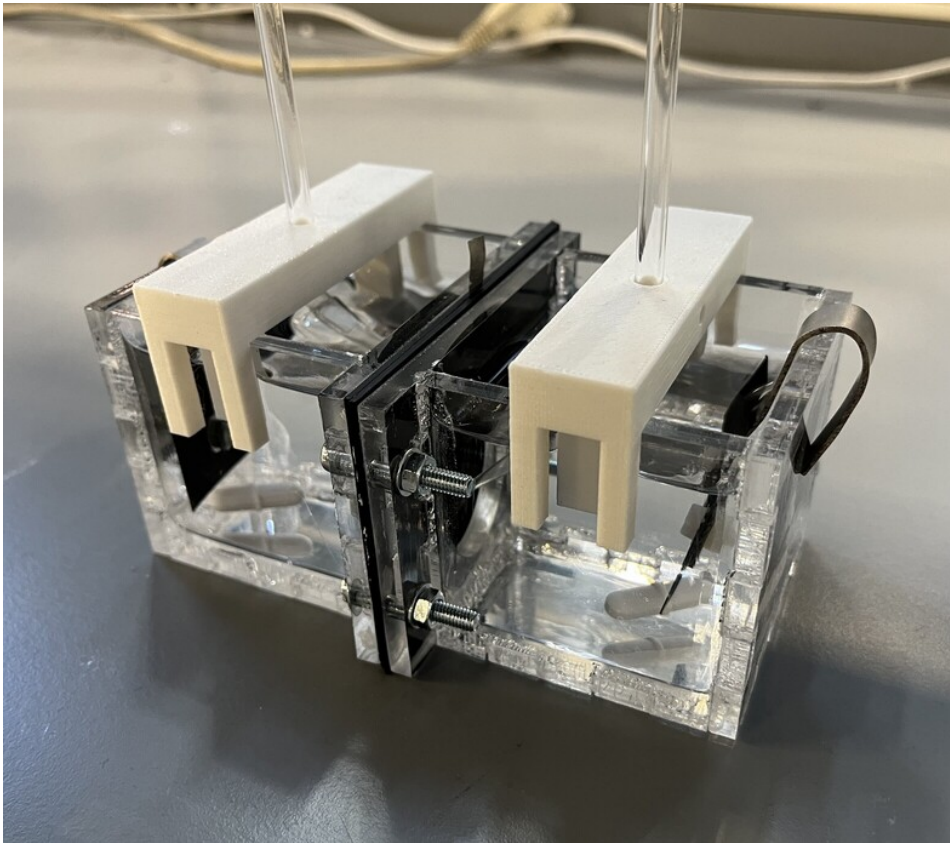


Figure 4.4: The fully completed cell

Table 4.2: Bill of materials of the cell

Item NO.	Component	Description	Quantity
1	Cell compartment	Two identical compartments were designed to hold the water.	2
2	Gasket	To prevent leaking of the cell.	2
3	CME	The membrane that is being measured.	1
4	Counter electrode	The counter electrodes have the purpose of being able to charge up the CME, as well as providing the means to measure the CME resistance.	1
5	Current collector	The current collector that sits on the CME, to provide a current to the CME. Made from titanium grade 1.	1
6	Clamp	The clamp that holds the counter electrode. It also serves as a current conductor for the counter electrode. Made from titanium grade 2.	1
7	Bolt 1	Bolt to hold cell together.	4
8	Screw 1	Screw to hold cell together.	4
9	O-ring	O-ring that rests on the flange of the compartments.	8
10	Bolt 2	To attach the counter electrode to the clamp. Titanium grade 2.	1
11	Screw 2	To attach the counter electrode to the clamp. Titanium grade 2.	1
12	Tubing	PMMA tubing that carries the signal from the membrane to the reference electrodes.	2
13	Pipette	To be able to measure closely to the membrane, a pipette is attached to the tubing.	2
14	Bracket	This bracket has the sole purpose of holding the tubing in place.	2
15	Mixing rods	Magnetic mixing rods supplied by the lab.	2

5

Results

In this chapter, the results from all measurements will be presented and reflected upon. Section 5.1 showcases how the measured potentials change over time. From the membrane potential, the permselectivity can be calculated. The following subsections show what variables affect the selectivity. The selectivity measurements are concluded by plotting the permselectivity against the electrical potential of the CME. Section 5.3 presents all the selectivity measurements, section 5.4 shows the pore size measurements, and finally section 5.5 shows the SEM imaging results.

5.1. Results of a typical experiment

This section showcases how the electrical potential and membrane potential of the CME change over time during a cycle. The selectivity can be calculated from the membrane potential, the known salt concentrations, and the thermal voltage. This is described by Equation 2.25 in section 2.11. As was described in subsection 3.2.3, during an experiment both the electrical potential V_{cme} and membrane potential V_m are being recorded over time. Figure 5.1 showcases what the results of a typical experiments look like. Please note that the x-axis has two time scales, a different time scale for both the positive curve and the negative curve. Figures 5.1a and 5.1c show how V_{cme} and V_m develop during a complete positive and negative charge cycle. The first half of each curve in Figures 5.1a and 5.1c is more or less uninterrupted, between $t=0$ [s] and $t \approx 1250$ [s]. (For the negative curve between $t \approx 3500$ [s] and $t \approx 4750$ [s]). This part denotes the charging phase of each cycle. The second half of these curves is repeatedly interrupted, this part denotes the floating phase. Subsection 5.2.2 discusses in detail why this part of the curve is interrupted.

Figures 5.1b and 5.1d are zoomed in on the floating phase of the curves from Figures 5.1a and 5.1c. For all subsequent measurements, only the floating phase is considered, because this is the relevant part of a measurement. There is of course a measurable membrane potential during the charging phase, but then the membrane potential is affected by the charging potential from the power supply. Meaning that the permselectivity is no longer a function of V_m , which means that Equation 2.25 is not valid during the charging phase. As was defined in section 2.11, the maximum selectivity cannot be greater than 1. For standard concentrations (see subsection 3.2.3), a selectivity of 1 corresponds with a membrane potential of 35.6 [mV]. During charging phases, it has been observed that V_m becomes much greater than 35.6 [mV]. Therefore, only the floating phase is considered when the permselectivity is concerned.

A final interesting point to note is that the positive and negative curves of V_m in Figure 5.1c seem to intersect close to zero, the x-axis. Meaning that the CME is completely discharged at the end of the floating phase. It also seems that the positive curves and negative curves look like each other's mirror image. These two observations indicate that the entire charging process is reversible, giving the confidence that the cell is working correctly.

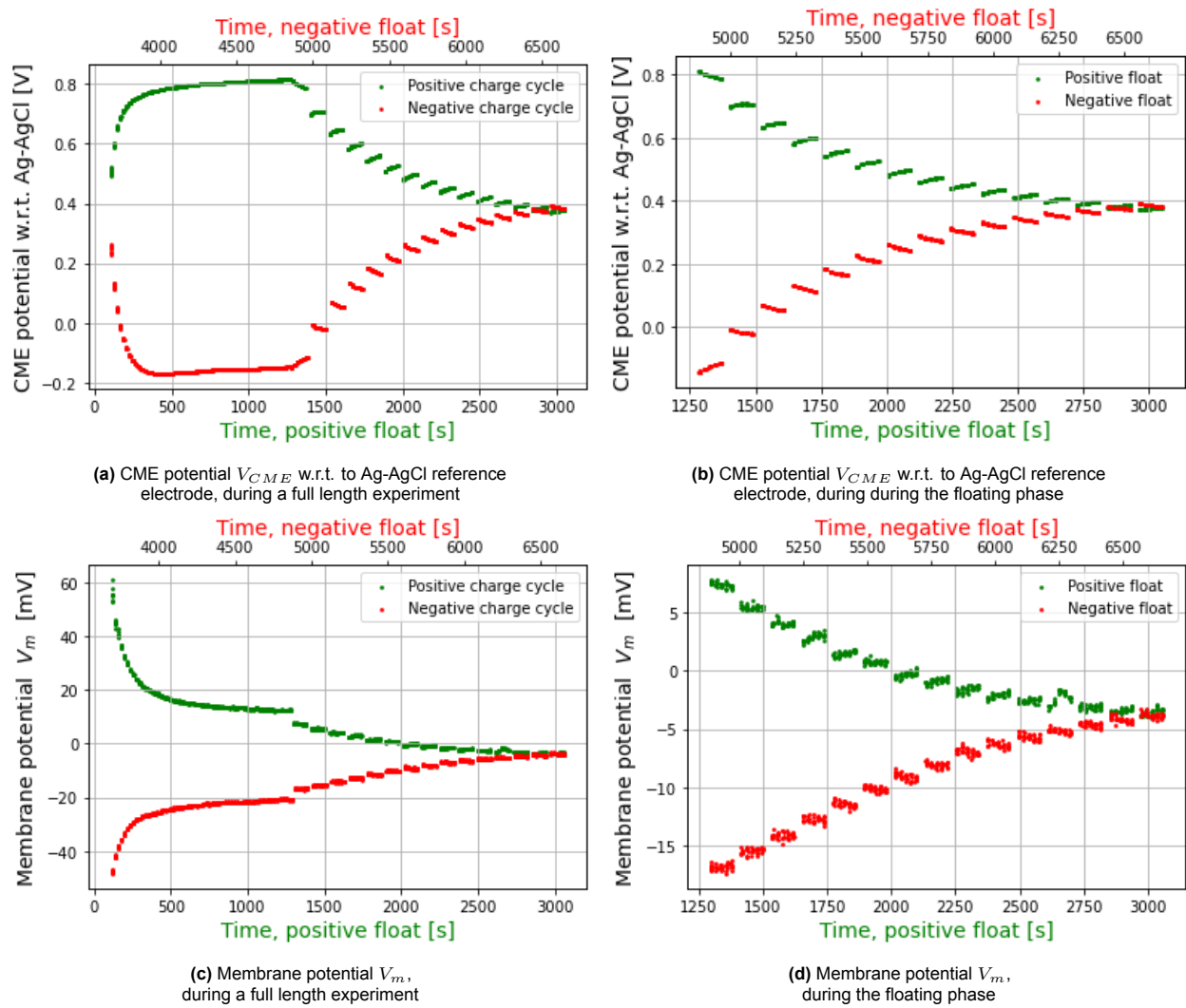


Figure 5.1: Membrane potentials during a typical experiment. The figures on the left show V_{CME} and V_m during full charge cycles. At around 1250 [s] (and 4750 [s]), there is a clear jump in the curves. This denotes the change from the charge phase to the floating phase. The figures on the right show V_{CME} and V_m during the floating phase.

5.2. Testing for various conditions

Before any conclusive measurements can be performed, first the testing setup must be tested as well. Therefore, various inputs and scenarios were changed to see what kind of an effect they have on the permselectivity. These results are presented in subsections 5.2.1 through 5.2.7, by showing the permselectivity over time. In these subsections, the steps in between are intentionally left out, to keep the results concise and straight to the point. The variables were tested in the following chronological order:

1. Increasing salt concentrations
2. Tuning the amount of short-circuit time
3. Using a different salt
4. Applying different charge potentials on the CME
5. Effect of stirring the mixtures
6. Reversing the concentrations
7. Effect of charge cycling the CME on the permselectivity

Points 1, 3, 4, and 7 test the permselectivity of a CME under different conditions. Points 2, 5, and 6 test the cell operation.

5.2.1. Varying amount of salt concentrations

For almost all experimental results discussed in this thesis, the salt concentrations during experiments are as follows: $C_L = 0.25 \text{ [g l}^{-1}\text{]}$ and $C_H = 1.00 \text{ [g l}^{-1}\text{]}$. Therefore, the concentrations were raised in two steps to observe the effect of different concentrations, while keeping the ratio between C_L and C_H the same. Figure 5.5 shows that the absolute maximum permselectivity goes down as the concentrations are tripled from Figure 5.2a to Figure 5.2b, and tripled again from Figure 5.2b to Figure 5.2c. Equation 2.25 describes the permselectivity, as both a function of the concentrations in the bulk (C_H and C_L), as well as a function of the concentrations inside the membrane (c_+ and c_-). Equation 2.25 suggests that the permselectivity should stay the same as long as the *ratio* of C_H and C_L stays the same. The same argument goes for c_+ and c_- . Looking closely at the equation, if both c_+ and c_- are increased by the same factor, then also, in that case, the permselectivity should not change. The c_+ and c_- concentrations inside the membrane are affected by the charge on the CME and the concentrations in the bulk. In Figure 5.2 a rise in concentrations in the bulk leads to lower permselectivities, which is contradicting with Equation 2.25.

Nature always tries to seek equilibrium when charged particles are separated. A capacitor will never spontaneously charge up for example. When there is an electrostatic charge on the CME, it will attract ions from the aqueous solution. These ions will form a thin layer (the so-called EDL) on the CME trying to bring the electrostatic charge into equilibrium. At higher concentrations, more ions are present in the solution and start to counteract the electrostatic charge. This lowers the measured membrane potential for the same charge level of the CME, and a lower membrane potential will diminish the permselectivity of the membrane.

Another observation is from Figure 5.2c. The data shows more fluctuations, meaning that at higher concentrations the cell is more easily disturbed. What exactly has caused this is uncertain. Knowing that only the concentrations have been changed, it might be due to fluctuations in the mixing of the solutions, see subsection 5.2.5.

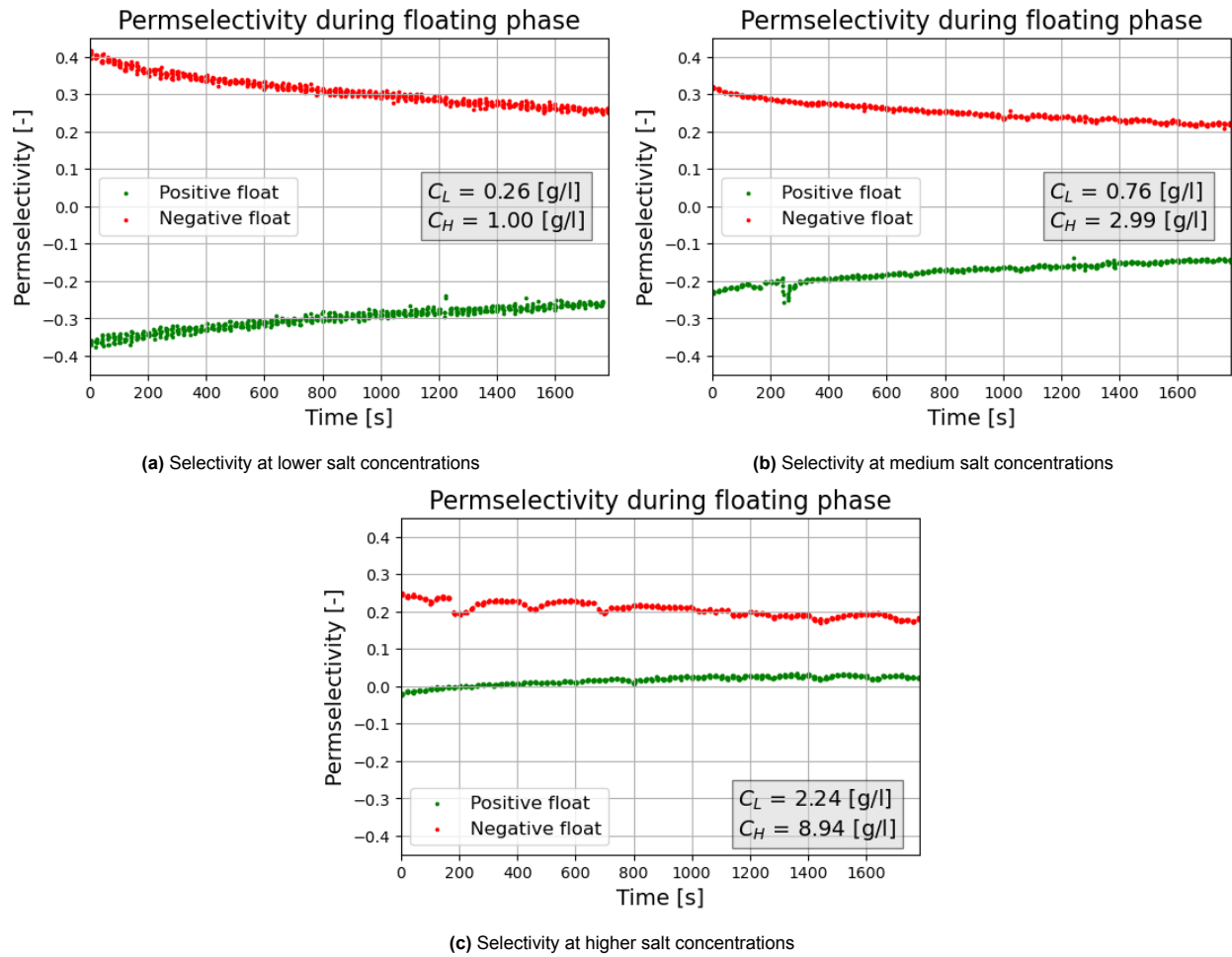


Figure 5.2: Increasing the salt concentrations reduces the permselectivity of the CME. It is hypothesised, that at higher concentrations more ions will be located in the EDL. This reduces the apparent membrane potential, which reduces the permselectivity.

5.2.2. Tuning the amount of discharge during floating phase

During measurements, it has been observed that the cell would not completely discharge during the floating phase, which can be observed in Figure 5.3a. It has been investigated how many times and for how long the short-circuit time would be optimal. Each short-circuit interval would take 20 [s], to keep it at the same length as 1 measuring block (10 [s] measuring V_{CME} + 10 [s] measuring V_m). Three short-circuit scenarios were tested, where the cell was short-circuited 3 times, 6 times, or 15 times during the floating phase. These numbers were no arbitrary choices, as they would evenly space the short-circuit intervals during a floating phase of 1800 [s]. As can be seen from Figure 5.4, short-circuiting the cell 15 times during the float phase seems sufficient to completely discharge the cell. The measurements from Figure 5.4 are also plotted together in Figure B.1 in Appendix B. Figure B.1 shows that the measurements nicely overlay each other. Here the permselectivity is plotted against the electrical potential of the CME w.r.t. one reference electrode. Section 5.3 discusses permselectivity vs electrical potential measurements.

Figure 5.3 shows two measurements that were done back to back, with a charge potential of 1.7 [V]. During the measurements from Figure 5.3b, the cell has been short-circuited 15 times. Each time the cell was short-circuited for 20 [s], which means that the total short-circuit time was $15 \cdot 20 = 300$ [s]. Estimating from Figure 5.3, without short-circuiting the cell it would take approximately: $(10 \text{ [mV]} - (-8 \text{ [mV]}) \cdot 1800 \text{ [s]} \approx 9 \text{ [hours]}$. This estimation would only be true if the discharge is linear, but looking at Figure 5.3a, the discharge is so slow that it is reasonable to assume that it is a linear process. Without short-circuiting the cell, performing all measurements would be a very time-consuming process. Therefore, it is beneficial to short-circuit the cell to get a complete picture in a timely manner.

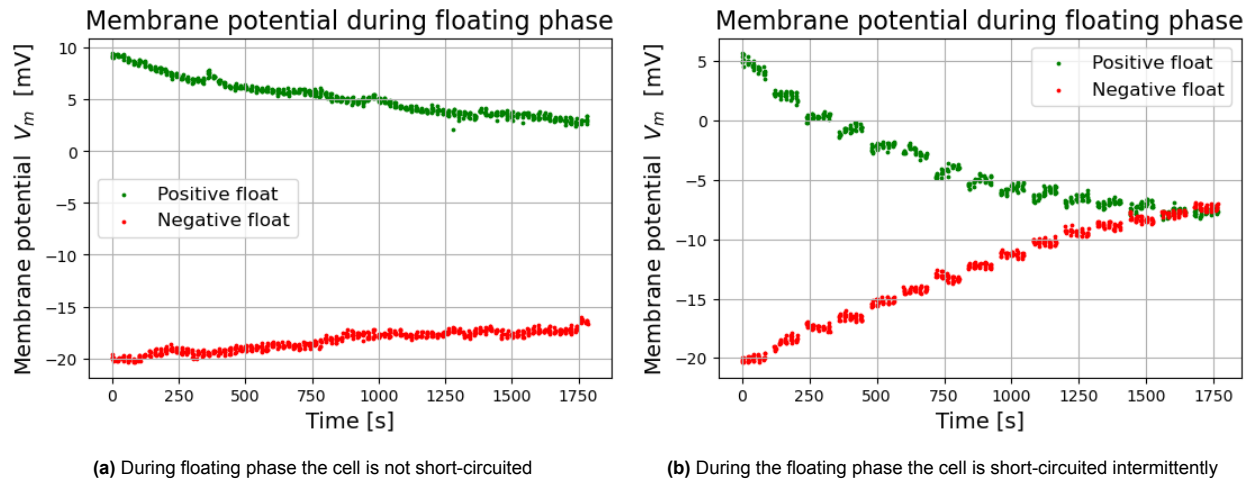


Figure 5.3: These two experiments were performed back to back. This clearly indicates that short-circuiting the cell during the floating phase is beneficial to get the complete discharge curve in a timely manner.

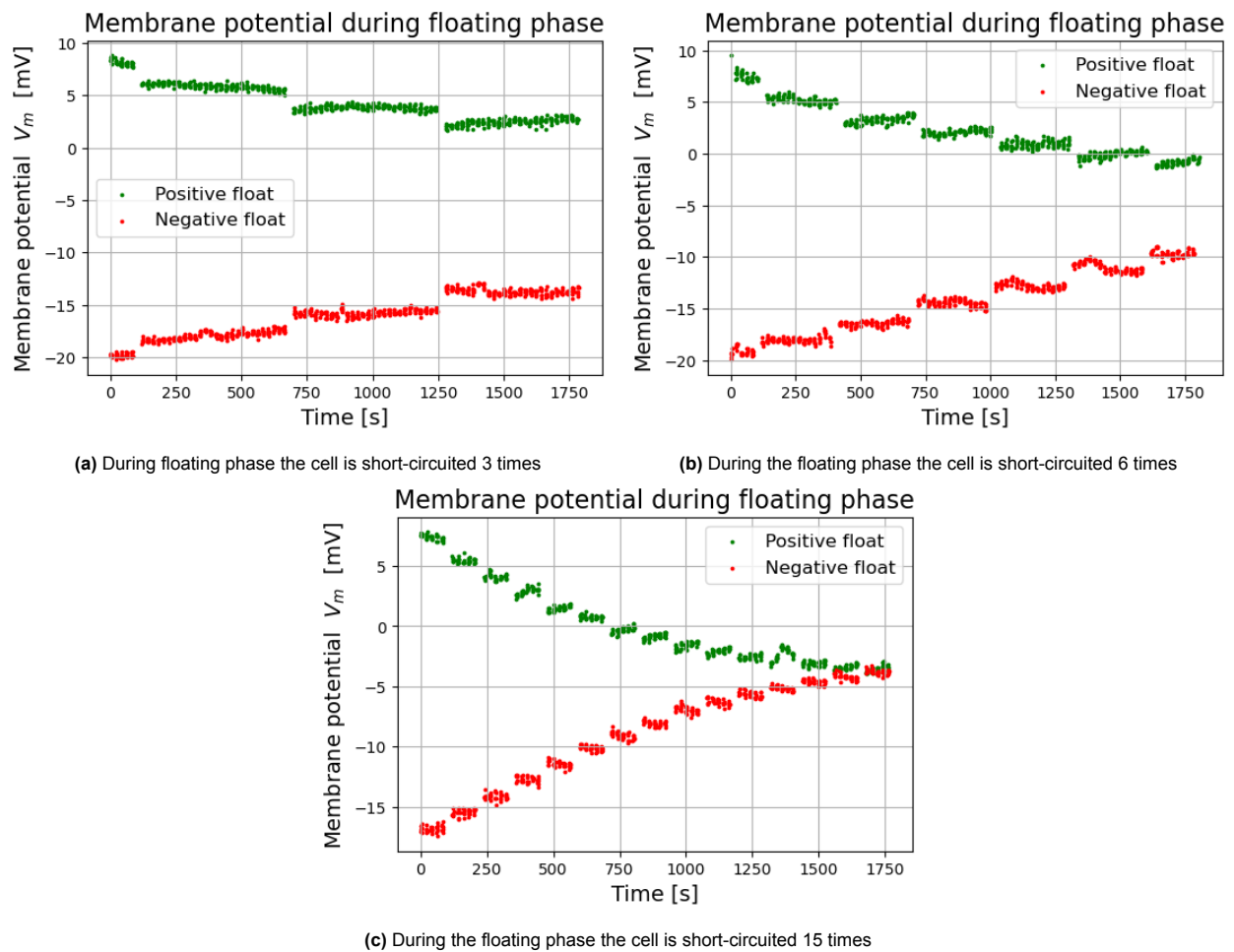


Figure 5.4: By increasing the number of short-circuit times during the floating phase, the more the CME gets discharged, and the smaller the membrane potential gets at the end of the floating phase. From these figures it is clear that 15 times makes sure that the CME is completely discharged.

5.2.3. Using a different salt

KCl was used during experiments, because K^+ and Cl^- have roughly equal diffusion constants [38]. The reasoning is that equal diffusion coefficients imply equal amounts of migration in the bulk of the fluid, which implies that it should not affect the measurements. Experiments conducted with KCl in the lab are under ideal conditions, this may not translate very well to experiments conducted in the field. In nature, plenty of other ions occur, such as Ca^{2+} [39]. To see the effect of using a different salt, $CaCl_2 \cdot 2H_2O$ was used. The diffusion coefficients of Ca^{2+} and Cl^- differ by a ratio of 2.56 ($D_{Cl^-} = 2.56 \cdot D_{Ca^{2+}}$). In this experiment, the same concentrations by mass [$g\ l^{-1}$] were used. However, this means that the molarity will be different due to a difference in molar mass. $M_{CaCl_2 \cdot 2H_2O} = 147.02\ [g\ mol^{-1}]$ vs $M_{KCl} = 74.55\ [g\ mol^{-1}]$. Demineralised water was taken and mixed with $0.25\ [g\ l^{-1}]$ $CaCl_2$ and $1.00\ [g\ l^{-1}]$ of $CaCl_2$ for low and high concentration respectively.

During the experiment with $CaCl_2$ it has been observed that the membrane potential becomes slightly positive, whereas the experiment with KCl has a slightly negative membrane potential. The permselectivity with $CaCl_2$ has also been calculated using Equation 2.25. The permselectivity is negative for a positive membrane potential, as described by Equation 2.25. What this implies is that the permselectivity is slightly positive in the KCl case, and slightly negative in the $CaCl_2$ case, see Figure 5.5

Ca^{2+} has a valence of 2+ which means that it has to be attracted by 2 electrons. The slightly positive membrane potential could indicate that there are not always 2 electrons available for each Ca^{2+} cation, causing the membrane potential to appear positive. This also indicates that Ca^{2+} encounters a higher resistance when migrating through the CME, resulting in a higher negative permselectivity of the CME.

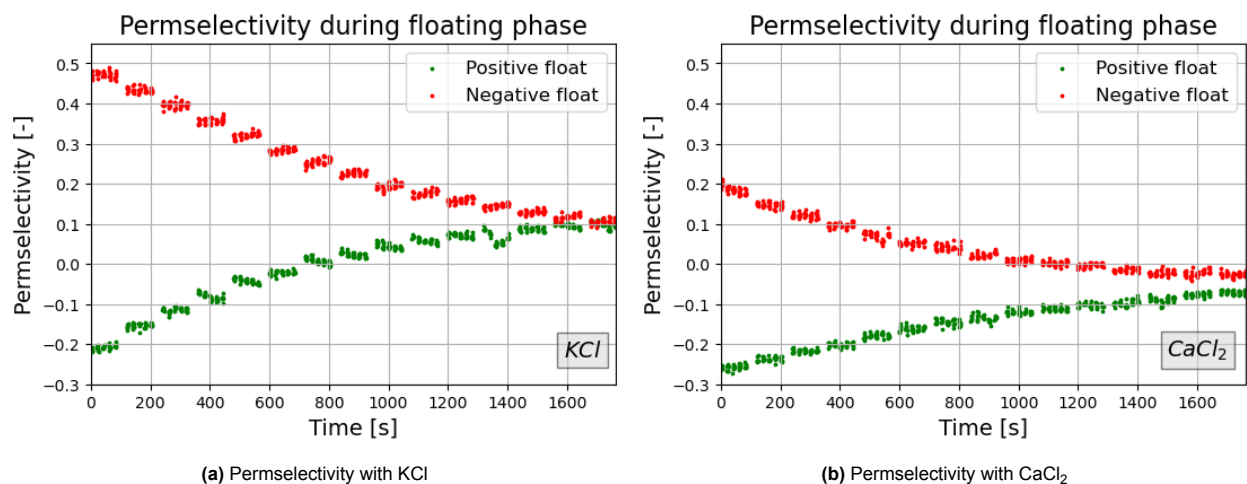


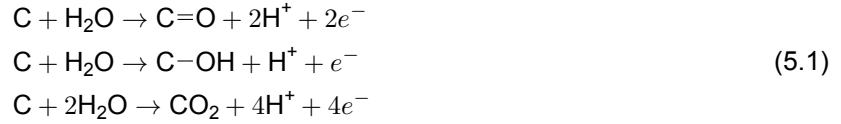
Figure 5.5: Permselectivity for a monovalent (KCl) salt on the left, and the permselectivity for a divalent salt ($CaCl_2$) on the right. Ca^{2+} has a much smaller diffusion coefficient, and it needs two electrons to be attracted by the CME. This leads to a different membrane potential and therefore a different permselectivity.

5.2.4. Applying different charge potentials

Different charging potentials were applied to find out if the permselectivity is affected by the charging itself. The charging potential was increased from $1.0\ [V]$ to $1.7\ [V]$, and again to $2.0\ [V]$. Afterwards, a control test was performed with $1.0\ [V]$ again. As was observed during experiments, the permselectivity increases with increasing CME potentials. However, it was observed that higher charge potentials can have permanent effects on the permselectivity at the end of the floating phase. Indicating a change within the material that lasts even when the CME is discharged again, as can be seen in Figure 5.6. In the $1.0\ [V]$ case permselectivity is around 0.1 at the end of the floating phase, which is close to zero. But as the charging potential is increased, so does the permselectivity become more positive. More interestingly after charging again with $1.0\ [V]$ during the control test, the permselectivity stays at a higher positive level. This seems to suggest that oxidation or damage to the membrane has occurred as a result of the higher charging potentials.

When you zoom in locally on the CME there is either a surplus of positive or negative electrostatic charge on the CME, when the CME is charged. This charge is balanced by the charged particles in the solution, forming

the so-called "electrical double layer" (EDL), see section 2.5. When the CME loses its charge, so does the EDL disappear. This means that in an uncharged state, the membrane potential should be close to or equal to zero. However, when charging potentials on a carbon electrode are elevated, other effects start occurring. Zhang *et al* [40] describe different mechanisms of faradaic reactions occurring in CDI cells at elevated potentials. One of these mechanisms involves the reduction of carbon (C) at the positive electrode, where carbon reacts with water molecules H_2O , forming hydroxyl groups, CO and CO_2 . The reactions are as follows [40]:



These reactions yield one or more electrons, trying to bring down the surplus of positive electrostatic charge on the CME. According to Zhang [40], the standard electrode potential where oxidation starts to occur is at 0.21 [V] vs standard hydrogen electrode (SHE). This corresponds with a cell voltage of 1.2 [V]. The measurements shown in Figure 5.6b and 5.6c were performed with potentials that were far above this threshold, which greatly accelerated the oxidation. The reactions shown in Equation 5.1 also produce highly reactive hydrogen ions. Higher H^+ concentrations will reduce the pH level of the solutions near the CME [41]. The acidic environment and the oxidation of the carbon material of the CME will chemically damage the surface, forming charged groups in the microstructure of the CME. These charged groups lower the membrane potential. The safe operating limit for a CDI cell is below 1.2 [V], to prevent this process from happening.

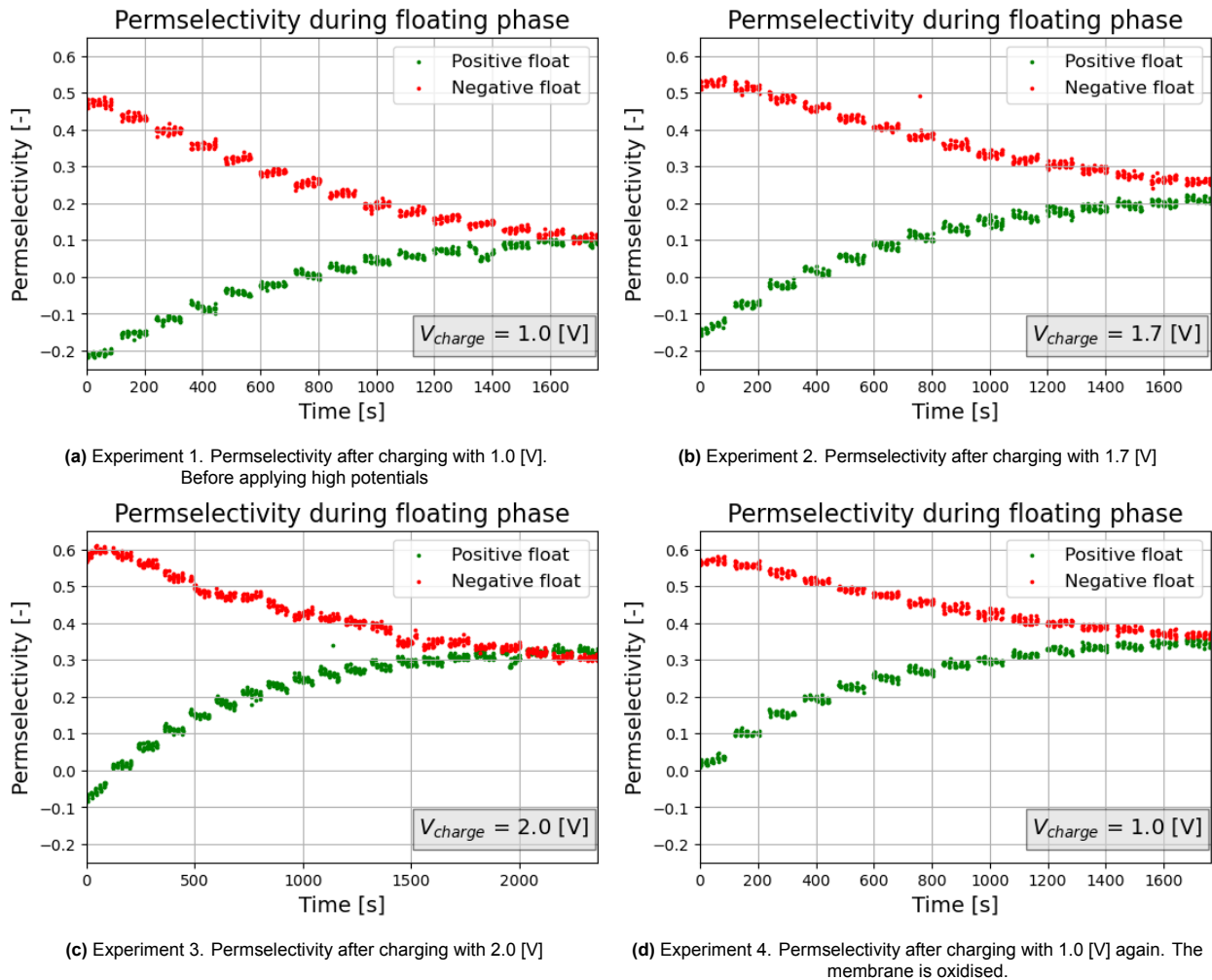


Figure 5.6: The permselectivity for increasing charge potentials on the CME. Increasing the charge potential has a lasting effect on the permselectivity, even when the CME is discharged. Which can be observed by comparing the permselectivities at the end of the floating phase, when the CME is discharged. Figure d shows the permselectivity of an oxidised membrane. The charge potential is 1 [V], but after two experiments with higher potentials.

5.2.5. Influence of stirring mixture on selectivity

At the start of the experimental phase of this research, it was assumed that stirring the solutions would benefit the selectivity of the CME. Stirring means that the solution is properly mixed in the bulk and that the local concentrations near the CME are constantly refreshed. To confirm this a short experiment with and without stirring was performed. In this case, only the positive cycle was tested. As can be seen in Figure 5.7 stirring does increase permselectivity, both in the positive and negative range, validating the stirring assumption. From Figure 5.7 it is also visible that there are more fluctuations in the unstirred case. Revisiting the statement in subsection 5.2.1 about the fluctuations occurring at high concentrations, it does indeed seem that not stirring or improper stirring is causing these fluctuations. Higher concentrations make the system more sensitive to improper stirring.

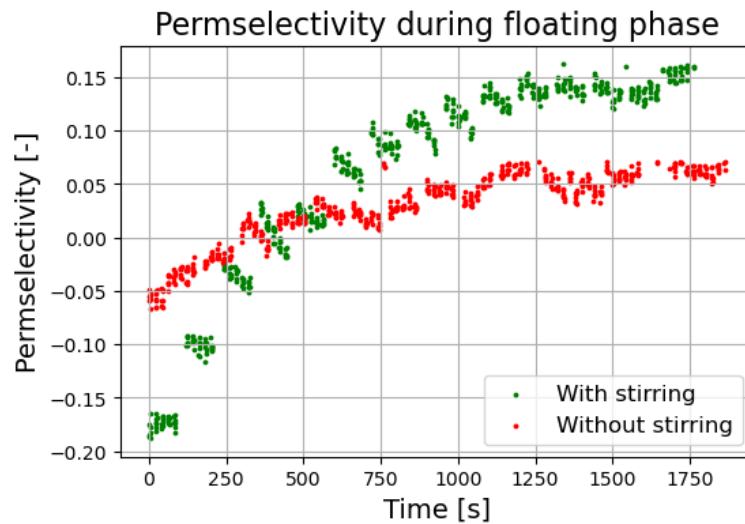


Figure 5.7: Permselectivity during positive floating, with and without stirring the solutions. From this figure, it is clear that stirring increases the permselectivity both in the positive and negative range.

5.2.6. Exchanging concentrations

Later samples that were tested showed higher membrane potentials than expected when they were new and uncharged. Due to these higher membrane potentials, the permselectivity was more negative, as can be seen in Figure 5.8a. Therefore, the concentrations were exchanged to check whether the measuring setup might be faulty, and how this translates to the permselectivity. With exchanged concentrations, one would expect the permselectivity to become inverted. Ions will now be transported in the opposite direction through the CME. This is also visible in Figure 5.8b, as the permselectivity has now become positive. Despite the fact that both green and red curves don't level out at the same permselectivity, it is true that both red and green curves have been mirrored along the x-axis and are shifted up. Exchanging the concentrations indicates that the system is working correctly.

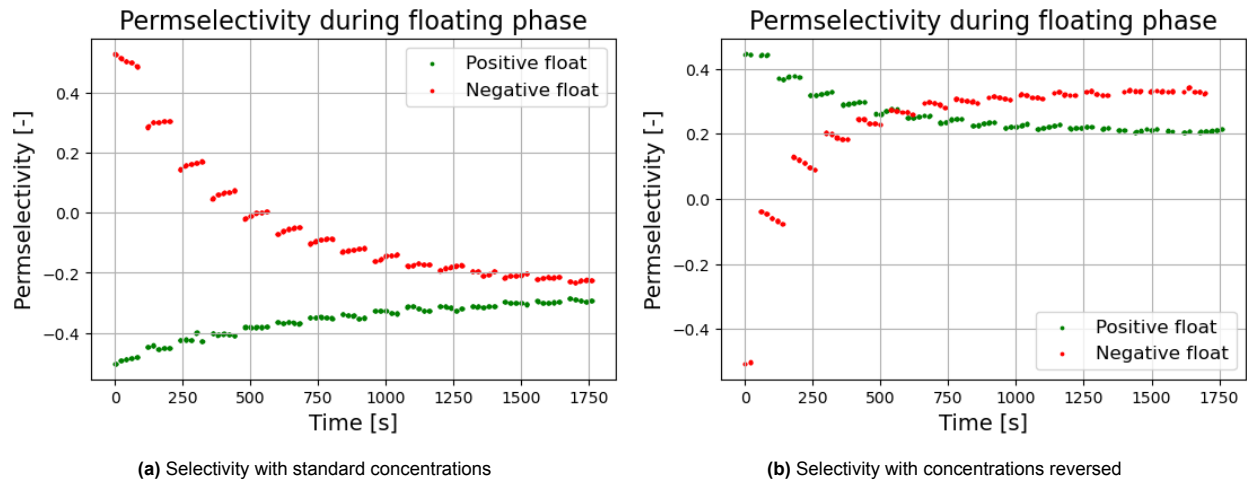


Figure 5.8: In the figure on the left permselectivity experiment was carried out with salt concentrations in the normal configuration. In the figure on the right, the concentrations were reversed. Meaning that the ions will now migrate in the opposite direction through the CME, resulting in a permselectivity that is inverted.

5.2.7. Reduction of CME selectivity after charge cycling

It has been observed after subsequent measurement with the same sample CME, that the resting membrane potential starts to become more and more negative. Indicating that the selectivity becomes more positive and that CME becomes more permselective for cations. This effect is also visible in Figure 5.6, but at a much-accelerated pace due to the higher charging potentials that were applied. Therefore, an experiment was conducted to see how much the permselectivity was affected after a certain amount of cycles. A fresh new membrane was cut, and the membrane potential was recorded before any charging was done. This membrane potential was 7.928 [mV]. Next, the CME was put under 10 cycles, where positive and negative cycles alternated. The applied charging potential was chosen to be 1.2 [V], and it was kept constant for each charge cycle. A slightly higher potential was chosen to speed up the oxidation of the CME, but not too high that damage might occur instantly.

What becomes apparent when looking at the data from Figure 5.9, is that a positive cycle is causing the selectivity to go up and will eventually become positive. A negative cycle has the opposite effect, but it is not capable of fully correcting the effect from the positive cycle. What is even more interesting to see, is that negative cycle number 2 over-corrects positive cycle number 1. However, for the subsequent cycles, the negative cycle does not seem to correct the full effect of the foregoing positive cycle. What exactly causes this non-linear effect is still unknown and needs further research.

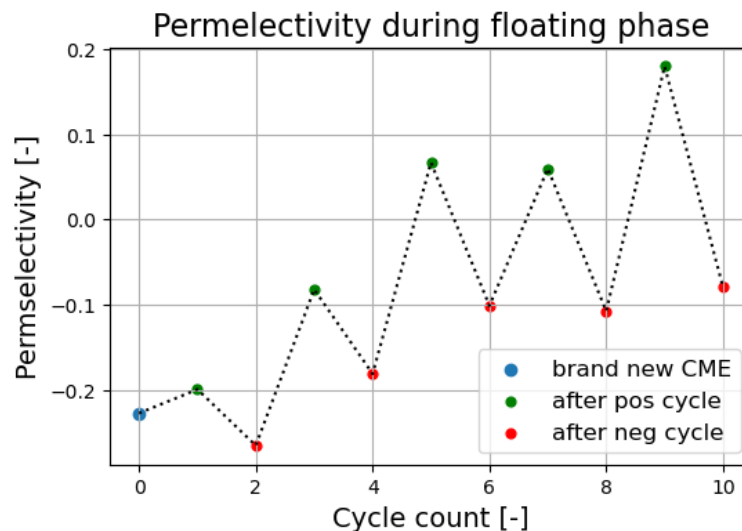


Figure 5.9: Selectivity after 10 cycles, where positive and negative cycles alternate. Each point in the graph is all the way at the end of a positive or negative cycle. Meaning that the CME is completely discharged.

5.3. Permselectivity and resistivity results

The final goal of the selectivity measurements is to measure the permselectivity w.r.t. the electrical potential of the CME (V_{CME}). For the final measurements all foregoing tested variables from subsections 5.2.1 through 5.2.7 were kept at ideal conditions. This means that KCl salt was used, at lower concentrations, with short-circuiting the cell 15 times during the floating phase, operating the cell at a charging potential of 1 [V], stirring the solutions of the cell, and letting the CME undergo only 1 positive and negative charge cycle.

Besides measuring the permselectivity w.r.t. V_{CME} , also the electrical resistance across the thickness of the membrane is measured. The electrical resistance across the thickness originates from the ionic resistance of the membrane. As both ions and electrons are charged particles. A highly selective CME with a high ion resistance is not considered ideal. Therefore, the ion resistance is an important parameter when assessing the permselectivity of a CME. Unfortunately, no resistance data is available for CME material 04/21, because no resistance measurements were performed for this material.

The data from Table 5.1 shows that the resistance is higher after the floating phase compared to before the floating phase. Intuitively this seems to be correct. When the CME is charged, more ions will locate in the pores inside the membrane. With higher concentrations inside, the lower the resistance will be across the thickness. This also correlates with the observation that a higher CME potential induces a higher permselectivity. A higher potential is causing higher ion concentrations inside the membrane, which induces higher permselectivity. It should be noted that the resistance data in Table 5.1 is calculated for the *entire* exposed CME area, as the current passes through the entire exposed CME.

Table 5.1: Permselectivity and resistance data for different CME materials

material	Positive cycle					Negative cycle				
	Selectivity fully charged	Maximum potential CME [V]	Ion resistance before float [Ω]	Selectivity discharged	Ion resistance after float [Ω]	Selectivity fully charged	Maximum potential CME [V]	Ion resistance before float [Ω]	Selectivity discharged	Ion resistance after float [Ω]
04/21	0.219	0.815	NA	-0.113	NA	-0.489	-0.171	NA	-0.092	NA
06/01#2	0.667	0.801	134.93	0.378	200.31	-0.743	-0.229	119.15	0.304	172.65
06/01#1	0.502	0.716	73.21	0.284	73.98	-0.529	-0.202	66.55	0.231	71.86
Gradient	0.634	0.843	83.84	0.241	135.82	-0.596	-0.249	95.32	0.454	102.69
09/04	0.397	0.83	26.71	0.247	20.56	-0.56	-0.309	19.91	0.275	16.76

The analysis is concluded by plotting the measured permselectivity of the membrane as a function of its voltage with respect to the reference electrode. These results are shown in the sub-figures below in Figure 5.11. The plot shows that for positive voltages the CME becomes negatively permselective, which indicates actually a strong preference for negative ions to be conducted through the CME. On the other hand, when the voltage of the CME becomes negative the CME becomes positively permselective. In this case, there is a strong

preference for the permeation of positive ions. The permselectivity curves resemble an "S" shape, where at some point a higher potential will not lead to an equally higher permselectivity. This is the point of diminished returns. The point where the positive and negative curves meet is the point when the CME is discharged. For each curve the positive floating curve comes first, the negative curve second. Over time the CME gets discharged, meaning that as time progresses, both curves move inward.

When looking at the Figures 5.11a - 5.11e and the data from Table 5.1, what becomes immediately apparent is that material 04/21 can become considerably less selective compared to the other tested materials. When trying to make a fair comparison between these membranes it is important to choose a performance metric. If for example two CMEs are equally selective, but one needs a lower potential to achieve this, then that one is considered to be better performing. Or a membrane may be highly selective, but also have a high ionic resistance. Therefore, the membranes are compared by looking at the permselectivity/resistance ratio (P/R_m) and permselectivity/electric potential ratio (P/V_{cme}). The ratios for the negative cycle have been made absolute to make easier comparisons. In Table 5.1, in an absolute sense the maximum positive CME potential is larger compared to the maximum negative CME potential. The middle point of the positive and negative curves in Figures 5.11a - 5.11e was taken as a reference point when calculating the ratio P/V_{cme} . For example, for material 04/21 that would be 0.38 [V].

The value of 0.38 [V] stems from the fact that the potential of the CME is measured w.r.t to the reference electrode. The charge potential from the power supply equals 1 [V] and charges the CME w.r.t. one counter electrode. A range of 1 [V] would be expected to be on the x-axes of the subfigures from Figure 5.11. This is the case, but it is at an offset of approximately -0.2 [V]. The standard potential of an Ag-AgCl reference electrode in 3M KCl solution at $T = 293$ K w.r.t. to a standard hydrogen electrode (SHE) is 0.210 [V] [42]. The total potential between the CME and the Ag-AgCl reference electrode is measured as V_{CME} , which is the sum of the absolute potential of the CME minus the standard potential of an Ag-AgCl reference electrode ($E_- = 0.210$ [V]).

$$E_{total} = V_{CME} = E_+ - E_-$$

Taking material 04/21 as an example, and taking its data from Table 5.1: the absolute potential of the CME at the middle point equals: $E^+ = 0.38 + 0.210 = 0.59$ [V]. $E_+ = 1.025$ [V] when $V_{CME} = 0.815$ [V], and $E_+ = 0.039$ [V] when $V_{CME} = -0.171$ [V].

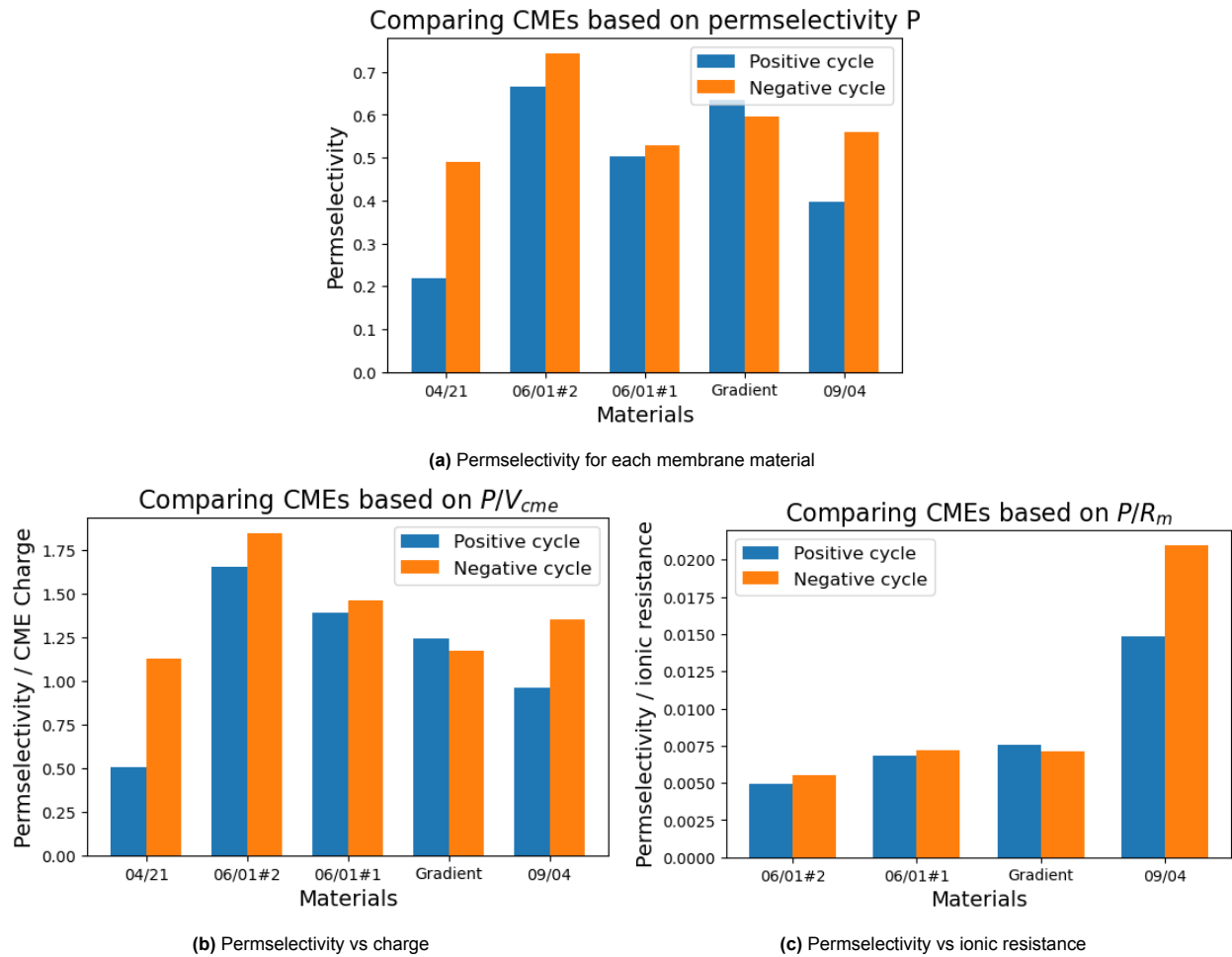


Figure 5.10: Comparing CME material based on two performance metrics

It should be noted that for material 04/21 there is no ionic membrane resistance data, meaning that it could not be compared in Figure 5.10c. For material 04/21 it is also clear that it was not a good performer when looking at P/V_{cme} . This means that other materials should be considered when choosing a material for a CDI cell. From the above figures, material 09/04 stands out. Material 09/04 is performing reasonable when looking at P/V_{cme} but performing exceptional when P/R_m is concerned. Material 09/04 is showing decent permselectivity, while offering low ionic resistance. These are desirable qualities in a CME material. A highly selective material that also has high ionic resistance is not very desirable, as high ionic resistance means that less salt will be transported through the membrane.

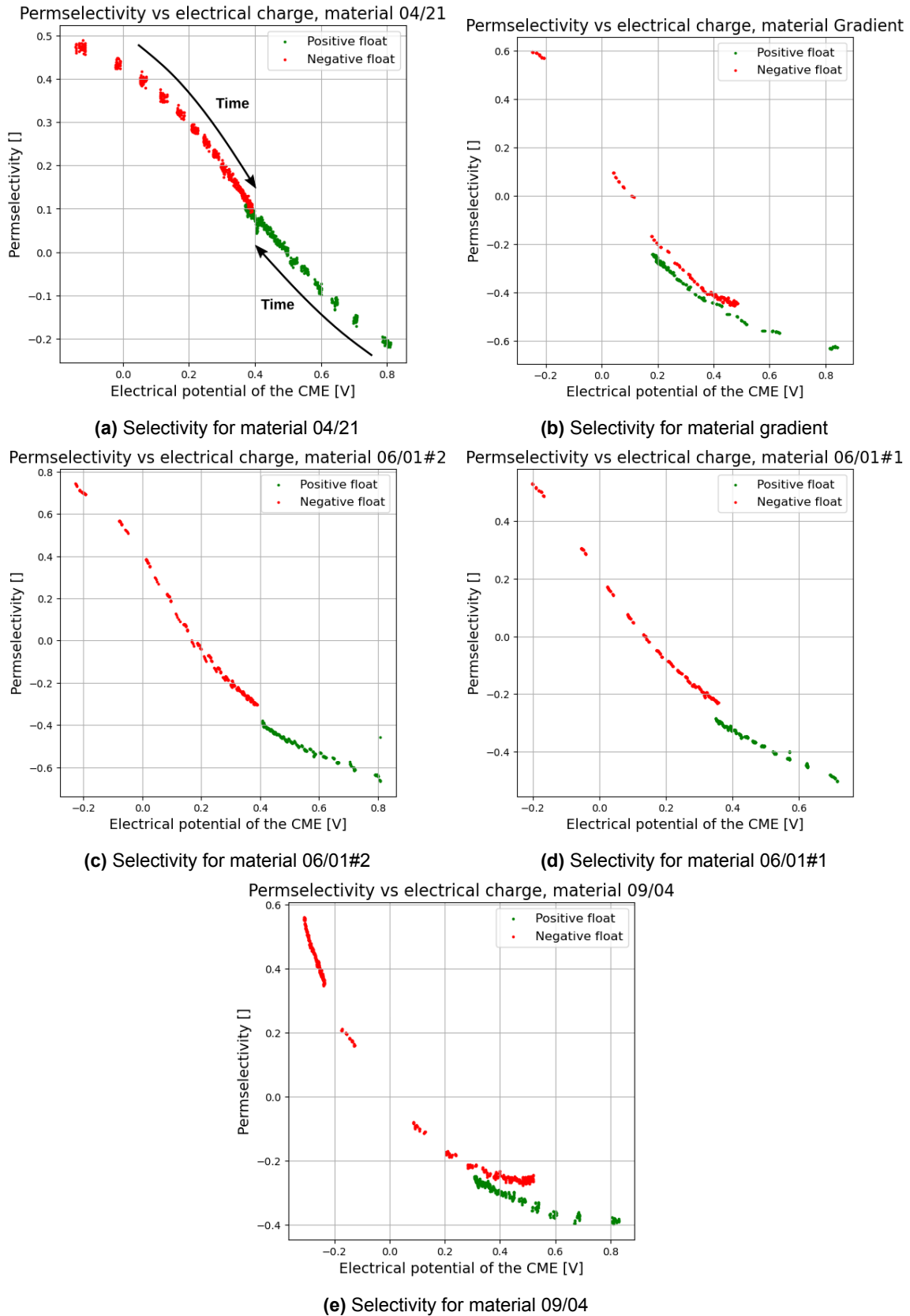


Figure 5.11: Permselectivity for different materials. For each figure the green curve correlates with the positive cycle (first occurring), and the red curve with the negative cycle (second occurring). As time progresses the curves move inward. The x-axis shows the electrical potential of the CME in Volts w.r.t. one reference electrode. The permselectivity is on the y-axis and has no units.

5.4. Porosity measurements

An overview of the results for the pore size measurements is given below in Table 5.2. The measurements were carried out with a Porolux Revo porometer, with a lower measuring limit of 19.4 [nm]. As was explained in section 3.3, the pore size is estimated from the pressure and fluid flow through the membrane. The Young–Laplace Equation 3.2, relates the capillary pressure to the pore diameter. The smaller the pore size to be measured, the higher the required pressure. The maximum operating pressure is at 40 [Bar], which correlates with the pore limit of 19.4 [nm]. Of each material, two samples were taken and tested. One observation from these results is that both materials 06/01#1 and 06/01#2 have considerably smaller maximum pore sizes. For the other materials, the maximum and minimum pore size seems to be very consistent across the board. The mean flow pore size (MFPS) does show some variation, however. For the MFPS also the pressure and volumetric flow rate are given. Later on, the flow rate can be compared with the electrical resistance from Table 5.1.

Nomenclature:

- MP = maximum pore size
- MPS = mean pore size
- SP = smallest pore size
- MFPS = mean flow pore size

Table 5.2: Pore size measurements for different membrane materials

Material	Material thickness [μm]	Sample number	MP [nm]	MPS [nm]	SP [nm]	MFPS [nm]	MFPS pressure [Bar]	MFPS, flow rate [l min ⁻¹]
Gradient	25	1	366.4	168	30.93	184.2	5.33	0.49
Gradient	25	2	365.2	93.94	28.82	119.4	3.45	0.39
09/04	20	1	363.7	69.39	20.48	60.83	10.76	3.3
09/04	20	2	363.4	63.5	22.82	59.64	10.66	3.06
06/01#2	45	1	92.08	39.54	22.35	44.56	14.27	0.55
06/01#2	45	2	122.5	49.65	24.78	56.45	11.27	0.83
06/01#1	75	1	73.7	41.76	23.04	36.78	17.29	1.39
06/01#1	75	2	122.5	45.45	20.48	39.96	15.92	2.09
04/21	65	1	363.5	68.35	27.43	79.28	8.02	0.44
04/21	65	2	365.3	82.77	23.23	62.64	10.15	2.73

Below in Figure 5.12a a typical graph is shown for a pore size measurement. During a measurement, the pressure is gradually increased until it reaches a predetermined maximum value. As the pressure is increased the porometer records the fluid flow in [l min⁻¹]. Section 3.3 explains how the software calculates the pore size for each respective pressure and flow rate. The bubble point is the point where the wet curve leaves the x-axis, and gas starts to run through the membrane. This point translates to the maximum pore size. The point where the dry curve meets the wet curve is the point that relates to the minimum pore size. Here, the gas flow for both wet and dry curves is equal, indicating that all the wetting liquid has been pushed out of the membrane. Finally, the point where the half-dry curve crosses the wet curve, is the point that relates to the mean flow pore size.

It should be noted that measuring the pore size distribution (PSD) was not a trivial task. In order to reliably find the minimum pore size, the dry curve and wet curve should converge and run parallel at high pressures, as shown for example in Figure 5.12a. However, this was not always the case. The dry and wet curves did not always intersect, or they did intersect but at the wrong point. The software from the Porolux can perform varying calculation methods, where the dry curve is calculated (instead of measured) to intersect with the wet curve. The software gives 3 calculation methods that are explained in the manual [43].

- The **first** calculation method draws a straight line between the origin and the last point where a pore opening should be detected. This point is on the linear part of the wet curve where the wet curve starts to become dry.
- The **second** calculation method draws a straight line between the origin and the point where the wet curve has the steepest gradient.

- The **third** calculation method draws an exponential curve fitted to three points. The origin, the last wet data point, and the third point is chosen close to the last point. The third point therefore lies in the "almost dry" part of the wet curve. By putting the 2nd and 3rd points close together, one makes sure that the calculated dry curve and measured wet curve run parallel at higher pressures.

All 3 calculation methods are an estimation method for the dry curve. The 1st and 2nd calculation methods were deemed to be crude methods to calculate a dry curve. Therefore, the 3rd calculation method was chosen in the case when the dry and wet curves did not converge. In appendix C all pore size measurements are shown. When the dry curve has a smooth curve, calculation number 3 was chosen. When the dry curve has markers on it, then that is the actual measured dry curve.

The Darcy equation is a linear equation [43], that describes the fluid through porous media as a function of the pressure gradient. The Darcy equation has the following assumptions [43]:

- The porous media has cylindrically shaped pores.
- The flow is laminar.
- The fluid is incompressible.

However, the dry curves in Figure 5.12a and in Appendix C are non-linear. This is true for both estimated dry curves and measured dry curves. The first assumption is difficult to verify without information about the microstructure of the CME materials. The Porolux software does have a shape correction factor of 0.715 to correct for variation in the shapes of the pores, but this is yet another assumption that may or may not apply. Figure 5.12a shows fluid flows in the order of 30 [L min⁻¹] at pressures of 35 [Bar], therefore it is very likely that the flow is turbulent and that the flow is compressible. Therefore, the second and third assumptions will not hold. From these observations, it can be said that the Darcy equation does not apply anymore for the measurements in Figure 5.12a and the figures in Appendix C.

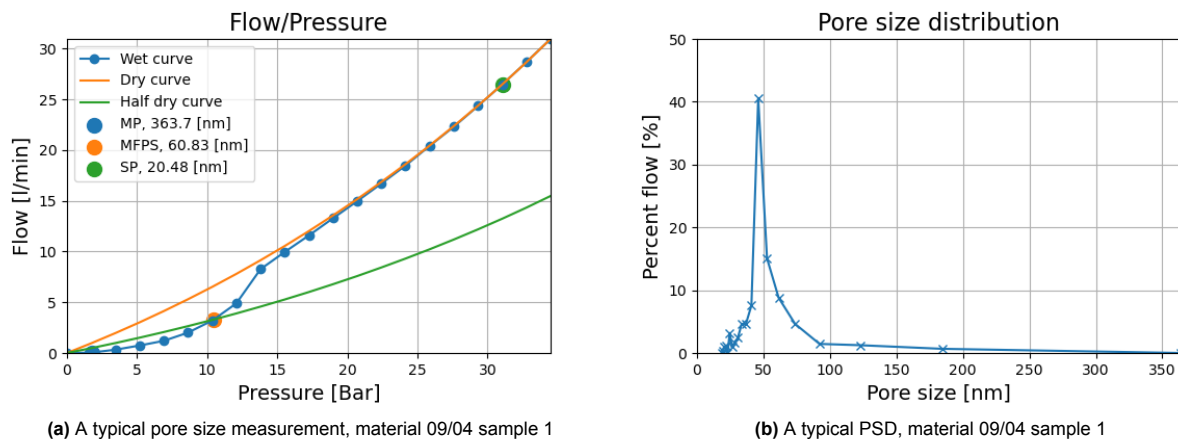


Figure 5.12: Pore size measurement results for material 09/04. This figure on the left shows the data points of the measurement, where the pressure data points were recorded with their respective fluid flows. The wet and dry curves did not converge, unfortunately. The porometer software has the capability to recalculate the dry curve with an exponential approximation. This is what happened in the figure on the left. The curve in the figure on the right is the calculated PSD from the data from the curve on the left. It is clear from this figure that most pores are between 20 and 80 [nm]. That is in the mesopore and lower macropore range. As was discussed in section 2.6, the mesopores play a key role in the permselectivity of CMEs.

5.5. SEM Imaging

The lower measuring limit of the Porolux Revo is 19.4 [nm]. To verify whether even smaller pores are present in the CME material, SEM imaging was performed. To limit the amount of time and resources used, the choice was made to only look at samples from the 04/21 material. Making sharp SEM images of other CME materials at reasonable magnification turned out to be very time-consuming. SEM images were taken at increasing magnifications until the highest possible magnification of 100,000 times was reached. Appendix D shows a gradual zoomed-in visual overview. At a magnification of 100,000 times, the individual pores and particles were visible, as can be seen in Figure 5.13. From the scale at the bottom of the figure, it can be

deduced that the pores at the surface were in the order of 20 [nm] or larger, and that only a few pores were smaller than 20 [nm]. The vast majority of pores are in the range of 20-30 [nm] or larger. This validates the pore size distribution measurements from section 5.4.

Sub 20 [nm] pores were not visible with the porometer, due to the lower measuring limit. Furthermore, it might very well be the case that high pressures are causing the smallest pores to collapse and close, well before the measuring limit of the porometer has been reached. This is visible in the PSD figures from appendix C. The PSDs do not abruptly stop at the 19.4 [nm] mark, but instead they taper off well before the limit is reached. On the other hand, from Figure 5.13 it becomes clear that even though there are pores smaller than the measuring limit from the porometer, these sub 20 [nm] pores are only small in numbers.

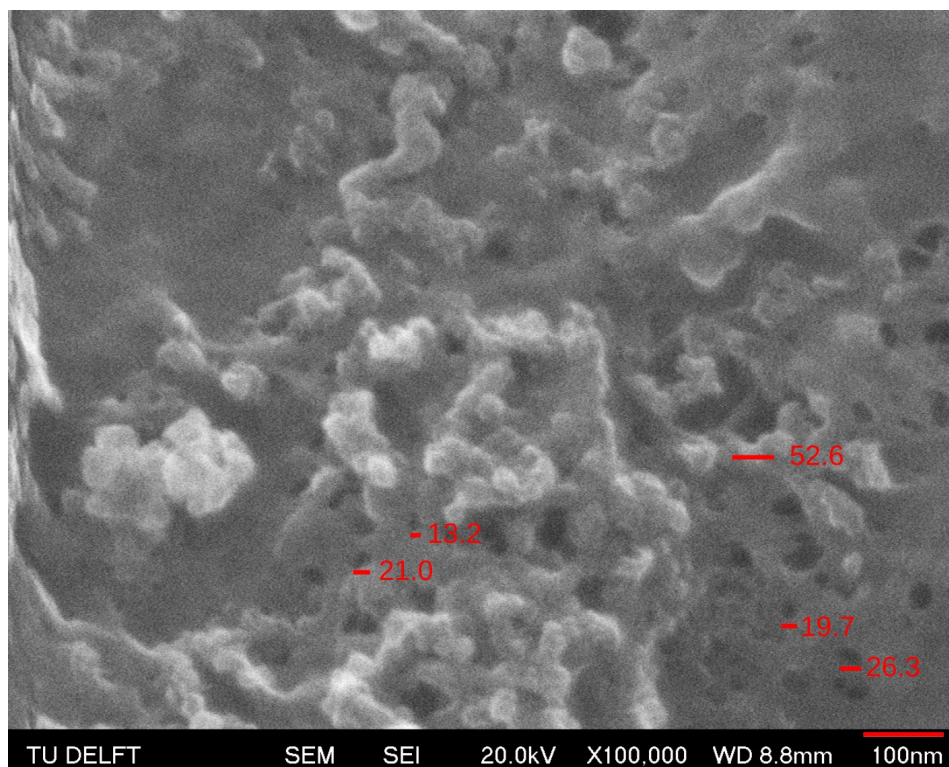


Figure 5.13: The surface of material 04/21 at a magnification 100,000x. From the scale at the bottom, it can be deduced that most pores are larger or in the order of 20 [nm]. Few pores are smaller than 20 [nm]. This validates the pore size measurements from the porometer which has a lower measuring limit of 19.4 [nm], see section 5.4.

Although the SEM measurement confirmed the presence of very small pores, which is essential for good permselectivity of the CME, these measurements do not provide any information about the underlying pore network *throughout* the membrane. Dead pores and blind pores will not contribute to the ion transport through the material. Therefore, SEM imaging was also used to look at the cross-section of the material. This allows us to verify whether the microstructure is homogeneous across the thickness of the material. First, the cross-section was studied by tearing the membrane and putting the membrane on its side in the electron microscope. When the images were taken of the torn cross-section, it looked like the microstructure had giant cavities with a lot of ragged edges. A very small content of carbon black particles was visible, indicating that the tear-line predominantly ran *through* the graphite particles, instead of in between. Tearing the CME gave SEM images that were completely opposite of what was expected. Therefore, cutting the CME was opted. The concern was that cutting is a shearing motion, compressing the microstructure of the material. But it turned out to cause much less damage to the microstructure compared to tearing the CME. Figure 5.14 shows that the spaces between the graphite flakes are filled up with carbon black particles and binder. As the carbon black and binder are filling the space between the larger graphite particles, it is therefore plausible that the carbon black and binder (i.e. pore structure) are running continuously through the thickness of the material.

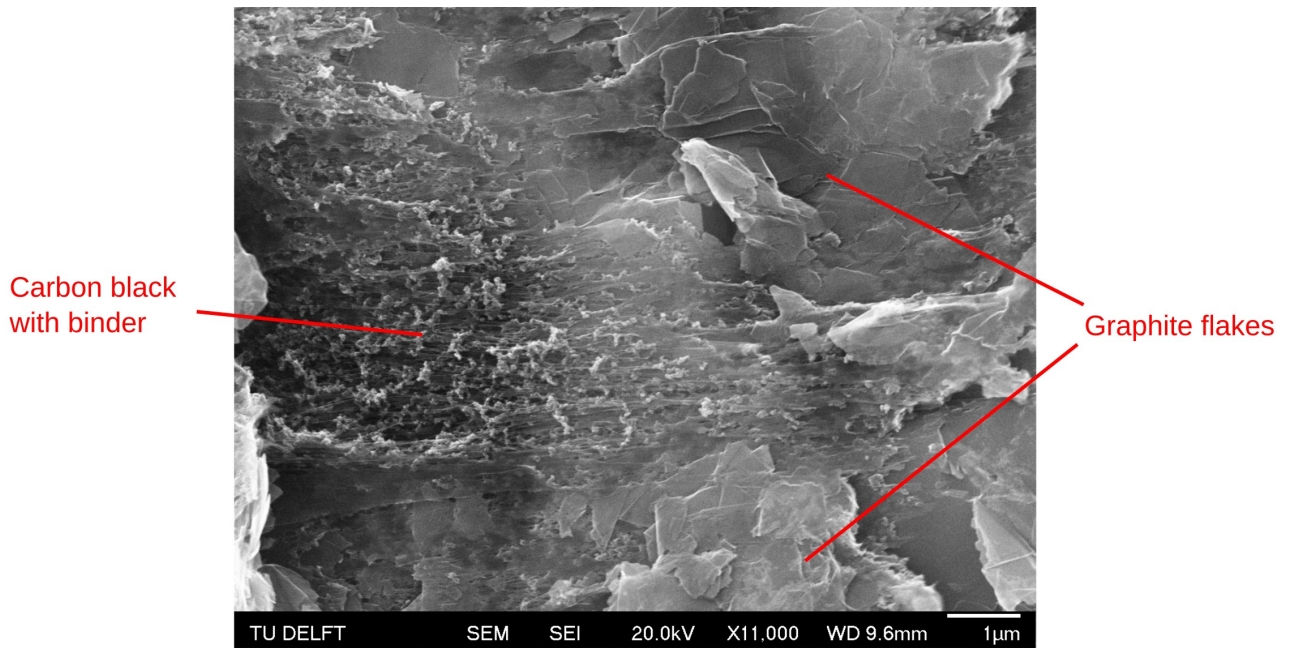


Figure 5.14: SEM figure of the cross-section of material 04/21 at a magnification 7,000x. A network of carbon black and binder is surrounded by graphite particles. As the carbon black and binder fill the space between the graphite particles, it is therefore plausible that the pore structure is running continuously through the thickness of the material.

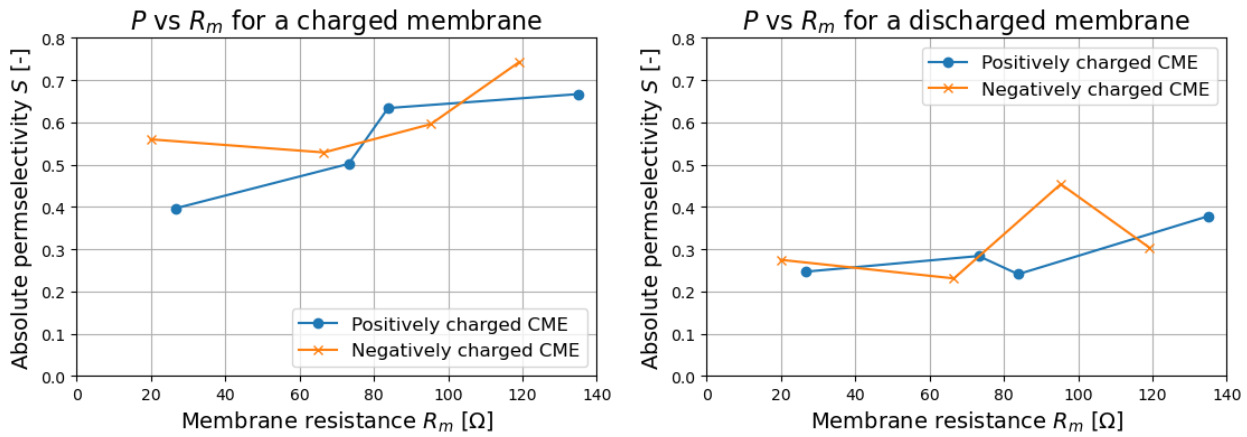
6

Discussion

Chapter 5 discussed the individual results from the permselectivity measurements, pore size measurements, and the SEM imaging. This chapter investigates whether there are correlations between these measurements. More specifically whether a correlation exists between the permselectivity and the pore size distribution data, as this will answer the main research question. Other correlations are investigated as well, such as: permselectivity vs membrane ionic resistance, fluid flow at MFPS vs membrane ionic resistance, and fluid flow at MFPS vs permselectivity. These correlations will be investigated in the subsequent paragraphs of this chapter.

Permselectivity vs membrane ionic resistance

The data from Table 5.1 shows that in general, membranes with a higher resistance had a higher permselectivity. A higher ion resistance would indicate a denser pore structure, with smaller pore sizes. However, this was not universally true. This trend becomes visible by plotting the absolute permselectivity vs the ionic membrane resistance, see Figure 6.1a. The only imperfection in the data is the upward kink in the negative curve on the left of the figure. This is considered to be a single anomaly that stems from the 09/04 material, and that in general can be stated that membranes with a higher ionic resistance have a higher permselectivity. Figure 6.1a plots the permselectivity with its respective resistance for four membranes. Due to the sample size being small, it cannot be stated that a physical correlation is proven. Furthermore, error bars are also not provided to estimate the uncertainty of the data points. The curves through the data points in Figure 6.1a merely guide the eye, to show that a higher membrane resistance generally indicates a higher permselectivity. In a discharged state there was no physical relation found between the permselectivity and membrane ionic resistance. When discharged, the permselectivity was similarly low for all membranes even though each membrane had a different resistance when uncharged. This can be seen in Figure 6.1b.



(a) The permselectivity plotted against membrane resistances from different membranes (b) The permselectivity plotted against membrane resistances from different membranes

Figure 6.1: The curves through the data point guide the eye, to show that generally speaking, a higher membrane resistance indicates a higher permselectivity.

Fluid flow at MFPS vs membrane ionic resistance

The data does suggest that there is a correlation between the membrane ionic resistance and the fluid flow at MFPS. It is expected that in the case of a highly porous membrane, the fluid may easily permeate through the microstructure. If this is the case for the fluid, then also the ions would easily permeate through, meaning that the ionic resistance of the membrane will also be low. The fluid flow data points were taken from Table 5.2, for each membrane the average fluid flow was calculated between two samples and compared with the membrane ionic resistance. The membrane resistance data points were taken from Table 5.1 before and after the floating phase. Even though the curves have an odd shape (at the lower right bottom they curve slightly upward) all data points are in fact close together. Also in the case of Figure 6.2 it should be noted that the sample size is small, and that a physical correlation cannot be proven. Error bars are also not present to estimate the uncertainty of the data points. The curves through the data points in Figure 6.2 merely indicate that a trend is present, namely that membranes with high ionic resistance show lower fluid permeation. Comparing these data points from two completely different measurement setups (the permselectivity measurements and the pore size measurements with the porometer), does give the confidence that there must be a connection between the physical properties and the electrical/permselectivity properties of a CME.

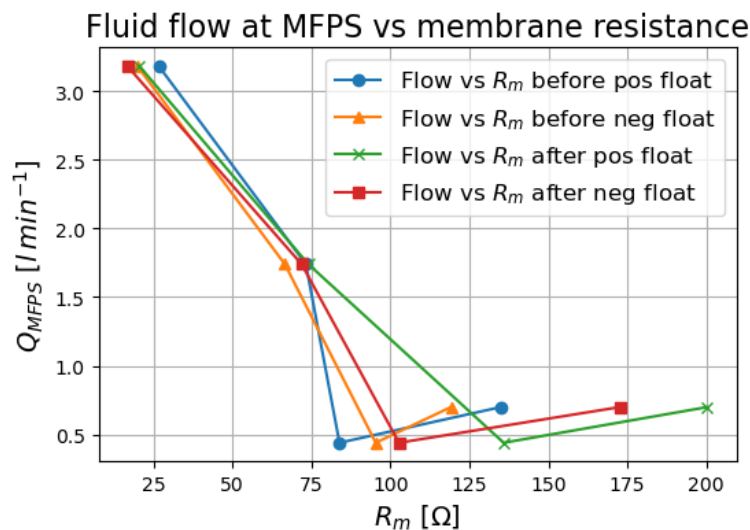


Figure 6.2: The data points of the fluid flow at MFPS are plotted against the 4 different membrane resistances of each material. The curves through the data points are drawn to indicate the trend that membranes with high fluid flow, also demonstrate low ionic resistance.

Pore size data and SEM discussion

When investigating the data of Table 5.2, it turned out that there were no correlations between many different combinations of pore size quantities. When the peak of a normal distribution is shifted to the left or the right, so do its edges shift to the left or the right. When looking at the pore size distributions, it would therefore be expected that a different mean pore size would lead to a different maximum and minimum pore size. However, this is not the case for the pore size data in Table 5.2. Samples from materials 09/04, 04/21, and gradient all have very similar maximum pore sizes, yet they have very different mean pore sizes and smallest pore sizes. This could be explained by looking at the composition of the membranes. The membrane materials from Table 3.2 are made out of the same ingredients. The graphite particles, carbon black particles, and PVDF have a finite size. The ingredients may be mixed at varying ratios, but the maximum and minimum pore sizes of the materials will probably stay the same due to the finite size of the particles.

The pore size measurements of the CMEs almost reached the measuring limit of 19.4 [nm] of the porometer. The measurements showed that the CME materials mostly had pore sizes smaller than 80 [nm], see Appendix C. To detect the smaller pore sizes higher operating pressures are needed. At elevated pressures pores might collapse, skewing the results. This might indicate that the capillary flow technique of the porometer is not suitable to accurately measure the pore size distribution for these types of membranes. On the other hand, SEM imaging showed that there were almost no pores smaller than the measuring limit of the porometer, to support the pore size measurements. However, with SEM imaging it is practically impossible to look at every square millimetre of the sample at a magnification of 100,000x. Therefore, it should be stated that the SEM figures give an indication of the validity of the pore size data, rather than truly verifying the validity of the pore size data. Microtrac, a company that produces pore size measuring equipment, states that "the bubble point method" (another name for capillary flow method) operates in the range of 50 [nm] until ≈ 100 [μm] [44]. For future research, using gas adsorption techniques such as BET (Brunauer, Emmett and Teller), may produce more reliable pore size data.

Fluid flow at MFPS vs permselectivity

Lastly, the fluid flow data at MFPS is compared with the permselectivity data. This comparison combines previous Figures 6.2 and 6.1a. From intuition, it is expected that higher fluid permeation through a membrane results in a lower permselectivity. A fluid will more easily permeate through a membrane that has a high pore count. If the fluid can easily permeate, then the ions will also permeate easily through the membrane, reducing the ionic resistance. Earlier it was established that membranes with low ionic resistance had lower permselectivities. Therefore, it is expected that membranes with high fluid permeation, also demonstrate lower permselectivities.

Looking at Figure 6.3, only the positive charge curve seems to show a correlation between the fluid flow and the permselectivity, where a high fluid flow corresponds with a low permselectivity. The correlation for the negative curve seems to be weak to non-existent. Again, there is a kink in the upper part of the negative curve, which corresponds to the kink in the negative curve of Figure 6.1a. To be able to prove that there is a correlation between the fluid flow through the CME and its permselectivity is not possible. Intuitively it can be said, that membranes that allow for higher fluid flows, also have lower permselectivities. This is what Figure 6.3 does seem to suggest.

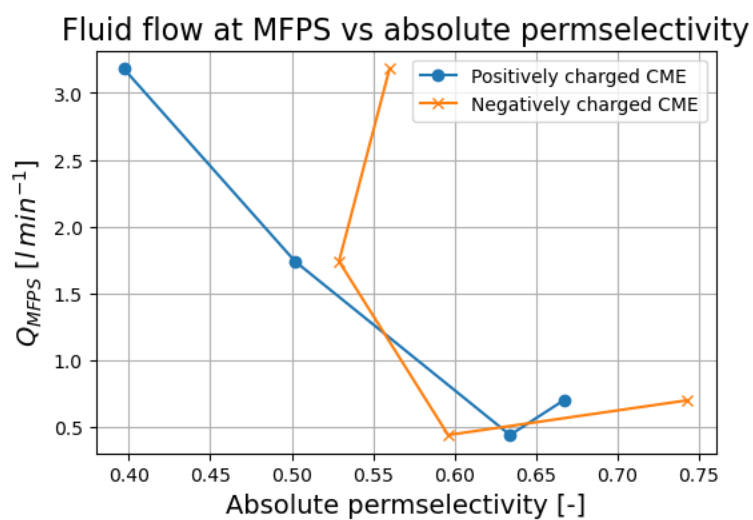


Figure 6.3: The fluid flow data is plotted w.r.t. the permselectivity data of each membrane. Only the positive curve suggests a trend that higher fluid flows lead to lower permselectivities. The negative curve does not show any correlation or trend. Also in this figure, the curves through the data points are merely a visual aid to help see a trend.

Conclusion & Recommendations

7.1. Conclusion

More areas around the world are being threatened by freshwater shortages. As a result, a lot of research is done on desalination and deionisation technologies. One of such technologies is capacitive deionisation (CDI). Recently, a multi-channel CDI architecture has been developed, where the capacitive membrane electrodes (CMEs) are between the separating channels. How selective these membranes are may depend on different factors. This thesis sought to find an answer to this question. The research is concluded by answering the research questions from the introduction:

How large is the effect of the pore size distribution on the ion transport and selectivity of porous carbon capacitive membrane electrodes?

The main research question cannot directly be answered as there did not seem to be a correlation in the data points of the pore size measurements. There is however a correlation between the "volumetric flow rate at the mean-flow-pore-size" with the ionic resistance of the porous carbon capacitive membrane electrodes (CME). This indicates that there must be a connection between the physical properties and the electrical/permselective properties of the CME. The data suggests that CMEs that allow for higher fluid flows have lower permselectivities. To reiterate, the main research question cannot be directly answered, with the pore size data from this research, it is impossible to quantify its effect on the selectivity of CME. When studying the data, it can at least be deemed plausible that the physical properties are connected to the electrical/permselective properties of the CME.

What will the experimental setup look like such that it can measure the ion transport and ion selectivity of a CME?

The membrane potential of a CME is used to determine the permselectivity of a CME. The membrane potential is measured in a cell by two probes close to the membrane, one on either side. The probes carry an ionic signal to the Ag-AgCl reference electrodes. The reference electrodes transduce the ionic signal in an electrical signal, which is measured by a source measuring unit (SMU). It was found that the system had a high internal resistance, in the order of 6.5 [MΩ]. An SMU has a high input resistance larger than 10 [GΩ], therefore an SMU was used to accurately measure the membrane potential. A power supply was used to charge the CME at 1 [V] w.r.t. a counter electrode in the cell. Magnetic stirrers were added to the setup to make sure that the solutions in the cell were properly mixed. The cells' charging behaviour and the input signal of the SMU were controlled by an Arduino and relay board combination. The measuring setup therefore consisted out of a cell, an Ag-AgCl reference electrode, an SMU, a power supply, magnetic stirrers, and an Arduino and relay board.

How can a mathematical model be built such that it can describe the permselectivity of the CME in terms of electrostatic potential and ion concentrations?

The permselectivity could mathematically be related to the membrane potential, the elementary charge, the Boltzmann constant, the temperature, and the natural logarithm of the concentration ratios. This mathematical

relation was derived from the chemical potential of two salt solutions separated by a membrane. One salt solution had a high salinity, the other a low salinity. In an isolated system, where the ions naturally migrate from high to low salinity, it can be stated that the flux for both positive (J_+) and negative (J_-) ions must be the same. By equating J_+ to J_- and substituting the chemical potential, a mathematical relation could be obtained for the permselectivity and the membrane potential. If the membrane potential was positive, then this would indicate a negatively permselective membrane. If a CME has a positive charge, then it will prefer the permeation of negative ions through its microstructure, and vice versa. The membrane is perfectly selective when the selectivity is equal to 1, and the membrane is not selective at all when the selectivity is equal to 0.

How can the pore size distribution of a CME be measured and which units quantify the pore size distribution?

The capillary flow technique can be used to measure the pore size distribution of porous CMEs. In the capillary flow technique, the fluid flow through and the pressure on the membrane are recorded over time. The pore size distribution was calculated with the pressure difference between the wet and dry measurements. The pressure difference stems from the capillary flow in the pores. A Porolux Revo porometer with a lower measuring limit of 20 [nm] was used to measure the pore size distribution. The porometer gives the following data points: the maximum pore size, the mean pore size, the mean flow pore size, the smallest pore size, and a pore size distribution. The pore size distribution is quantified by assigning an X percentage of fluid flow per pore size. SEM imaging was used to verify the validity of the pore size measurements. SEM figures pointed out that the vast majority of pores were 20 [nm] or larger.

Unfortunately, no correlations were found in the pore size data. For example, multiple membrane materials showed a similar maximum pore size, but had differing mean pore sizes. It is suspected that the capillary flow technique is not suitable for CME, as the measurements were performed close to the measuring limit of the porometer. Therefore, it is recommended for CMEs that the pore size distributions are measured with an alternative technique, such as gas adsorption techniques.

How can the measured pore size distributions be linked to the experimental values for ion selectivity and transport capability?

Selectivity measurements and pore size measurements were performed with 5 different membrane materials. The membrane materials were made with the same ingredients, but with varying ratios of these ingredients. The selectivity data was compared with the pore size data for each membrane. Due to the small sample size and the fact that no error bars could be given, no physical relationships can be *proven*. There are a few trends visible in the comparisons, however. It was observed that membranes with high fluid permeation showed lower permselectivities and lower ionic resistances. If a membrane allows for high fluid permeation (due to a large number of pores), then also the ions will easily permeate through the microstructure, indicating lower ionic resistance. Intuitively, when the ion resistance of a membrane is lower, then both positive and negative ions can migrate more easily through the membrane, which would indicate lower permselectivity.

7.2. Recommendations for future research

Below a list of points is given for recommended research in the future.

- The pore size measurements were carried out with a Porolux Revo porometer that utilises the capillary flow technique. The measurements were performed at the measuring limit of the machine. Therefore, it is recommended for future research that pore size measurements are carried out with a different technology, such as gas adsorption or mercury intrusion techniques.
- The sample size of the comparison carried out in chapter 6 is too small to draw any meaningful conclusion. Therefore, the sample size of tested membranes should be increased.
- During testing the cell had some minor leaks. To make sure that this does not affect the measurements, improvements of the cell are needed such that the design is 100 % leak-free.
- During testing two potentials were measured. Because only one SMU was present, an Arduino controlled relay board was added to the setup. Allowing to switch input signals to the SMU repetitively. If budget permits, a second SMU should be added to the setup to measure two potentials simultaneously. This leads to less information being lost in the data.
- The thickness of the CME has been recorded, as the porometer required this as an input. It is recommended to investigate if the thickness of a CME can be correlated to other CME properties, such as: the

membrane ionic resistance, permselectivity, and porosity.

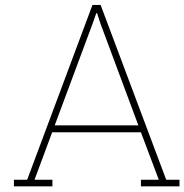
- It had been discovered that the CME starts to oxidise for charging potentials at or above 1.2 [V]. This effect happened during positive cycles, where the membrane potentials started to become smaller and smaller. Negative cycles seemed to reverse this effect, but not completely. It should be investigated how this mechanism exactly works, and how long a negative cycle should last to completely counteract the effect of membrane oxidation. Using different charge potentials for the positive cycle and negative cycle should also be tested. Does a negative cycle allow for higher potentials compared to positive cycles without damaging the CME? Also, SEM images should be taken before and after the oxidation has taken place, to verify how oxidation affects the microstructure of the CME.

References

- [1] TutorChase. *Why is it important to use distilled water in experiments?* URL: <https://www.tutorchase.com/answers/igcse/chemistry/why-is-it-important-to-use-distilled-water-in-experiments>. *date accessed: 07 apr 2024*.
- [2] T. Arunkumar et al. "Energy efficient materials for solar water distillation - A review". In: *Renewable and Sustainable Energy Reviews* 115 (2019), p. 109409. DOI: 10.1016/J.RSER.2019.109409.
- [3] CapeCoralBreeze. *The history of Cape Coral utilities at a glance*. URL: <https://www.capecoralbreeze.com/cape-history/cape-corals-50th-anniversary/2020/09/18/the-history-of-cape-coral-utilities-at-a-glance/>. *date accessed: 07 apr 2024*.
- [4] Muhammad Qasim et al. "Reverse osmosis desalination: A state-of-the-art review". In: *Desalination* 459 (2019), pp. 59–104. DOI: 10.1016/J.DESAL.2019.02.008.
- [5] Mohan Qin et al. "Comparison of energy consumption in desalination by capacitive deionization and reverse osmosis". In: *Desalination* 455 (2019), pp. 100–114. DOI: 10.1016/J.DESAL.2019.01.003.
- [6] Shu Yuan Pan et al. "Brackish water desalination using reverse osmosis and capacitive deionization at the water-energy nexus". In: *Water Research* 183 (2020), p. 116064. DOI: 10.1016/J.WATRES.2020.116064.
- [7] S Porada et al. "Direct prediction of the desalination performance of porous carbon electrodes for capacitive deionization". In: *Energy Environ Sci* 6 (2013), pp. 3700–3712. DOI: 10.1039/c3ee42209g. URL: www.rsc.org/ees.
- [8] Xudong Zhang et al. "Selective ion separation by capacitive deionization (CDI) based technologies: a state-of-the-art review". In: *Environ. Sci.: Water Res. Technol* 6 (2020), pp. 243–257. DOI: 10.1039/c9ew00835g.
- [9] M E Suss et al. "Water desalination via capacitive deionization: what is it and what can we expect from it?". In: *Energy Environ. Sci* 8 (2015), pp. 2296–2319. DOI: 10.1039/c5ee00519a. URL: www.rsc.org/ees.
- [10] Xitong Liu et al. "Cost Comparison of Capacitive Deionization and Reverse Osmosis for Brackish Water Desalination". In: *ACS ES and T Engineering* 1.2 (Feb. 2021), pp. 261–273. ISSN: 26900645. DOI: 10.1021/ACSESTENG.0C00094/SUPPL{_}FILE/EE0C00094{_}SI{_}001.PDF. URL: <https://dx.doi.org/10.1021/acsestengg.0c00094>.
- [11] Lutfi Agartan et al. "Influence of operating conditions on the desalination performance of a symmetric pre-conditioned Ti3C2Tx-MXene membrane capacitive deionization system". In: *Desalination* 477 (2020), p. 114267. DOI: 10.1016/J.DESAL.2019.114267.
- [12] Zhizhao He et al. "Optimization of constant-current operation in membrane capacitive deionization (MCDI) using variable discharging operations". In: *Water Research* 204 (2021), p. 117646. DOI: 10.1016/J.WATRES.2021.117646.
- [13] Lin Chen, Fudong He, and Fangqing Li. "Denitrification enhancement by electro-adsorption/reduction in capacitive deionization (CDI) and membrane capacitive deionization (MCDI) with copper electrode". In: *Chemosphere* 291 (2022), p. 132732. DOI: 10.1016/J.CHEMOSPHERE.2021.132732.
- [14] Robert McNair, Gyorgy Szekely, and Robert A W Dryfe. "Ion-Exchange Materials for Membrane Capacitive Deionization". In: *ACS EST Water* 1 (2021), pp. 217–239. DOI: 10.1021/acsestwater.0c00123. URL: <https://dx.doi.org/10.1021/acsestwater.0c00123>.
- [15] Robert McNair, Gyorgy Szekely, and Robert A.W. Dryfe. "Sustainable processing of electrodes for membrane capacitive deionization (MCDI)". In: *Journal of Cleaner Production* 342 (2022), p. 130922. DOI: 10.1016/J.JCLEPRO.2022.130922.
- [16] Filtration Separation. *Voltea helps secure water supply for manufacturer in South Africa*. URL: <https://www.filtsep.com/content/features/voltea-helps-secure-water-supply-for-manufacturer-in-south-africa/>. *Date accessed: 01 jun 2023*.
- [17] Xin Gao et al. "Surface charge enhanced carbon electrodes for stable and efficient capacitive deionization using inverted adsorption-desorption behavior †". In: *Energy & Environmental Science* 8 (2015), pp. 897–909. DOI: 10.1039/c4ee03172e. URL: www.rsc.org/ees.

- [18] P. M. Biesheuvel, S. Porada, and J. E. Dykstra. "The difference between Faradaic and Nonfaradaic processes in Electrochemistry". In: *arXiv:1809.02930 [physics.chem-ph]* (2018). URL: <http://arxiv.org/abs/1809.02930>.
- [19] Changyong Zhang et al. "Flow Electrode Capacitive Deionization (FCDI): Recent Developments, Environmental Applications, and Future Perspectives". In: *Environ. Sci. Technol* 55 (2021), pp. 4243–4267. DOI: 10.1021/acs.est.0c06552. URL: <https://doi.org/10.1021/acs.est.0c06552>.
- [20] Yong Uk Shin et al. "Improving the feasibility and applicability of flow-electrode capacitive deionization (FCDI): Review of process optimization and energy efficiency". In: *Desalination* 502 (2021), p. 114930. DOI: 10.1016/J.DESAL.2021.114930.
- [21] N.J.H. Boon. *Patent | Deionization device and method for at least partially deionizing a feed liquid in which an electrolyte is dissolved, and apparatuses using such devices*. URL: <https://www.patentguru.com/search?q=US11772992B2>. Patent no: US11772992B2.
- [22] J.D. Seader, Ernest J. Henley, and D. Keith Roper. *Separation Process Principles - Third Edition*. 2010, pp. 527–530. ISBN: 978-0-470-48183-7.
- [23] Chen Zhang et al. "A positive-negative alternate adsorption effect for capacitive deionization in nanoporous carbon aerogel electrodes to enhance desalination capacity". In: *Desalination* 458 (2019), pp. 45–53. DOI: 10.1016/J.DESAL.2019.01.023.
- [24] Jung Eun Cha et al. "A practical approach to measuring the ion-transport number of cation-exchange membranes: Effects of junction potential and analyte concentration". In: *Journal of Membrane Science* 635 (2021). DOI: 10.1016/j.memsci.2021.119471.
- [25] Ali Hemmatifar, Michael Stadermann, and Juan G. Santiago. "Two-Dimensional Porous Electrode Model for Capacitive Deionization". In: *Journal of Physical Chemistry C* 119.44 (2015), pp. 24681–24694. DOI: 10.1021/acs.jpcc.5b05847.
- [26] Martin Z. Bazant. *Lecture 24: Diffuse Charge in Electrolytes MIT Student 1. Poisson-Nernst-Planck Equations*. Tech. rep. Massachusetts Institute of Technology, 2011.
- [27] Zhen Chao, Weihua Geng, and Robert Krasny. "Integral equation method for the 1D steady-state Poisson-Nernst-Planck equations". In: *Journal of Computational Electronics* 22 (2023), pp. 1396–1408. DOI: 10.1007/s10825-023-02092-y. URL: <https://doi.org/10.1007/s10825-023-02092-y>.
- [28] Allen Flavell et al. "A conservative finite difference scheme for Poisson-Nernst-Planck equations". In: *J Comput Electron* 13 (2014), pp. 235–249. DOI: 10.1007/s10825-013-0506-3.
- [29] Viktoria R T Hsu. "Almost Newton method for large flux steady-state of 1D Poisson-Nernst-Planck equations". In: *Journal of Computational and Applied Mathematics* 183 (2005), pp. 1–15. DOI: 10.1016/j.cam.2004.12.024. URL: www.elsevier.com/locate/cam.
- [30] B Matejczyk et al. "Asymptotic models for transport in large aspect ratio nanopores †". In: *Jnl of Applied Mathematics* 30 (2019), pp. 557–584. DOI: 10.1017/S0956792518000293. URL: <https://doi.org/10.1017/S0956792518000293>.
- [31] Marina Micari et al. *Reverse electrodialysis heat engine (REDHE)*. Woodhead Publishing, Jan. 2022, pp. 127–162. ISBN: 9780081028476. DOI: 10.1016/B978-0-08-102847-6.00004-8.
- [32] Lidieta Giorno, Enrico Drioli, and Heiner Strathmann. "Permselectivity of Ion-Exchange Membranes". In: *Encyclopedia of Membranes* (2016). Ed. by Enrico Drioli and Lidieta Giorno, pp. 1490–1493. DOI: 10.1007/978-3-662-44324-8_{1435}. URL: https://link.springer.com/referenceworkentry/10.1007/978-3-662-44324-8_1435.
- [33] Juxiu Tong et al. "Experimental study on soluble chemical transfer to surface runoff from soil". In: *Environmental Science and Pollution Research* 23.20 (Oct. 2016), pp. 20378–20387. DOI: 10.1007/S11356-016-7248-2. URL: https://www.researchgate.net/publication/305636160_Experimental_study_on_soluble_chemical_transfer_to_surface_runoff_from_soil.
- [34] Tektronix. *2450 SourceMeter SMU Instrument Datasheet*.
- [35] Sigma Aldrich. *Aldrich® glass reference electrode*. URL: <https://www.sigmaaldrich.com/NL/en/product/aldrich/z113085>. date accessed: 10 apr 2024.
- [36] Engineering Toolbox. *Water - Density, Specific Weight and Thermal Expansion Coefficients*. URL: https://www.engineeringtoolbox.com/water-density-specific-weight-d_595.html.
- [37] IB-FT GmbH. *Training slides Porolux revo*. Berlin, Germany, 2023.
- [38] Aqion. *Table of Diffusion Coefficients*. URL: <https://www.aqion.de/site/diffusion-coefficients>. Date accessed: 15 mar 2024.
- [39] Britannica. *Seawater*. URL: <https://www.britannica.com/science/seawater>. date accessed: 29 mar 2024.

- [40] Changyong Zhang et al. "Faradaic reactions in capacitive deionization (CDI) - problems and possibilities: A review". In: *Water Research* 128 (Jan. 2018), pp. 314–330. DOI: 10.1016/J.WATRES.2017.10.024.
- [41] LibreTexts Chemistry. *8.6: The pH Concept*. URL: [https://chem.libretexts.org/Courses/University_of_Kentucky/UK%3A_CHE_103_-_Chemistry_for_Allied_Health_\(Soult\)/Chapters/Chapter_8%3A_Properties_of_Solutions/8.6%3A_The_pH_Concept](https://chem.libretexts.org/Courses/University_of_Kentucky/UK%3A_CHE_103_-_Chemistry_for_Allied_Health_(Soult)/Chapters/Chapter_8%3A_Properties_of_Solutions/8.6%3A_The_pH_Concept). *date accessed: 12 apr 2024*.
- [42] Sensortechnik Meinsberg. *Standard potentials of reference electrodes*. URL: <https://www.meinsberger-elektroden.de/en/ueberblick/potential.html>. *date accessed: 11 apr 2024*.
- [43] IB-FT GmbH. *Operating Manual Porometer POROLUX Revo*. Berlin, Germany, 2023.
- [44] Microtrac. *Expression of Pore Size Distribution*. URL: <https://www.microtrac.com/applications/knowledge-base/expression-of-pore-size-distribution/>. *Date accessed: 29 mar 2024*.



Code files

Section A.1 shows the python code that was used to filter, process and analyse the data. Section A.2 shows the Arduino code that controls the relay board.

A.1. Python Code

```
1 #!/usr/bin/env python3
2 # -*- coding: utf-8 -*-
3 """
4 Created on Wed Nov  8 16:29:54 2023
5
6 @author: ruben
7 """
8
9 import csv
10 import math
11 import pandas as pd
12 import numpy as np
13 import matplotlib.pyplot as plt
14
15 ### Positive cycle
16 #import the data and extract positive charge cycle and reference measurements
17 df = pd.read_csv('/home/ruben/Documents/Universiteit/university documents 5/ME55035 ME-EFPT MSc
18 Thesis/E Measurements/20231106/laadcyclus.csv', skiprows=8) #read the csv file
19 df = df.filter(items=["Reading","Relative Time"]) #discard any irrelevant information
20 df.rename(columns = {'Relative Time':'Time'}, inplace = True) #rename last column
21 pos = df[(df.Time > 103) & (df.Time < 3080)] #seperate positive charge cycle
22 ref = df[(df.Time < 55) + (df.Time > 7361) & (df.Reading < 0)] #collect reference potentials
23
24 #plot reference data
25 V_ref = np.array(ref["Reading"]*1000)
26 t_ref = np.array(ref["Time"])
27 plt.figure(0)
28 plt.plot(t_ref,V_ref)
29 plt.axis([min(t_ref),max(t_ref),min(V_ref)-0.05,max(V_ref)+0.05])
30 plt.xlabel("Time [seconds]")
31 plt.ylabel("Measured potential [mV]")
32 plt.title("Reference potential, date 2023-11-06")
33 plt.grid()
34
35 # Calculate the average reference potential
36 ref = ref.to_numpy() # Convert df to array
37 avg = sum(ref[:,0])/len(ref[:,0])*1000 # Calculate average in [mV]
38 print("The reference potential is: ",avg,"[mV]")
39
40 #####
41 # separate the CME electrical potential from the data frame pos
42 V_meas = pos # V_meas becomes a dataframe
43 V_meas = V_meas.to_numpy() # Convert V_meas from df to array
```

```

43
44 # Filter out any peaks that occurred due to switching the measured signal
45 # This is done by designing a pulse train. The pulse train is 0 where peaks
46 # occur in the original signal. This is done by tuning the parameters below
47 pulse_width = 7 # Width of each pulse (in seconds)
48 total_duration = len(V_meas[:,0]) # Total duration of the pulse train (in seconds)
49 pulse_interval = 24.23 # Time between the start of each pulse (in seconds)
50 pulse_offset = 2.7 # The initial offset w.r.t. the y-axis of the pulse
51
52 time = np.arange(0, total_duration, 1) # Time values from 0 to total_duration, steps of 1 second
53
54 pulse_train = np.zeros(len(time)) # Initialize an array of zeros
55 for t in np.arange(0, total_duration, pulse_interval):
56     start_index = int(t+pulse_offset) # Convert time to an index
57     end_index = start_index + int(pulse_width) # Convert pulse_width to indices
58     pulse_train[start_index:end_index] = 1
59
60
61 V_cme = V_meas[:,0]*pulse_train # Multiply the measurements with the pulse train
62 t = V_meas[:,1]*pulse_train # Multiply the time values with the pulse train
63 V_cme = np.delete(V_cme, np.where((V_cme == 0))[0], axis=0) # Delete all zeros from array
64 t = np.delete(t, np.where((t == 0))[0], axis=0) # Delete all zeros from array
65
66 # plot the electrical potential of the CME
67 plt.figure(2)
68 plt.plot(t,V_cme)
69 plt.axis([0,max(t),0,max(V_cme)+0.05])
70 plt.xlabel("Time [seconds]")
71 plt.ylabel("CME potential [V]")
72 plt.title("Electric potential during positive charge cycle, date 2023-11-06")
73 plt.grid()
74
75
76 #####
77 # separate the membrane potential from the data frame pos
78 V_meas = pos # V_m becomes a dataframe
79 V_meas = V_meas.to_numpy() # Convert V_cme from df to array
80
81 # Filter out any peaks that occurred due to switching the measured signal
82 # This is done by designing a pulse train. The pulse train is 0 where peaks
83 # occur in the original signal. This is done by tuning the parameters below
84 pulse_width1 = 7 # Width of each pulse (in seconds)
85 total_duration1 = len(V_meas[:,0]) # Total duration of the pulse train (in seconds)
86 pulse_interval1 = 24.23 # Time between the start of each pulse (in seconds)
87 pulse_offset1 = 14.7 # The initial offset w.r.t. the y-axis of the pulse
88
89 time1 = np.arange(0, total_duration1, 1) # Time values from 0 to total_duration, steps of 1 second
90
91 pulse_train1 = np.zeros(len(time1)) # Initialize an array of zeros
92 for t1 in np.arange(0, total_duration1, pulse_interval1):
93     start_index1 = int(t1+pulse_offset1) # Convert time to an index
94     end_index1 = start_index1 + int(pulse_width1) # Convert pulse_width to indices
95     pulse_train1[start_index1:end_index1] = 1
96
97
98 V_m = (V_meas[:,0]*pulse_train1*1000) # Multiply the measurements with the pulse train
99 t1 = V_meas[:,1]*pulse_train1 # Multiply the time values with the pulse train
100 V_m = np.delete(V_m, np.where((V_m == 0))[0], axis=0) # Delete all zeros from array
101 V_m = V_m - avg
102 t1 = np.delete(t1, np.where((t1 == 0))[0], axis=0) # Delete all zeros from array
103
104
105 # plot the membrane potential
106 plt.figure(3)
107 plt.plot(t1,V_m)
108 plt.axis([min(t1),max(t1),min(V_m)-0.05,40])
109 plt.xlabel("Time [seconds]")
110 plt.ylabel("Membrane potential [mV]")
111 plt.title("Corrected mem. pot; CH/CL = 1.00[g/L] / 0.25 [g/L], date 2023-11-06")
112 plt.grid()
113

```



```

114 #####
115 # plot the membrane potential vs the electrical potential
116 # only the discharge phase is considered
117 # data during short circuit is omitted
118 A = np.column_stack((t,V_cme,t1,V_m))
119 A = np.delete(A, np.where((V_m < -8.3)|(V_m>10))[0], axis=0)
120
121
122 plt.figure(4)
123 plt.scatter(A[:,1],A[:,3],s=3)
124 plt.axis([min(A[:,1]),max(A[:,1]),min(A[:,3])-0.5,max(A[:,3])+0.5])
125 plt.xlabel("Electrical potential of the CME [V]")
126 plt.ylabel("Membrane potential [mV]")
127 plt.title("Positive charge cycle, membrane potential vs the electrical potential, date 2023-11-06")
128 plt.grid()
129
130
131 ### Negative cycle
132 #import the data and extract negative charge cycle and reference measurements
133 df = pd.read_csv('/home/ruben/Documents/Universiteit/university documents 5/ME55035 ME-EFPT MSc
134 Thesis/E Measurements/20231106/laadcyclus.csv', skiprows=8) #read the csv file
135 df = df.filter(items=["Reading","Relative Time"]) #discard any irrelevant information
136 df.rename(columns = {'Relative Time':'Time'}, inplace = True) #rename last column
137 neg = df[(df.Time > 3678) & (df.Time < 6673)] #seperate negative charge cycle
138 ref = df[(df.Time < 55) + (df.Time > 7361) & (df.Reading < 0)] #collect reference potentials
139
140 # Calculate the average reference potential
141 ref = ref.to_numpy() # Convert df to array
142 avg = sum(ref[:,0])/len(ref[:,0])*1000 # Calculate average in [mV]
143 print("The reference potential is: ",avg,"[mV]")
144 #####
145 # separate the CME electrical potential from the data frame neg
146 V_meas = neg # V_meas becomes a dataframe
147 V_meas = V_meas.to_numpy() # Convert V_meas from df to array
148
149 # Filter out any peaks that occurred due to switching the measured signal
150 # This is done by designing a pulse train. The pulse train is 0 where peaks
151 # occur in the original signal. This is done by tuning the parameters below
152 pulse_width = 7 # Width of each pulse (in seconds)
153 total_duration = len(V_meas[:,0]) # Total duration of the pulse train (in seconds)
154 pulse_interval = 24.23 # Time between the start of each pulse (in seconds)
155 pulse_offset = 2.5 # The initial offset w.r.t. the y-axis of the pulse
156
157 time = np.arange(0, total_duration, 1) # Time values from 0 to total_duration, steps of 1 second
158
159 pulse_train = np.zeros(len(time)) # Initialize an array of zeros
160 for t in np.arange(0, total_duration, pulse_interval):
161     start_index = int(t+pulse_offset) # Convert time to an index
162     end_index = start_index + int(pulse_width) # Convert pulse_width to indices
163     pulse_train[start_index:end_index] = 1
164
165
166 V_cme = V_meas[:,0]*pulse_train # Multiply the measurements with the pulse train
167 t = V_meas[:,1]*pulse_train # Multiply the time values with the pulse train
168 V_cme = np.delete(V_cme, np.where((V_cme == 0))[0], axis=0) # Delete all zeros from array
169 t = np.delete(t, np.where((t == 0))[0], axis=0) # Delete all zeros from array
170
171 # plot the electrical potential of the CME
172 plt.figure(6)
173 plt.plot(t,V_cme)
174 plt.axis([min(t),max(t),min(V_cme)-0.05,max(V_cme)+0.05])
175 plt.xlabel("Time [seconds]")
176 plt.ylabel("CME potential [V]")
177 plt.title("Electric potential during negative charge cycle, date 2023-11-06")
178 plt.grid()
179
180
181 #####
182 # separate the membrane potential from the data frame neg
183 V_meas = neg # V_m becomes a dataframe

```

```

184 V_meas = V_meas.to_numpy()      # Convert V_cme from df to array
185
186 # Filter out any peaks that occurred due to switching the measured signal
187 # This is done by designing a pulse train. The pulse train is 0 where peaks
188 # occur in the original signal. This is done by tuning the parameters below
189 pulse_width1 = 7 # Width of each pulse (in seconds)
190 total_duration1 = len(V_meas[:,0]) # Total duration of the pulse train (in seconds)
191 pulse_interval1 = 24.23 # Time between the start of each pulse (in seconds)
192 pulse_offset1 = 14.6 # The initial offset w.r.t. the y-axis of the pulse
193
194 time1 = np.arange(0, total_duration1, 1) # Time values from 0 to total_duration, steps of 1 second
195
196 pulse_train1 = np.zeros(len(time1)) # Initialize an array of zeros
197 for t1 in np.arange(0, total_duration1, pulse_interval1):
198     start_index1 = int(t1+pulse_offset1) # Convert time to an index
199     end_index1 = start_index1 + int(pulse_width1) # Convert pulse_width to indices
200     pulse_train1[start_index1:end_index1] = 1
201
202
203 V_m = (V_meas[:,0]*pulse_train1*1000) # Multiply the measurements with the pulse train
204 t1 = V_meas[:,1]*pulse_train1 # Multiply the time values with the pulse train
205 V_m = np.delete(V_m, np.where((V_m == 0))[0], axis=0) # Delete all zeros from array
206 V_m = V_m - avg
207 t1 = np.delete(t1, np.where((t1 == 0))[0], axis=0) # Delete all zeros from array
208
209
210 # plot the membrane potential
211 plt.figure(7)
212 plt.plot(t1,V_m)
213 plt.axis([min(t1),max(t1),min(V_m)-0.005,max(V_m)+0.005])
214 plt.xlabel("Time [seconds]")
215 plt.ylabel("Membrane potential [mV]")
216 plt.title("Corrected neg. mem. pot; C_H/C_L = 1.00 [g/L] / 0.25 [g/L], date 2023-11-06")
217 plt.grid()
218
219 #####
220 # plot the membrane potential vs the electrical potential
221 # only the discharge phase is considered
222 # data during short circuit is omitted
223 V_cme = np.delete(V_cme, -1)
224 t = np.delete(t, -1)
225 B = np.column_stack((t,V_cme,t1,V_m))
226 B = np.delete(B, np.where((V_m < -19)|(V_m > 0))[0], axis=0)
227
228 plt.figure(8)
229 plt.scatter(B[:,1],B[:,3],s=3)
230 plt.axis([min(B[:,1]),max(B[:,1]),min(B[:,3])-0.5,max(B[:,3])+0.5])
231 plt.xlabel("Electrical potential of the CME [V]")
232 plt.ylabel("Membrane potential [mV]")
233 plt.title("Negative charge cycle, membrane potential vs the electrical potential, date 2023-11-06")
234 plt.grid()
235
236
237 ### Combined cycles
238 # Plot the membrane potential vs the electrical potential and combine the cycles
239 plt.figure(9,figsize=(8,8))
240 plt.scatter(A[:,1],A[:,3],s=3)
241 plt.scatter(B[:,1],B[:,3],s=3)
242 plt.axis([min(B[:,1])-0.01,max(A[:,1])+0.01,min(B[:,3])-0.5,max(A[:,3])+0.5])
243 plt.xlabel("Electrical potential of the CME [V]")
244 plt.ylabel("Membrane potential [mV]")
245 plt.title("combined cycles, membrane potential vs the electrical potential, date 2023-11-06")
246 plt.legend(['Positive discharge', 'Negative discharge'])
247 plt.grid()
248 plt.show()
249
250
251 # Define some constants
252 e = 1.60217663E-19 # Elementary charge
253 k_b = 1.380649E-23 # Boltzmann constant
254 T = 298 # Temperature in Kelvin

```

```

255 V_t = k_b*T/e          # Calculate the thermanl potential
256 C_H = 1.000            # High salt concentration [g/L]
257 C_L = 0.250            # Low salt concentration [g/L]
258 D1 = 1
259 D2 = 1
260
261 # Calculate the selectivity with the above constants and the membrane potential
262 # data from matrices A and B
263 S_A = []
264 for i in A[:,3]:
265     S = ((V_t*math.log(C_H/C_L))*(D1-D2) + (i/1000)*(D1+D2))/((V_t*math.log(C_H/C_L))*(D1+D2) + (i
        /1000)*(D1-D2))
266     S_A.append(S)
267
268 S_B = []
269 for i in B[:,3]:
270     S = ((V_t*math.log(C_H/C_L))*(D1-D2) + (i/1000)*(D1+D2))/((V_t*math.log(C_H/C_L))*(D1+D2) + (i
        /1000)*(D1-D2))
271     S_B.append(S)
272
273
274 print('Highest selectivity =', max(S_A))
275 print('Highest selectivity =', min(S_B))
276
277 # Plot the selectivity vs the electical potential of the CME
278 plt.figure(10,figsize=(6,6),dpi=300)
279 plt.scatter(A[:,1],S_A,s=3,color='green')
280 plt.scatter(B[:,1],S_B,s=3,color='red')
281 plt.axis([min(B[:,1])-0.05,max(A[:,1])+0.05,min(S_B)-0.05,max(S_A)+0.05])
282 plt.xlabel("Electrical potential of the CME [V]", fontsize=14)
283 plt.ylabel("Perm selectivity []", fontsize=14)
284 plt.title("Selectivity vs electrical charge, material 04/21", fontsize=16)
285 plt.legend(['Positive float', 'Negative float'], fontsize=12)
286 plt.grid()
287 plt.show()
288
289 ##### Plot both mebrane potentials #####
290 m = A[0,2]
291 for j in range(0,len(A)):
292     A[j,2] = A[j,2]-m
293 n = B[0,2]
294 for k in range(0,len(B)):
295     B[k,2] = B[k,2]-n
296
297 plt.figure(11,figsize=(6,4),dpi=300)
298 plt.scatter(A[:,2],S_A, color='green', s=3, label='Positive Float')
299 plt.scatter(B[:,2],S_B, color='red', s=3, label='Negative Float')
300 plt.axis([0,max(max(A[:,2]),max(B[:,2])), -0.65,0.25])
301 plt.xlabel('Time [s]', fontsize=14)
302 plt.ylabel('Perm selectivity [-]',fontsize=14)
303 plt.title('Selectivity during floating phase', fontsize=16)
304 plt.grid()
305 plt.legend(['Positive float', 'Negative float'], loc='upper right', fontsize=12)
306 textstr = '$V_{charge}$ = 1.0 [V]'
307 plt.text(0.65, 0.10, textstr, fontsize=14, transform=plt.gca().transAxes,
308         verticalalignment='center', bbox=dict(facecolor='lightgrey', alpha=0.5))
309
310 print("highest absolute selectivity" , max(max(S_A), -1*min(S_B)))
311 print("Maximum charge" , max(V_cme),-1*min(V_cme))
312 print("lowest absolute selectivity" , max(max(S_A), min(S_B)))

```

A.2. Arduino code

```

1 /*
2  NOMENCLATURE:
3  RE = refence electrode
4  CME = capacitive membrane electrode
5  CE = counter electrode
6  R+ = positive pole resistor
7  R- = negative pole resistor

```

```

8
9   This script was written to alternate between measuring the potential over the two REs and the
    potential of the CME w.r.t. one of the REs.
10  Next, 6 charging and discharging phases of the cell are controlled and looped by this script.
11
12  Written by N.J.H Boon 06 oct 2023
13  Rewritten by G.H.R. Vos 22 dec 2023
14
15  */
16
17  const int Rdat = 13;          // the number of the LED pin
18  const int Lat = 12;           // the number of the LED pin
19  const int Clk = 11;           // the number of the LED pin
20  #define NRModes 10
21  int8_t Setting[NRModes];
22  long Times[NRModes];
23  long NextSwitchTime=0;
24  long NextMeasurementTime=0;
25  long NextSCTime=0;
26  int CurrentMode=-1;
27  int MeasureMode=-1;
28  int SCmode=-1;
29
30  //=====
31  //define the charge and discharge phases, by determining which relays have to be turned on and for
    how long
32  void setup() {
33    // initialize serial communications at 9600 bps:
34    Serial.begin(115200);
35    pinMode(Rdat, OUTPUT);
36    pinMode(Lat, OUTPUT);
37    pinMode(Clk, OUTPUT);
38    Setting[0] = B01100000; Times[0]=1200;          //Positive charging. Relay 2 & 3 turned on
39    Setting[1] = B01101000; Times[1]=20;            //Put current through CME
40    Setting[2] = B01000000; Times[2]=1800;          //Positive floating. Relay 2 turned on to keep
    negative pole connected
41    Setting[3] = B01101000; Times[3]=20;            //Put current through CME
42    Setting[4] = B01010000; Times[4]=600;           //Short circuit cell. To completely discharge CME
43    Setting[5] = B10010000; Times[5]=1200;          //Negative charging. Relay 1 & 4 turned on
44    Setting[6] = B10011000; Times[6]=20;            //Put negative current through CME
45    Setting[7] = B00010000; Times[7]=1800;          //Negative floating. Relay 4 turned on to keep
    negative pole connected
46    Setting[8] = B10011000; Times[8]=20;            //Put negative current through CME
47    Setting[9] = B01010000; Times[9]=600;           //Short circuit cell. To completely discharge CME
48  }
49
50  void Relay(int RdatState)
51  {int i=0;
52   int ClkState=0;
53
54   for(i=0;i<8;i++){
55     digitalWrite(Rdat, RdatState &1);
56     ClkState=!ClkState;
57     digitalWrite(Clk, ClkState);
58     ClkState=!ClkState;
59     digitalWrite(Clk, ClkState);
60     RdatState=RdatState>>1;
61   }
62   digitalWrite(Lat, 0);
63   digitalWrite(Lat, 1);
64   digitalWrite(Lat, 0);
65  }
66
67  void loop() {
68    //=====
69    //loop to go through the charging and discharging phases of the cell
70    //each phase is set up setting is defined above
71    if (millis() > NextSwitchTime)
72    {
73      CurrentMode++;
74      if (CurrentMode>=NRModes) CurrentMode=0;      //go back to first mode

```

```

75     NextSwitchTime += Times[CurrentMode]*1000;    //
76     SCmode=-1;    //reset the SCmode
77     NextSCTime=millis();    //reset the sc timer
78     MeasureMode=-1;    //reset the measuremode
79     NextMeasurementTime=millis();    //reset the measure timer
80 }
81
82 //=====
83 //loop to short circuit cell during discharge
84 //There are X amount of "modes" to loop throught. The final mode short circuits the cell
85 //Example: 6 modes of each 20 seconds = 2 minutes. Of which 100 second measuring and 20 seconds
86     short circuiting
87     int8_t CurrentSetting = Setting[CurrentMode];
88     if (millis() > NextSCTime)
89     {
90         SCmode++;
91         if (SCmode>5) SCmode=0;    //6 short circuit modes
92         NextSCTime += 20000;    //add X amount of milliseconds
93     }
94
95     //if SCmode in final mode (step), and in discharge state 1 or 4, short circuit cell
96     if ((SCmode==5) && ((CurrentMode == 2) || (CurrentMode == 7)))
97     {
98         CurrentSetting = B01010000;    //Short circuit the cell
99     }
100
101     else
102     {
103         CurrentSetting = Setting[CurrentMode];    //Keep current setting
104     }
105 //=====
106 //loop to alternate between measuring the potential over the REs and the potential of the CME w.r.t
107     one of the REs
108 //there are therefore 2 measuring modes
109 if (millis() > NextMeasurementTime)
110 {
111     MeasureMode++;
112     if (MeasureMode>=2) MeasureMode=0;    // 2 measuring modes
113     NextMeasurementTime += 10000;    // Each mode takes 10 seconds (10000 milli seconds)
114 }
115
116 //for second mode turn relay on, keep currentsetting
117 if ((MeasureMode==1) && ((CurrentMode == 0) || (CurrentMode == 2) || (CurrentMode == 4) || (
118     CurrentMode == 5) || (CurrentMode == 7) || (CurrentMode == 9)))
119 {
120     Relay(B00000100 | CurrentSetting);
121 }
122
123 //for second mode turn relay on, keep currentsetting
124 if ((MeasureMode==1) && ((CurrentMode == 1) || (CurrentMode == 3) || (CurrentMode == 6) || (
125     CurrentMode == 8)))
126 {
127     Relay(B00000100 | CurrentSetting);
128 }
129
130 //for second mode turn relay on, keep currentsetting
131 if ((MeasureMode==0) && ((CurrentMode == 1) || (CurrentMode == 3) || (CurrentMode == 6) || (
132     CurrentMode == 8)))
133 {
134     Relay(B00000011 | CurrentSetting);
135 }
136
137 //for other modes turn relay of, keep currentsetting
138 if ((MeasureMode==0) && ((CurrentMode == 0) || (CurrentMode == 2) || (CurrentMode == 4) || (
139     CurrentMode == 5) || (CurrentMode == 7) || (CurrentMode == 9)))
140 {
141     Relay(B00000000 | CurrentSetting);
142 }
143
144 delay(100); //0.1 seconde
145 }

```

B

Combined short-circuit measurements

The figure below shows that the permselectivity measurements, with varying amounts of short-circuit intervals, are overlaying. During the floating phase, the cell was short-circuited 3, 6, or 15 times, to investigate how well the cell would discharge. The blue, green and purple curves are negatively permselective and correspond with positive membrane potentials. Orange, red and brown curves are positively permselective and correspond with negative membrane potentials. The 3 and 6 short-circuit curves do not meet in the middle, indicating that the cell is not completely discharged in those cases.

Permselectivity for varying amounts of short-circuit times

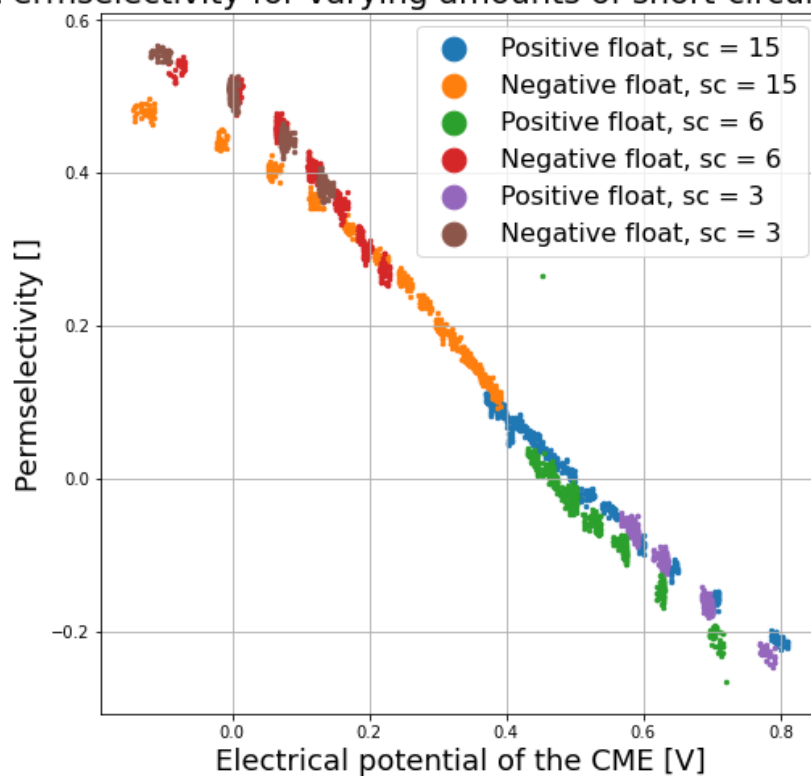
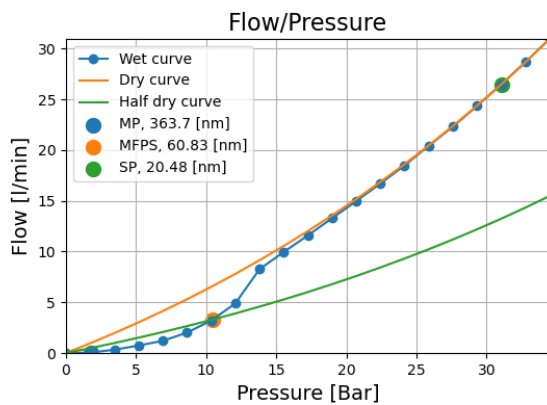


Figure B.1: Overlaying permselectivity curves for 3 experiments with varying amount short-circuit intervals. The curves from short-circuiting 3 times and 6 times do not meet at the middle point. Indicating that the CME has not been completely discharged yet.

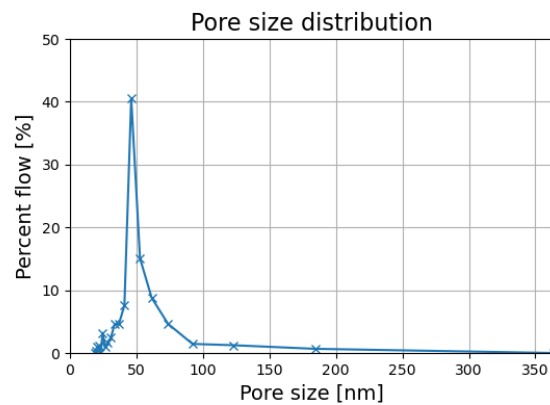
C

Pore size measurements

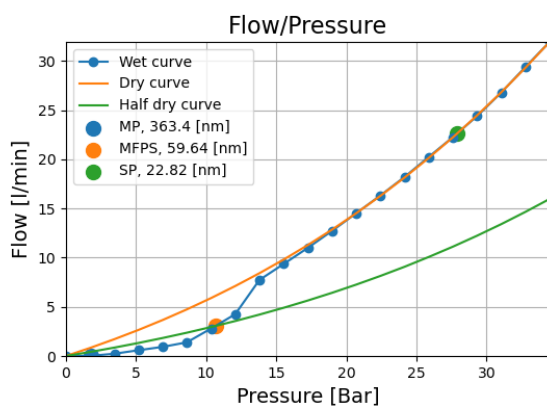
These are all the pore size measurement results. For all figures on the left, when the dry curve has a smooth curve, it was calculated using calculation method 3 described in 5.4. When the dry curve has markers on it, it is the actual measurement. MP = maximum pore size, MPFS = mean-flow-pore-size, SP = smallest pore size.



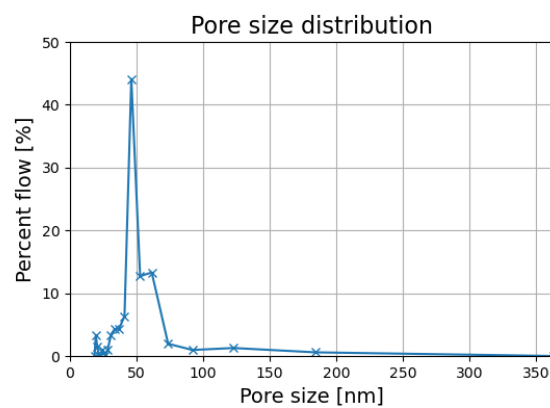
(a) CME 09/04 sample 1



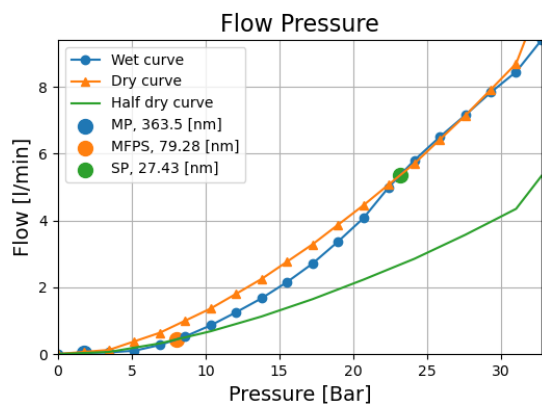
(b) PSD CME 09/04 sample 1



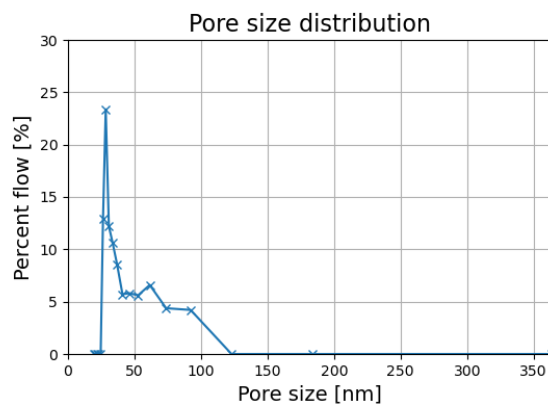
(c) CME 09/04 sample 2



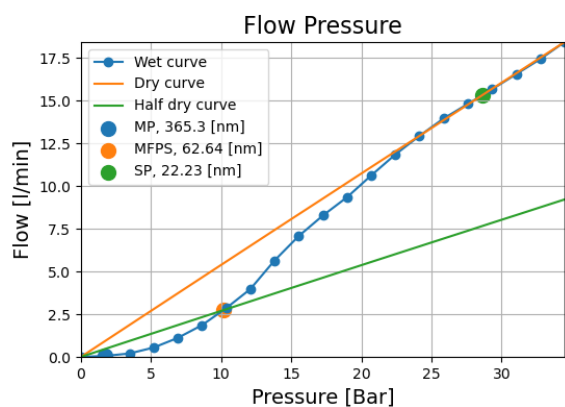
(d) PSD CME 09/04 sample 2



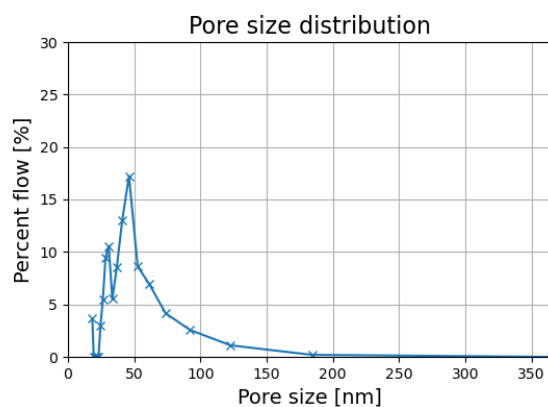
(e) CME 04/21 sample 1



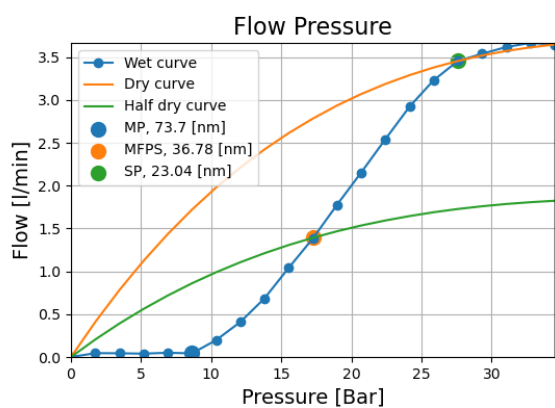
(f) PSD 04/21 sample 1



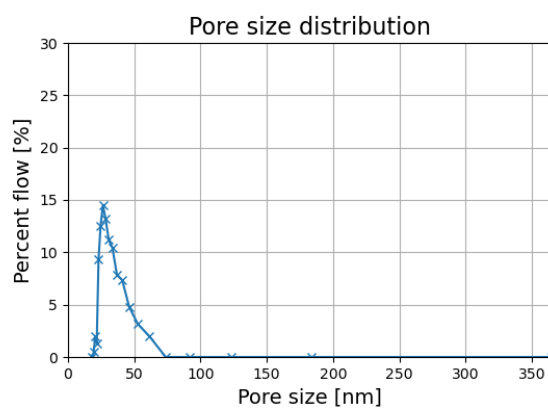
(g) CME 04/21 sample 2



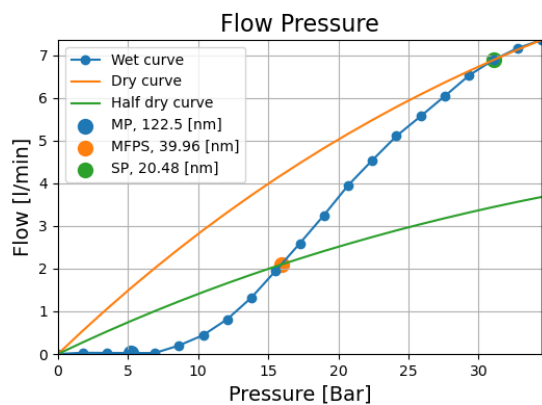
(h) PSD 04/21 sample 2



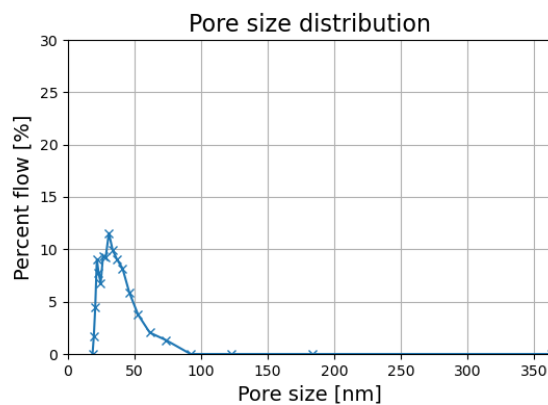
(i) CME 06/01#1 sample 1



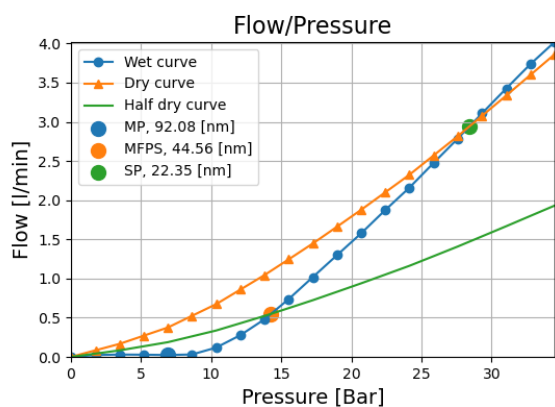
(j) PSD 06/01#1 sample 1



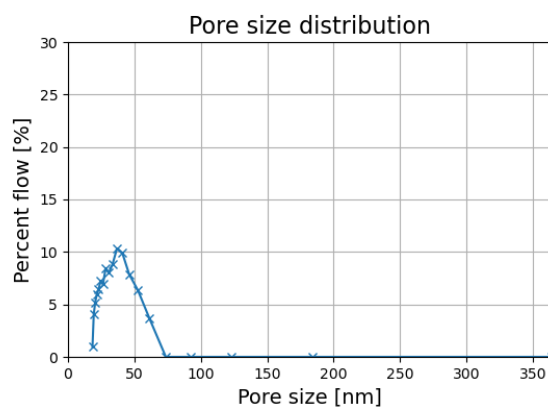
(k) CME 06/01#1 sample 2



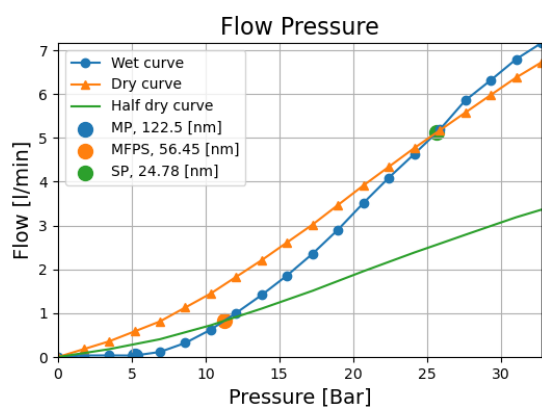
(l) PSD 06/01#1 sample 2



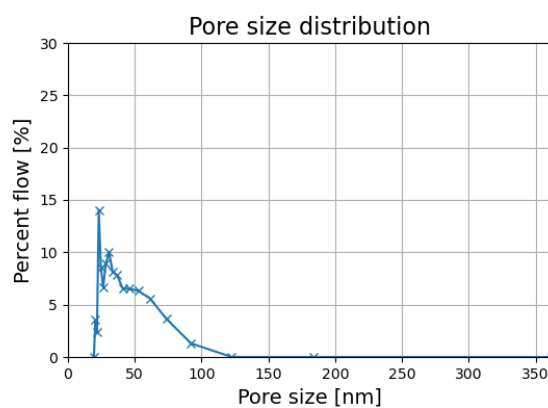
(m) CME 06/01#2 sample 1



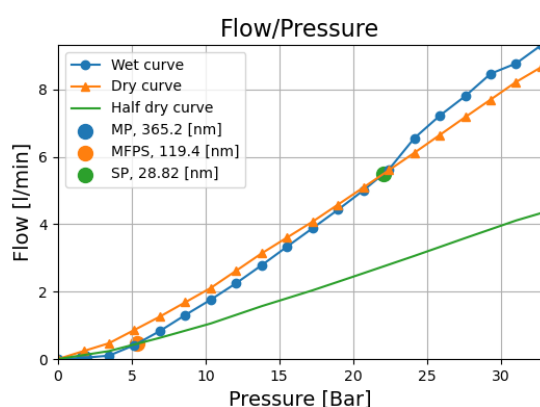
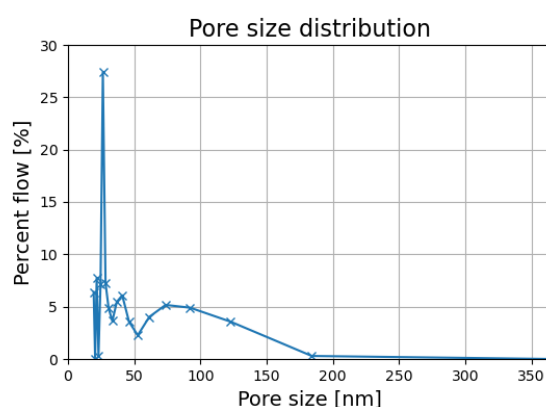
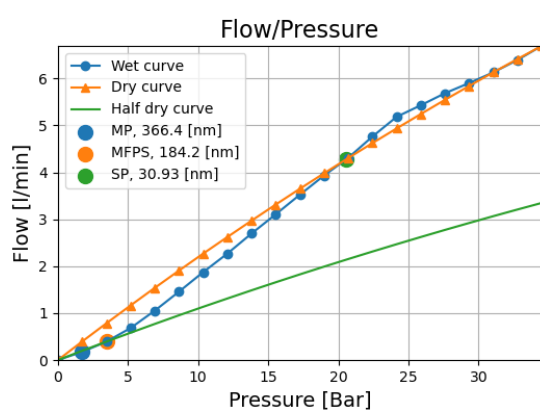
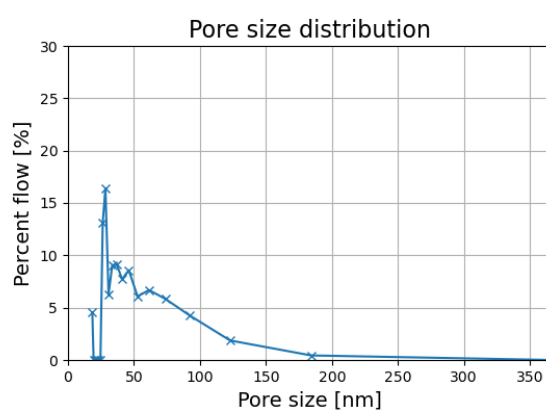
(n) PSD 06/01#2 sample 1



(o) CME 06/01#2 sample 2



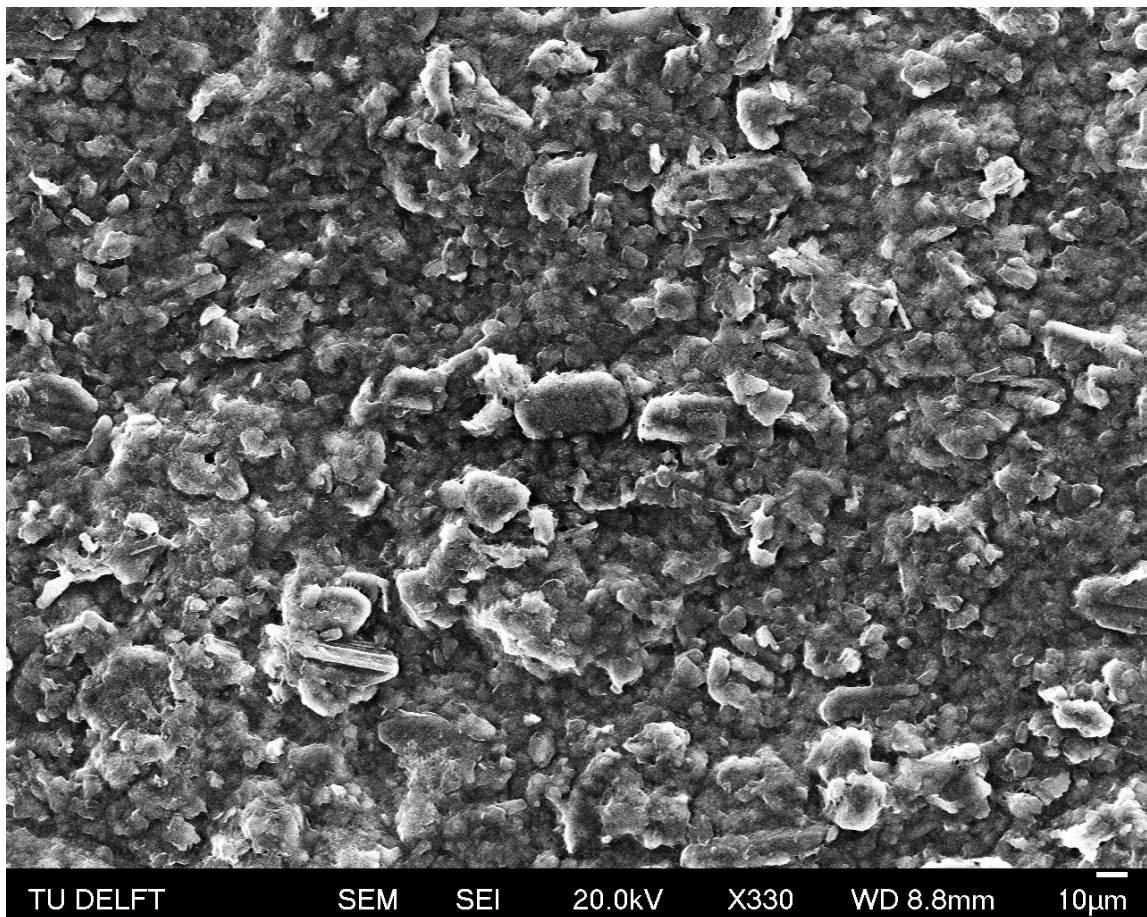
(p) PSD 06/01#2 sample 2

**(q)** CME gradient sample 1**(r)** PSD gradient sample 1**(s)** CME gradient sample 2**(t)** PSD gradient sample 2

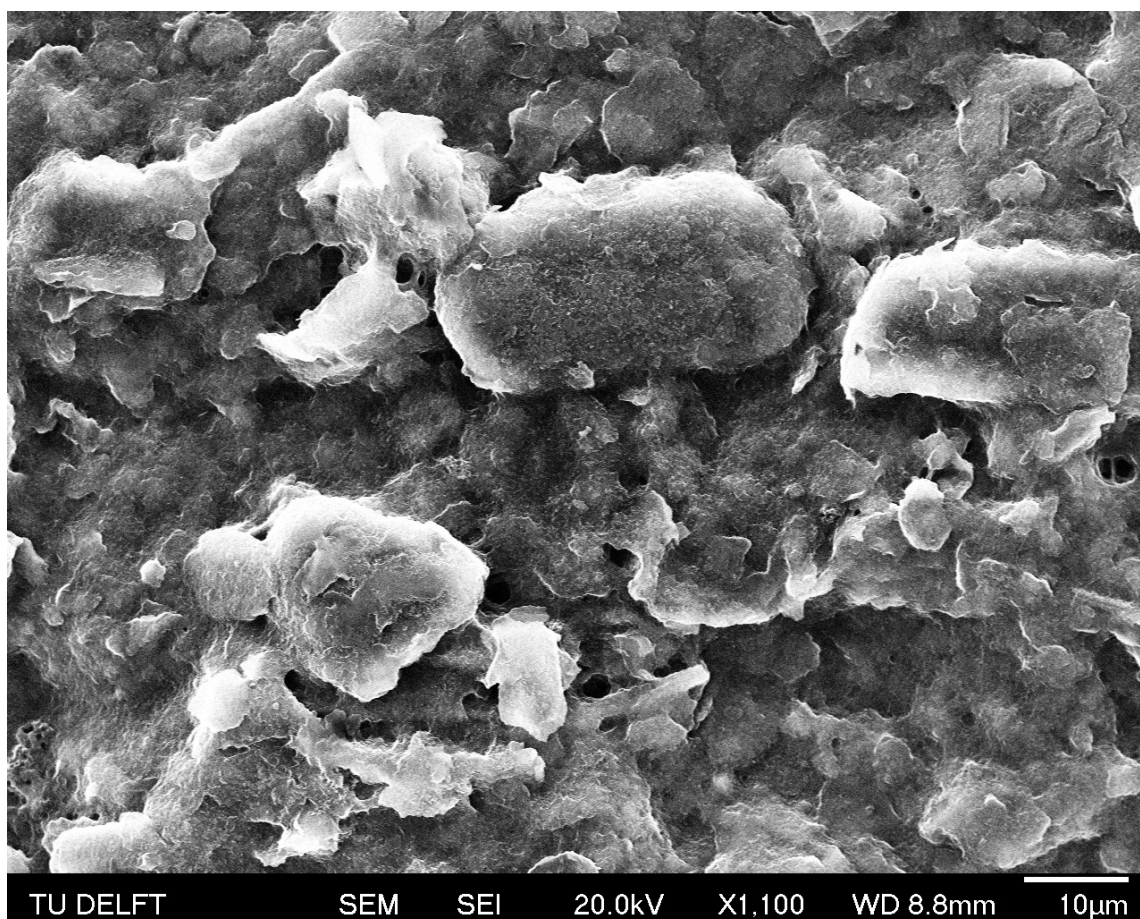
D

SEM figures

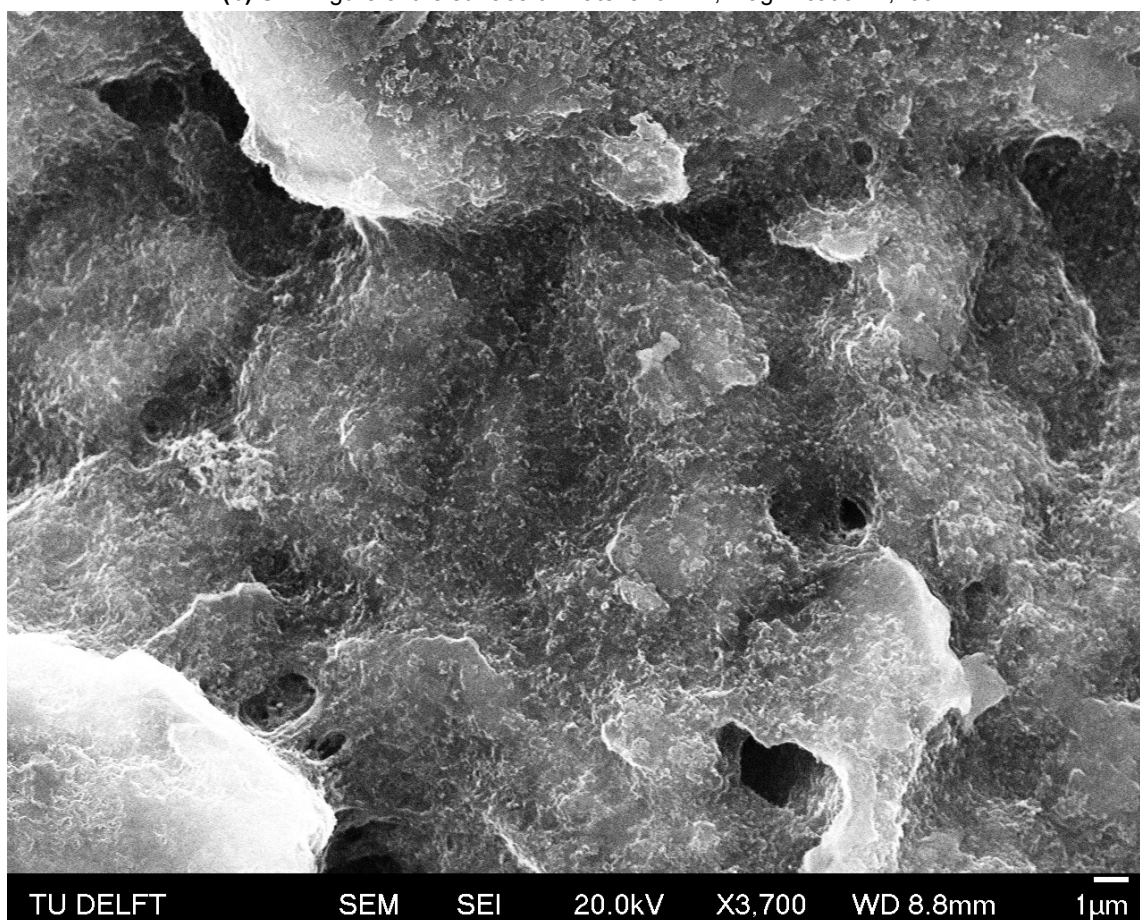
The sub-figures D.1 show a gradual magnification of the surface of material 04/21. Sub-figures D.2 show a gradual magnification of the cross-section of material 04/21.



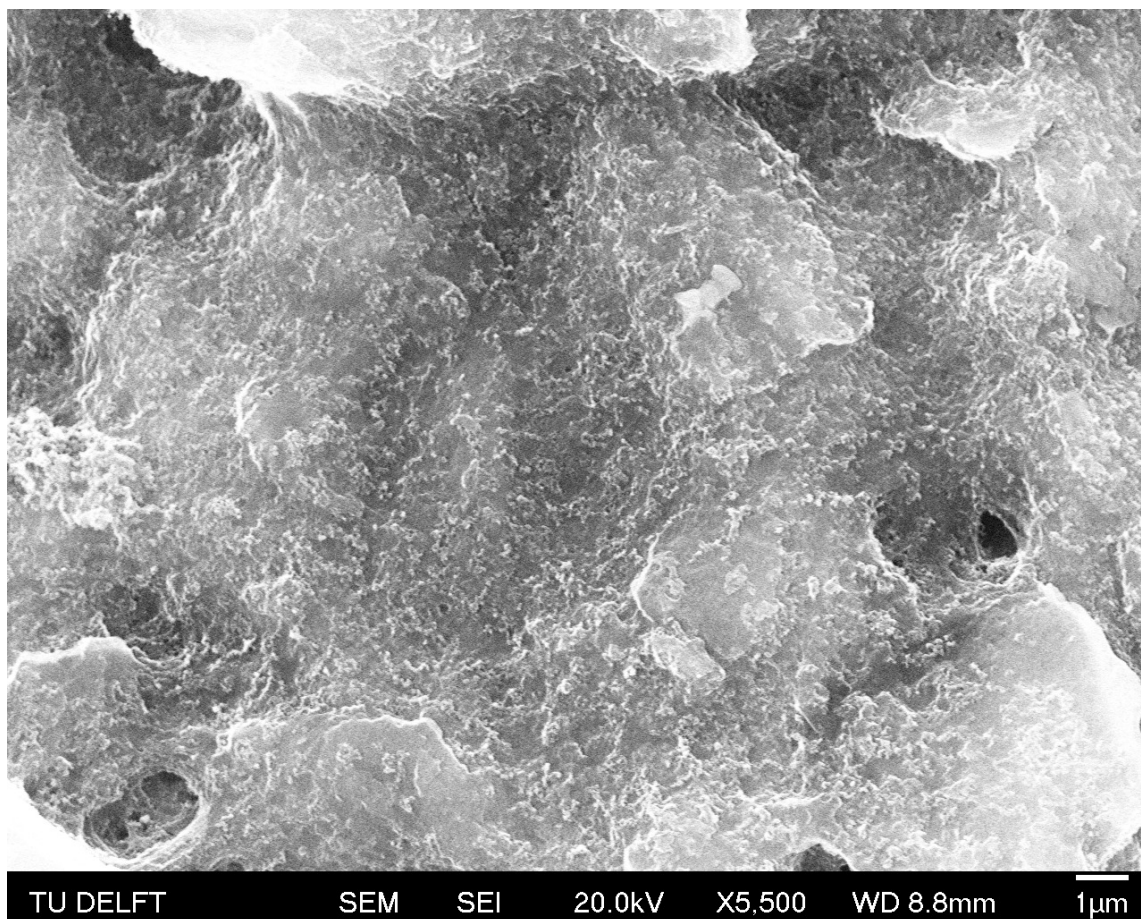
(a) SEM figure of the surface of material 04/21, magnification 330



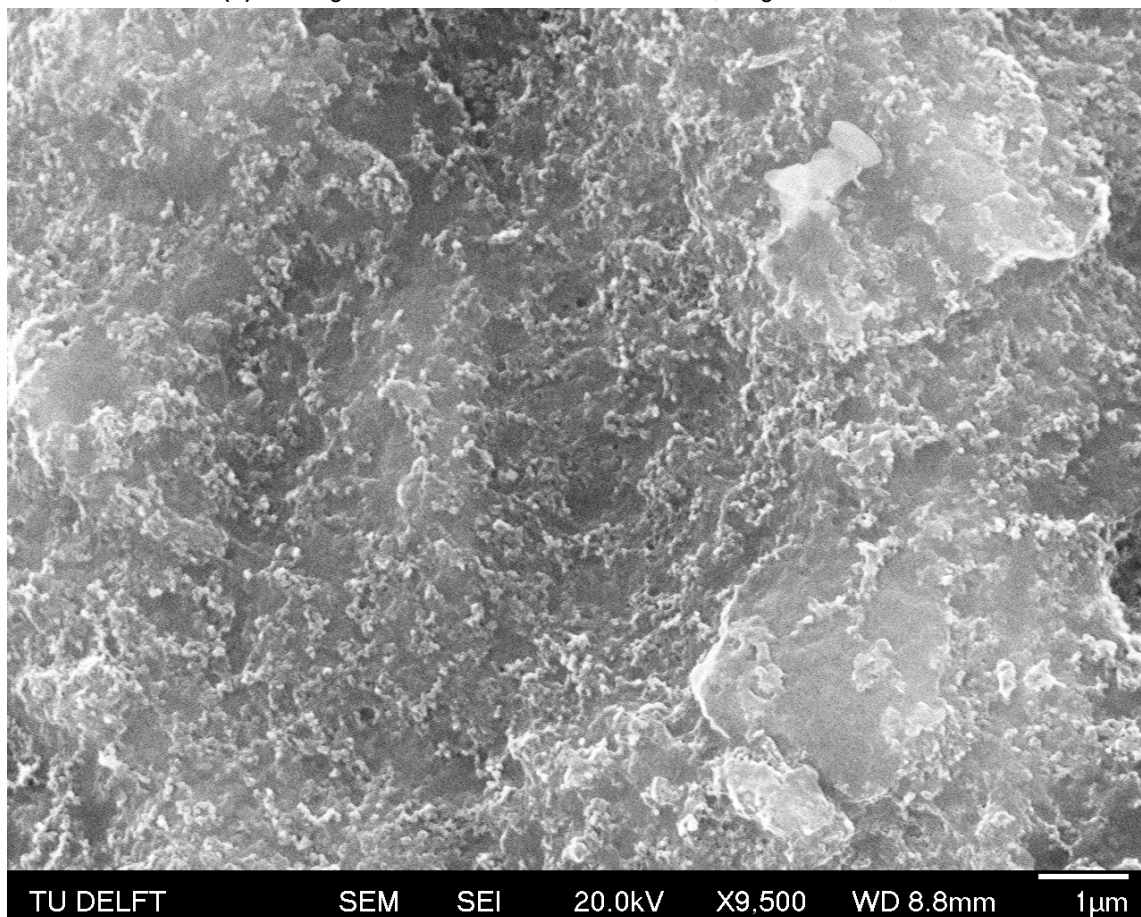
(b) SEM figure of the surface of material 04/21, magnification 1,100



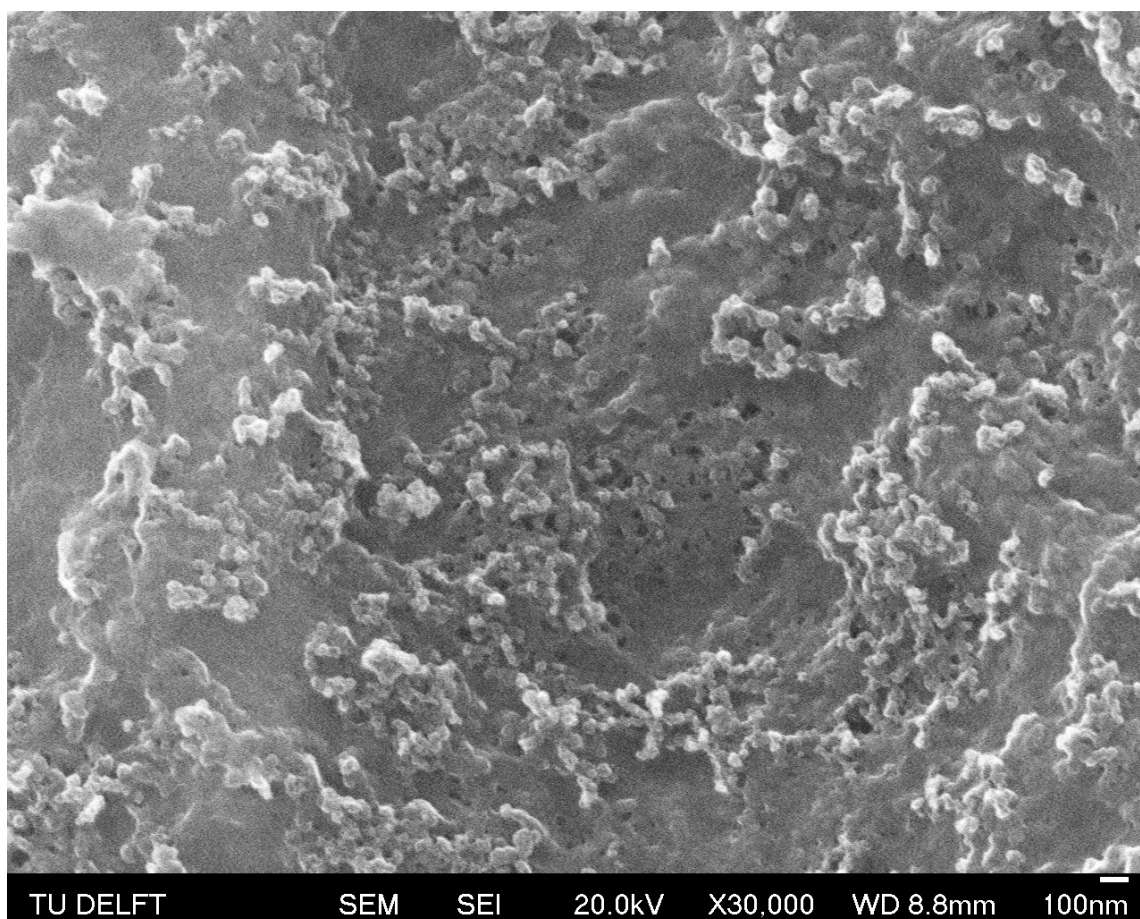
(c) SEM figure of the surface of material 04/21, magnification 3,700



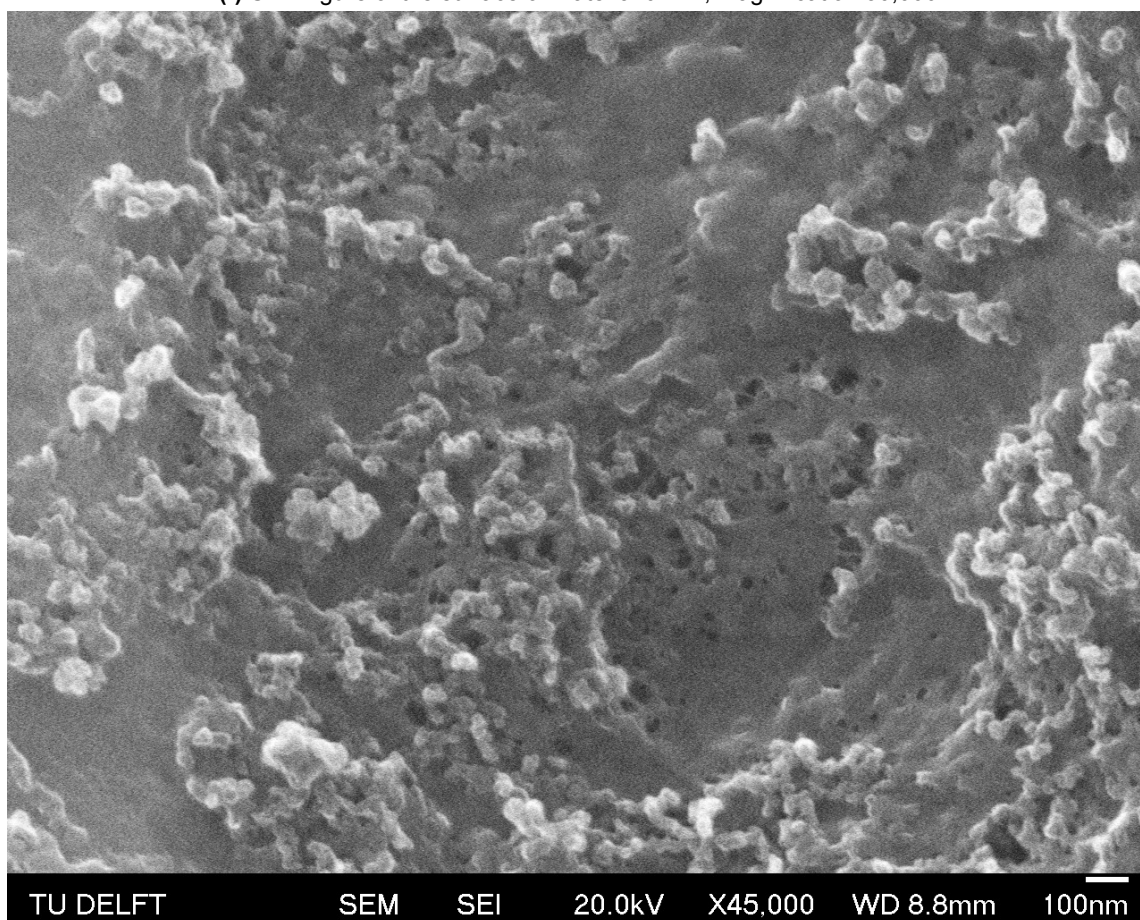
(d) SEM figure of the surface of material 04/21, magnification 5,500



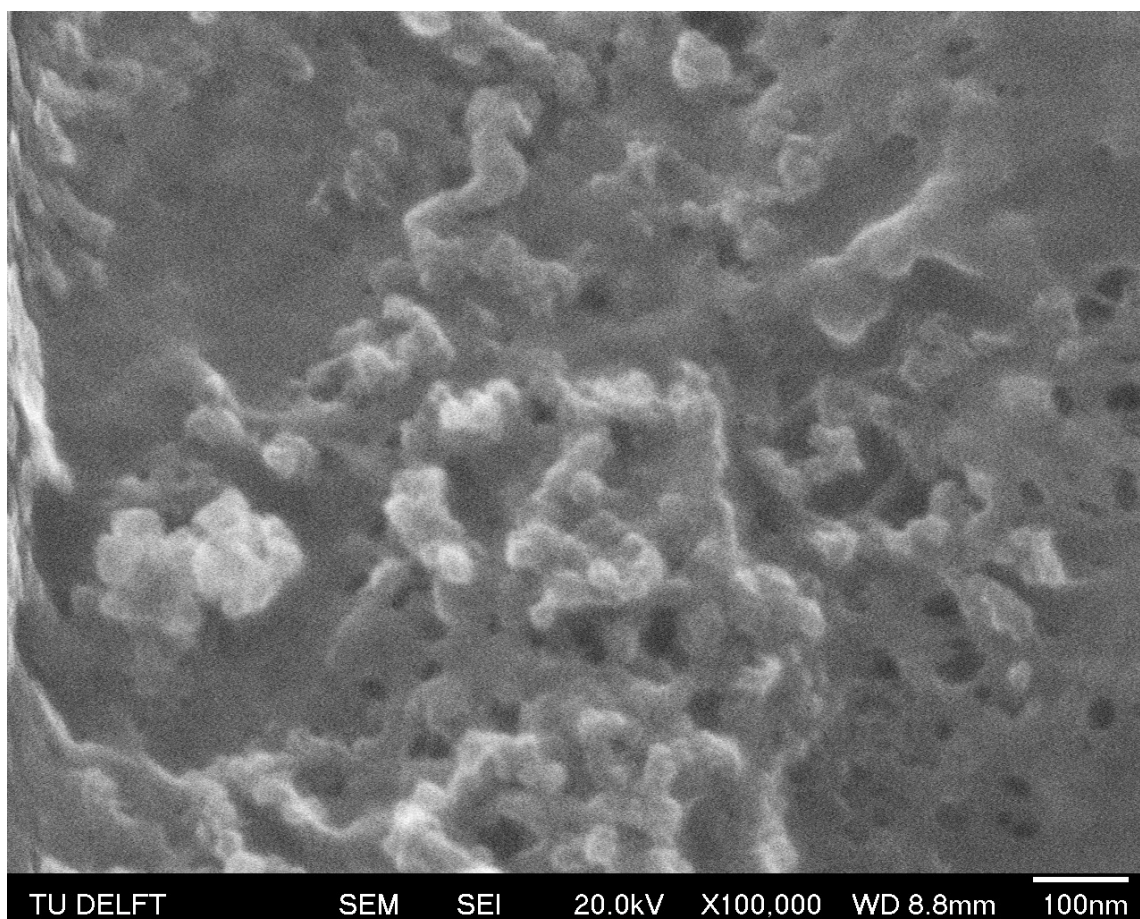
(e) SEM figure of the surface of material 04/21, magnification 9,500



(f) SEM figure of the surface of material 04/21, magnification 30,000

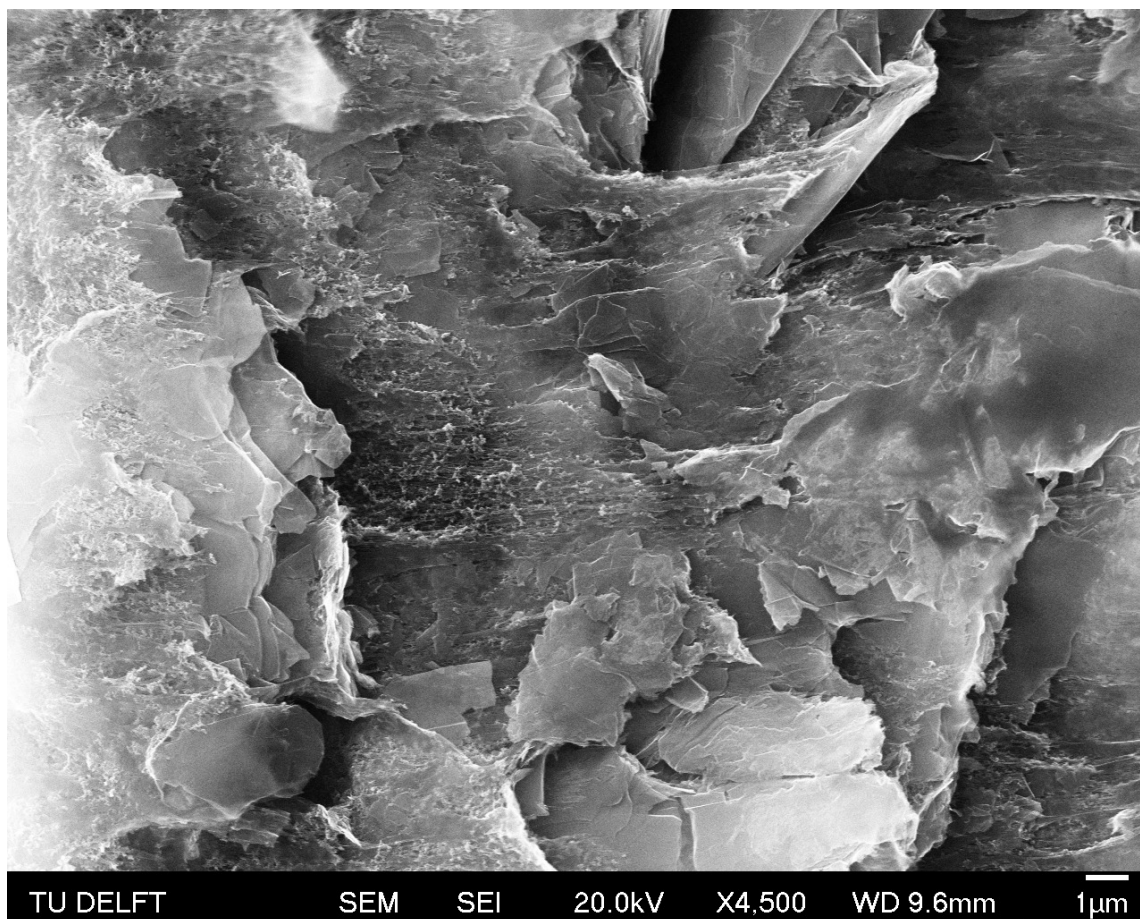


(g) SEM figure of the surface of material 04/21, magnification 45,000

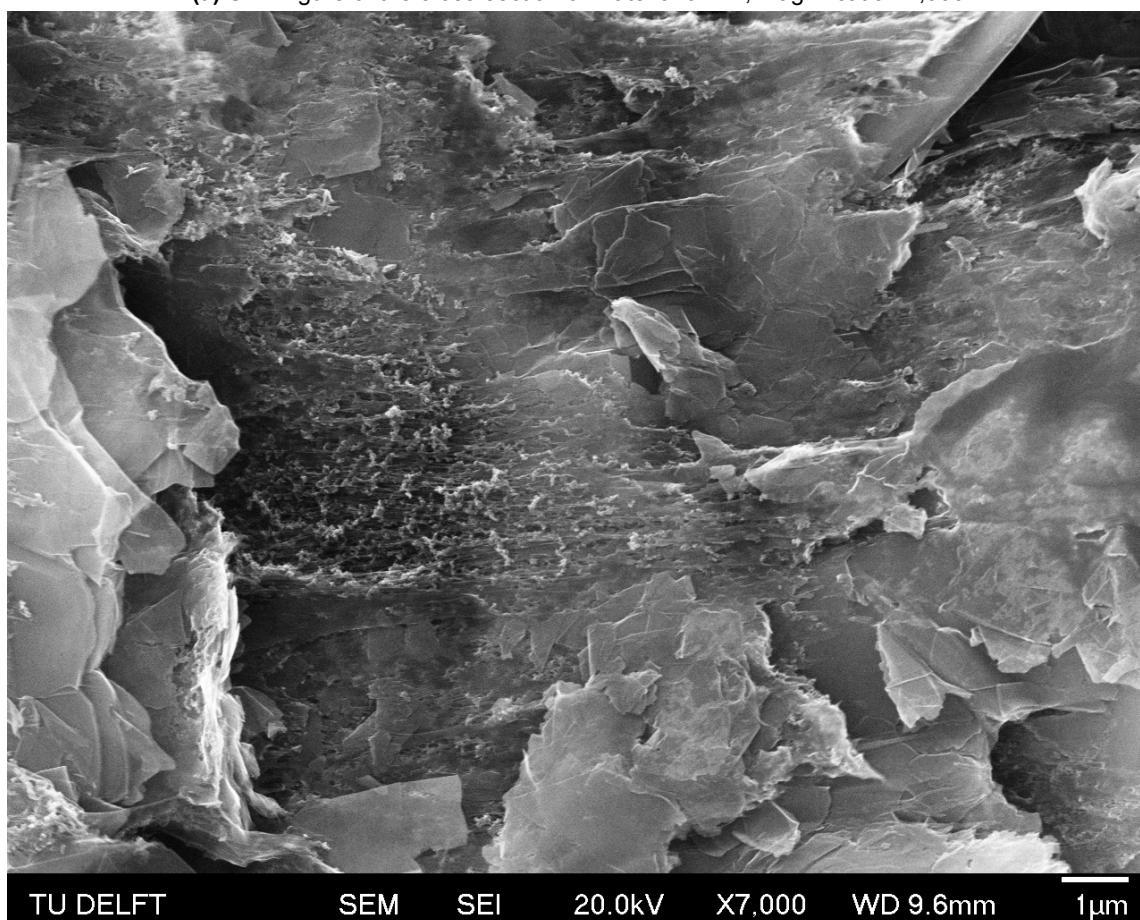


(h) SEM figure of the surface of material 04/21, magnification 100,000

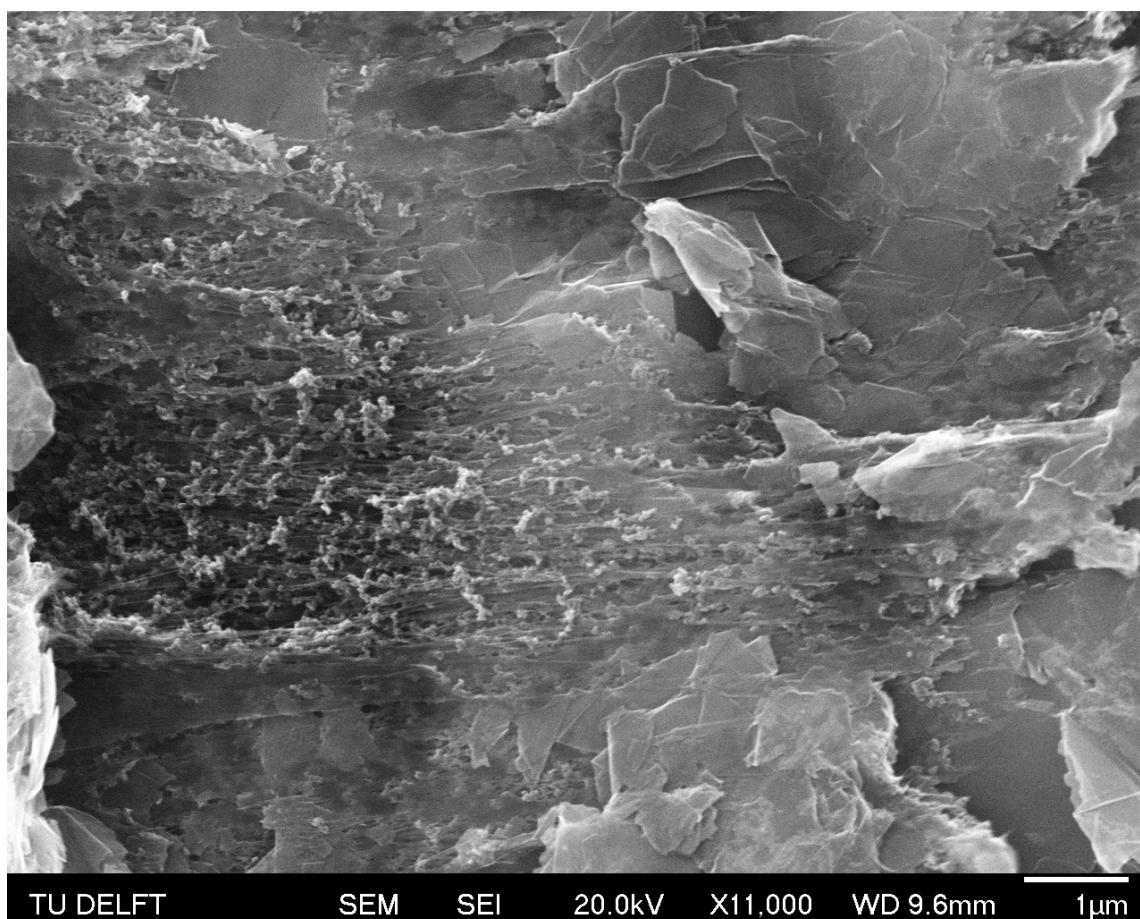
Figure D.1: SEM figures with increasing magnification of the surface of material 04/21



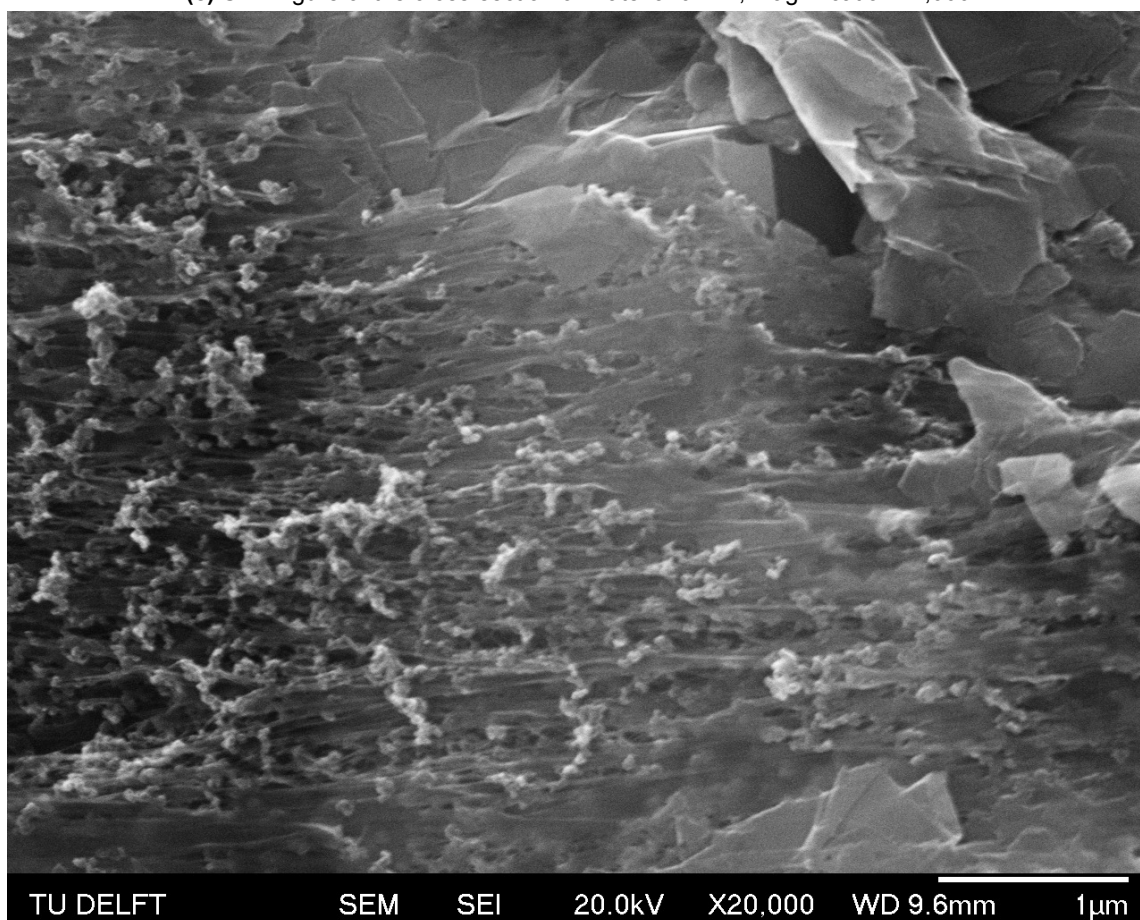
(a) SEM figure of the cross-section of material 04/21, magnification 4,500



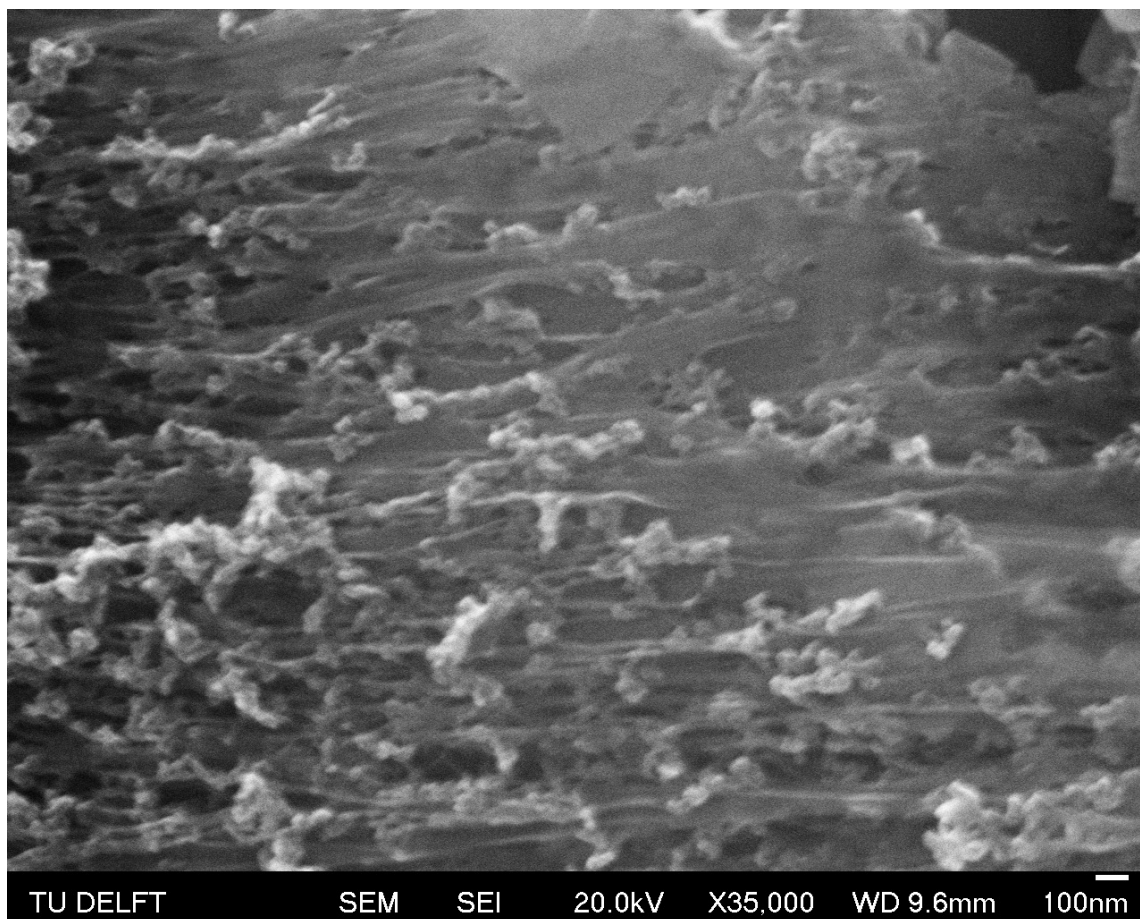
(b) SEM figure of the cross-section of material 04/21, magnification 7,000



(c) SEM figure of the cross-section of material 04/21, magnification 11,000



(d) SEM figure of the cross-section of material 04/21, magnification 20,000



(e) SEM figure of the cross-section of material 04/21, magnification 35,000

Figure D.2: SEM figures with increasing magnification of the cross-section of material 04/21